

JUL 17 1996

~~Print Media, 12615~~
~~MS 0619~~

CONTRACTOR REPORT

SAND96-1246
Unlimited Release
UC-1211

Probabilistic Fatigue Methodology and Wind Turbine Reliability

Clifford H. Lange
Civil Engineering Department
Stanford University
Stanford, CA 94305

Prepared by Sandia National Laboratories Albuquerque, New Mexico 87185
and Livermore, California 94550 for the United States Department of Energy
under Contract DE-AC04-94AL85000

Printed May 1996

RECEIVED
JUL 24 1996
OSTI

DISTRIBUTION OF THIS DOCUMENT IS UNLIMITED

MASTER

Issued by Sandia National Laboratories, operated for the United States Department of Energy by Sandia Corporation.

NOTICE: This report was prepared as an account of work sponsored by an agency of the United States Government. Neither the United States Government nor any agency thereof, nor any of their employees, nor any of their contractors, subcontractors, or their employees, makes any warranty, express or implied, or assumes any legal liability or responsibility for the accuracy, completeness, or usefulness of any information, apparatus, product, or process disclosed, or represents that its use would not infringe privately owned rights. Reference herein to any specific commercial product, process, or service by trade name, trademark, manufacturer, or otherwise, does not necessarily constitute or imply its endorsement, recommendation, or favoring by the United States Government, any agency thereof or any of their contractors or subcontractors. The views and opinions expressed herein do not necessarily state or reflect those of the United States Government, any agency thereof or any of their contractors.

Printed in the United States of America. This report has been reproduced directly from the best available copy.

Available to DOE and DOE contractors from
Office of Scientific and Technical Information
PO Box 62
Oak Ridge, TN 37831

Prices available from (615) 576-8401, FTS 626-8401

Available to the public from
National Technical Information Service
US Department of Commerce
5285 Port Royal Rd
Springfield, VA 22161

NTIS price codes
Printed copy: A05
Microfiche copy: A01

Unlimited Release
Printed March 1996

PROBABILISTIC FATIGUE METHODOLOGY AND WIND TURBINE RELIABILITY

Clifford H. Lange
Civil Engineering Department
Stanford University
Stanford, CA 94305

Sandia Contract: AC-9051

Abstract

Wind turbines subjected to highly irregular loadings due to wind, gravity, and gyroscopic effects are especially vulnerable to fatigue damage. The objective of this study is to develop and illustrate methods for the probabilistic analysis and design of fatigue-sensitive wind turbine components. A computer program (CYCLES) that estimates fatigue reliability of structural and mechanical components has been developed. A FORM/SORM analysis is used to compute failure probabilities and importance factors of the random variables. The limit state equation includes uncertainty in environmental loading, gross structural response, and local fatigue properties. Several techniques are shown to better study fatigue loads data. Common one-parameter models, such as the Rayleigh and exponential models are shown to produce dramatically different estimates of load distributions and fatigue damage. Improved fits may be achieved with the two-parameter Weibull model. High b values require better modeling of relatively large stress ranges; this is effectively done by matching at least two moments (Weibull) and better by matching still higher moments. For this purpose, a new, four-moment "generalized Weibull" model is introduced. Load and resistance factor design (LRFD) methodology for design against fatigue is proposed and demonstrated using data from two horizontal-axis wind turbines. To estimate fatigue damage, wind turbine blade loads have been represented by their first three statistical moments across a range of wind conditions. Based on the moments $\mu_1 \dots \mu_3$, new "quadratic Weibull" load distribution models are introduced. The fatigue reliability is found to be notably affected by the choice of load distribution model.

Foreword

This report comprises the Ph.D. thesis dissertation of the author, submitted to the Department of Civil Engineering of Stanford University in March 1996. The principal advisor of this research at Stanford has been Steven R. Winterstein. Other thesis readers have been C. Allin Cornell at Stanford, and Paul S. Veers at Sandia.

Chapter 2 describes a computer program, **CYCLES**, useful for estimating the fatigue reliability of structural and mechanical components. This program, developed as a general reliability program for various applications, served as a preliminary version of the more broadly distributed fatigue reliability program for wind turbines, **FAROW**. The **FAROW** program has been tailored to wind turbine applications by including an upper-bound cutoff wind speed and a variable cycle rate (e.g., as a function of wind speed). The **FAROW** code also has a more user-friendly interface. The capabilities of the two codes are nearly identical and the description given in Chapter 2 is applicable to both the **CYCLES** and **FAROW** programs.

This project, developed at Stanford University, was supported by Sandia National Laboratories Wind Energy Technology Department, and the Reliability of Marine Structures Program of the Civil Engineering Department at Stanford University.

Contents

Foreword	ii
1 Introduction	1
1.1 Organization	3
2 CYCLES Fatigue Reliability Formulation	5
2.1 CYCLES Overview	5
2.2 General Fatigue Formulation: Assumptions	8
2.2.1 Load Environment	8
2.2.2 Gross Response	9
2.2.3 Failure Measure	9
2.3 General Fatigue Formulation: Results	10
2.4 Analytical Fatigue Formulation	11
2.5 Solution Algorithm for Failure Probability	15
2.6 Program CYCLES Capabilities	17
2.7 Example Application: The Sandia 34-m Test Bed VAWT	21
2.7.1 Definition of Input	21
2.7.2 Results: Base Case	27
2.7.3 Lognormal versus Weibull Distribution for $S-N$ Parameter: C	27
3 Load Models for Fatigue Reliability	30
3.1 Fatigue Data and Damage Densities	31
3.2 One and Two Parameter Load Models	34
3.3 Generalized Four-Parameter Load Models	38

3.3.1	Model versus Statistical Uncertainty	39
3.3.2	Underlying Methodology	40
3.3.3	Generalized Weibull Model for Fatigue Loads	42
3.3.4	Generalized Gumbel and Generalized Gaussian Load Models	43
3.4	Fatigue Damage Estimates	50
3.5	Uncertainty Due to Limited Data	51
3.6	Summary	54
4	LRFD for Fatigue	55
4.1	Scope and Organization	55
4.2	Background: Probabilistic Design	57
4.2.1	Probabilistic Design against Overloads.	57
4.2.2	Probabilistic Design against Fatigue	57
4.3	Fatigue Load Modeling	60
4.3.1	Fatigue Loads for Given Wind Climate	60
4.3.2	Fatigue Loads Across Wind Climates	63
4.4	LRFD Assumptions and Computational Procedure	69
4.5	Variations with Load Distribution	72
4.6	LRFD Calculations	73
4.6.1	Turbine 1 Results	75
4.6.2	Turbine 2 Results	77
4.7	Effects of Limited Data	81
4.8	Summary	86
5	Summary and Recommendations	88
5.1	Overview of Important Conclusions	88
5.2	General Recommendations of Future Work	90
5.3	Specific Recommendations to Extend Current Work	91
5.4	Challenges for Future Study	92
	References	96

CONTENTS

v

A Statistical Moment Estimation

100

List of Tables

2.1	Sandia 34-m Test Bed VAWT, CYCLES Base Case Input Summary . . .	26
2.2	Sandia 34-m Test Bed VAWT, CYCLES Reliability Results	28
2.3	Effect of S-N Intercept Distribution Type with Reduced Uncertainty .	29
4.1	Random variables in reliability analyses.	70
4.2	Turbine 1 reliability results; effect of load distribution type	72
4.3	Turbine 1 reliability results; all results with same normalized fatigue load L_{nom}	74
4.4	Turbine 2 reliability results; all results with same normalized fatigue load L_{nom}	80
4.5	Most Damaging Wind Speeds (m/s) from Reliability Analyses	84

List of Figures

2.1	FORM and SORM approximations to $g(U) \leq 0$	16
2.2	Flow chart, general CYCLES code execution.	19
2.3	Flow chart, initial processing of CYCLES random variables.	20
2.4	Wind speed distributions from Amarillo, Bushland, and the theoretical Rayleigh distribution with $\bar{V} = 6.3$ m/s	23
2.5	Measured RMS Stresses at the Blade Upper Root	23
2.6	Effective stress amplitude versus cycles to failure for 6063 aluminum alloy	25
3.1	Histogram; Flapwise Data.	33
3.2	Damage Density; Flapwise Data.	33
3.3	Exponential and Rayleigh Models; Flapwise Data.	36
3.4	Weibull Model of Flapwise Data.	36
3.5	Weibull and Generalized Weibull models; Flapwise data	42
3.6	Histogram; edgewise data	44
3.7	Damage Density; Edgewise Data.	44
3.8	Weibull and Generalized Weibull Models; Edgewise Data (Ranges Plotted on Shifted Axis, $S-S_{min}$).	45
3.9	Generalized Gumbel Distribution for Annual Extreme Wave Height-19 Data.	46
3.10	Comparison of Generalized Gaussian, Gumbel, and Weibull Distributions for Annual Extreme Wave Height.	47
3.11	Oscillator Response; 30% Damping.	49
3.12	Oscillator Response; 10% Damping.	49

3.13	Normalized Damage per cycle; flapwise data	51
3.14	Damage coefficient of variation; flapwise data	52
4.1	Distribution of normalized loads (Turbine 1: $V = 11.5$ m/sec, $I = .16$).	61
4.2	Estimated mean of normalized loads.	64
4.3	Estimated load coefficient of variation (COV).	64
4.4	Estimated load skewness.	65
4.5	Standard deviation, estimated mean load.	67
4.6	Standard deviation, estimated load COV.	67
4.7	Standard deviation, estimated load skewness.	68
4.8	Load factors, Turbine 1. Note that these factors apply to a load defined in units of cycles (Eqs. 4.18–4.19).	76
4.9	Resistance factors, Turbine 1. Note that these factors apply to a resistance defined in units of cycles (Eq. 4.7).	76
4.10	Load factors needed, for Turbine 1, if nominal load is based only on the mean stress for wind speed $V=50$ m/s.	78
4.11	Load factors, Turbine 2. Note that these factors apply to a load defined in units of cycles (Eqs. 4.18–4.19).	79
4.12	Resistance factors, Turbine 2. Note that these factors apply to a resistance defined in units of cycles (Eq. 4.7).	79
4.13	Load factors, Turbine 2. Note that these factors apply to a load defined in units of stress (Eq. 4.23).	82
4.14	Resistance factors, Turbine 2. Note that these factors apply to a resistance defined in units of stress (Eq. 4.23).	82
4.15	Estimated Mean of Normalized Loads showing range of measured data	85
A.1	Effect of Ignoring Bias: Wave Height Example.	102

Chapter 1

Introduction

The deterioration of engineering structures due to fatigue has been a difficult problem facing engineers for many decades. This is due in part to the complex nature of the fatigue process, which makes a deterministic engineering description of the problem difficult. Traditional deterministic fatigue analyses have often employed rather large safety factors, in order to compensate for the large degree of uncertainty involved.

Recently, within the last few decades, probabilistic design techniques which account for statistical distributions of stress, strength, geometry, etc., have promised to provide a more rational and consistent design approach for fatigue (Committee on Fatigue and Fracture Reliability, 1982). The use of stationary random (or stochastic) processes to define statistical loads models for earthquakes, wind, ocean wave forces, and vehicle environments have played an important role in probabilistic analyses. The advantage of a probabilistic approach to fatigue design lies in the logical framework for analyzing design uncertainties and the quantitative basis for assessing structural integrity in the form of the risk or probability of unfavorable performance.

Wind turbines used to produce electrical energy from the wind are especially vulnerable to fatigue damage. Highly irregular loadings due to wind, gravity, and gyroscopic effects combined with extremely variable material properties make an efficient design against fatigue a challenging task. Virtually all turbines built in California in the early 1980's and operating in energetic sites (average wind speeds ≥ 7 m/s) have experienced fatigue problems (Sutherland et al, 1994). Although significant progress

has been achieved through inspection, maintenance programs, operating experience, and research activities, deterministic design approaches currently employed by the industry have serious shortcomings as evidenced by continued turbine failures.

The objective of this study is to develop and illustrate methods for the probabilistic analysis and design of fatigue-sensitive wind turbine components. (Note that while the specific focus lies with wind turbines, the methods shown here may be of use across a range of problems of damage accumulation, crack growth, etc.) We seek to capitalize on a rapidly evolving set of computational methods, grouped broadly under the topic of "structural reliability" (e.g., Madsen et al, 1986, Thoft-Christensen and Baker, 1982, Melchers, 1987). In particular, powerful asymptotic numerical techniques known as "FORM/SORM" (First- and Second-Order Reliability Methods) have been found quite efficient in estimating probabilities of rare failure events, associated with well-designed engineering systems. Simulation techniques—both ordinary Monte-Carlo and more sophisticated importance sampling schemes (e.g., Rubinstein, 1981, Melchers, 1987)—give a useful alternative for systems with higher failure rates, for which FORM/SORM may become inaccurate.

The net result is that computational analysis methods are available to estimate the reliability of complex engineering systems, which may involve

- A large number of random variables (e.g., tens to hundreds)
- Arbitrary probability distributions, given analytically or through numerical algorithms
- Arbitrary probabilistic dependence among variables (defined through a sequence of conditional distributions; e.g. Madsen et al, 1986)

Since we have gained this generality of analysis capabilities, the burden has been shifted back to the task of appropriate probabilistic modeling. We are free to use whatever probability distribution is most "correct" given the available data. With this freedom comes the associated need for more flexible distribution models, more robust distribution fitting techniques, methods to include uncertainty due to limited data, and finally a vehicle to propagate all of these to estimate the net consequence on

fatigue reliability. These topics are addressed in the following chapters of this work. An overview of each chapter follows below.

1.1 Organization

Each of the following three thesis chapters is devoted to a particular topic of interest for wind turbine fatigue reliability. These are described in turn below. A brief concluding chapter is also offered to suggest topics of future work.

CYCLES Fatigue Reliability Formulation (Chapter 2). A FORM/SORM based computer code capable of computing failure probabilities of wind turbine components has been developed. Based on Miners law to predict fatigue failure, it utilizes a closed-form expression for the limit state equation made possible by simplifying assumptions for distributions of wind speed and structural response. The resulting analytical form of the limit-state equation facilitates study of important parametric variations, e.g., of distribution parameters, $S-N$ curve properties, etc. An example that demonstrates the impact of distribution type (for the $S-N$ parameter C) on predicted reliability is given.

Load Models for Fatigue Reliability (Chapter 3). The availability of load models (e.g., probability distributions) that adequately reflect wind turbine response to environmental loading is required for a probabilistic fatigue analysis. Therefore, empirically based load models that are useful for describing structural response for a wide range of wind turbine components are established. Exponential, Rayleigh, and Weibull distributions are investigated from the standpoint of goodness of fit, damage density, and implications on predicted fatigue damage. A new "generalized" Weibull distribution is proposed and shown to offer improved modeling characteristics in some cases.

Load and Resistance Factor Design for Fatigue (Chapter 4). LRFD methodology for design against fatigue damage is proposed. The methodology is implemented using data from two different wind turbine rotor blades. The effects of

turbine design and limited data are discussed and shown to be important on the resulting partial safety factors. Results are presented for different load models (Chapter 3) and appropriate load models are shown to be highly important to the reliability calculations. The usefulness of LRFD in moving probabilistic fatigue methodology from a research topic to design practice is emphasized.

Chapter 2

CYCLES Fatigue Reliability Formulation

CYCLES is an algorithm and computer program that estimates the fatigue reliability of structural and mechanical components. It includes a rather flexible model of uncertainty, both in distribution parameters of randomly varying quantities (e.g., load environment parameters such as wind speed) and in uncertain material properties (e.g., $S-N$ fatigue properties). The formulation is intended to be of general applicability across a range of fatigue problems.

2.1 CYCLES Overview

The CYCLES algorithm is based on a deterministic fatigue life formulation specifically for structural components operating in a continuously varying load environment. The fatigue formulation is intended to be of rather general applicability. Originally developed by Veers, (1990), and since extended at Stanford with wind turbine applications in mind, it is equally useful for offshore applications (Winterstein and Lange, 1994).

The fatigue formulation employed by CYCLES is intended to reflect uncertainty in environmental loading, gross structural response, and local fatigue properties. Fatigue damage is modeled probabilistically using Miner's Rule, including the effects of variable loads, mean stress effects, and stress concentration factors. A critical

distinction here is between continuously varying quantities such as an environmental parameter (e.g., significant wave height H_S , mean wind speed V , applied stress level S versus time, etc.) and fixed parameters which may be uncertain (e.g. fatigue law coefficients, distribution parameters of H_S , V , S given either H_S or V , etc.). Continuously varying quantities are reflected here implicitly, through their average effect on fatigue damage. In contrast, parameter uncertainty doesn't "average out" over fatigue life, and is modeled here explicitly.

The *CYCLES* analysis assumes specific functional forms for the controlling quantities of fatigue life. The assumed functional forms enable the derivation of a closed form expression for fatigue damage in terms of the various parameters in the functions such as S - N coefficient and exponent, RMS stress level at a characteristic wind speed, average wind speed, etc.. These parameters can then be treated as constants or random variables in the probabilistic analysis. The trade-off is in the level of generality, the restrictive assumptions catalogued in section 2.4 that permit definition of the entire problem with a condensed data set. The emphasis has been on keeping the input simple and easy to use.

The assumed functional forms "built in" to the *CYCLES* formulation do restrict its generality. An obvious constraint is the use of only one environmental variable with predetermined distribution type (e.g. Weibull). Other assumptions regarding the load distribution and its dependence on the environment limit the program's ability to model measured load distributions across a range of environmental states. This is demonstrated in Chapter 4 where it is also shown that for some wind turbines the *CYCLES* formulation may work quite well. Therefore, the *CYCLES* limit state formulation, while not the most complex or detailed model that could be established, represents a useful compromise between its level of detail in mechanical and probabilistic modeling, and the state of knowledge of many structures and mechanical components to which it may be applied.

In contrast to the deterministic fatigue analysis code *LIFE2* (Sutherland, 1989) used by the wind industry, *CYCLES* computes a probability of failure for wind turbine components. *LIFE2* on the other hand gives only a projected time to failure as it treats all analysis parameters as constants. Furthermore the input to *LIFE2* is

achieved numerically with various "look-up" tables used to define various aspects of the input. While adding generality to the code the input procedure can become tedious. CYCLES however with its closed form limit state formulation requires only the distribution types and associated parameters for each of the 14 random variables used

The probability of failure is calculated using the general purpose FORM/SORM (first and second order reliability methods) package developed by Golweitzer et al, (1988). Enhancements to the way the basic algorithm treats correlation between random variables have been added (Winterstein et al, 1989). Section 2.5 describes the technique used to include the correlation. Importance factors and sensitivities are calculated as well.

2.2 General Fatigue Formulation: Assumptions

Whether fatigue or an alternate failure condition is considered, a complete reliability formulation generally includes uncertainty in three distinct aspects:

1. The loading environment;
2. The gross level of structural response given the load environment; and
3. The local failure criterion given both load environment and gross stress response.

The following treatment is intended to provide a general approach to fatigue modeling and at the same time produce a limit state equation that can be implemented in a FORM analysis. For the fatigue limit state of interest, each of these aspects is examined in turn below.

2.2.1 Load Environment

Characterizing Variable: X =dominant environmental parameter.

For the subsequent analysis, the load environment is assumed to be well characterized by a single controlling random variable, herein denoted X for generality. Therefore its probability density function, $f_X(x)$, is required as input to the fatigue reliability analysis. This will commonly be estimated from site-specific environmental data.

The environmental parameter X usually represents an "average" value over a relatively short time period. Problems involving fixed offshore platforms typically take $X=H_S$, the "significant wave height" during a period when the wave elevation process $\eta(t)$ can be assumed to be stationary (i.e., in a statistical steady-state condition). This period of assumed stationarity can be anywhere between one and six hours. Following common convention, the significant wave height is defined to be 4 times the standard deviation (RMS) of the wave elevation process, e.g. $H_S=4\sigma_\eta$. It is also roughly equal to the mean of the highest one-third of all wave heights (peak-trough distances), provided the common Gaussian model of $\eta(t)$ is assumed to hold. For wind, a common scalar definition of X is to choose V , some measure of average

wind speed over a reference period of approximately ten minutes, and at a reference elevation.

Note that other environmental variables may be significant in various applications. Offshore problems may include significant effects due to wave period T_z , current U , wave direction θ , etc. Additional wind parameters of interest include the turbulence intensity (ratio of RMS to mean wind speed), direction, and other spectral parameters in one or more directions. In the basic **CYCLES** formulation documented here, these variables are fixed, either at representative or worst-case values given knowledge of the dominant variable X . (More general models involving several variables, e.g., mean wind speed, V , and turbulence intensity, I_t , have also been implemented. These are discussed further in Chapter 4.)

2.2.2 Gross Response

Characterizing Variable: S =amplitude of local stress process.

The stress response at the location of interest will typically not be regular (i.e., sinusoidal). Nonetheless, it is assumed that some method, such as rainflow counting, is available to identify amplitudes of stress "cycles." Statistics of an arbitrarily chosen amplitude S will generally depend on the underlying environmental variable X . Thus the conditional probability density $f_{S|X}(s|x)$, over all possible values of the environmental variable x , is required.

This conditional distribution of S may be fit directly from observed stress histories. One might first sort the histories into bins according to the value of the environmental variable x (wave height, wind speed, etc.). The resulting histories may be rainflow counted and a density $f_{S|X}(s|x)$ fit for each bin. An example of this approach will be considered in Chapter 4. An alternative analytical model, tied to the RMS stress $\sigma(x)$ as a function of x , is used here in the following analytical formulation (section 2.4).

2.2.3 Failure Measure

Characterizing Variable: \bar{D} =mean value of Miner's damage.

It is assumed that fatigue tests at constant stress amplitude S are available to estimate the "S-N" curve; that is, the number of cycles $N_f(s)$ to failure as a function of stress amplitude s . Miner's rule is then used, assigning damage $1/N_f(S_i)$ due to a single stress cycle of amplitude S_i . This damage is assumed to grow linearly at its mean rate \bar{D} , ignoring local variations in this rate due to variability in the cyclic amplitudes S_i . (This will tend to average out quickly for the high-cycle fatigue applications of interest here.) As a result, fatigue behavior is characterized by only the mean damage rate \bar{D} .

2.3 General Fatigue Formulation: Results

To summarize from the previous section, the general fatigue formulation requires three functional inputs: $f_X(x)$, $f_{S|X}(s|x)$, and $N_f(s)$ to characterize the load, response, and fatigue damage respectively. A convenient scalar quantity on which to focus is the mean damage \bar{D} . This is found by integrating/summing over all load and response levels, x and s :

$$\bar{D} = \int_{x=0}^{\infty} \int_{s=0}^{\infty} \frac{f_{S|X}(s|x)f_X(x)}{N_f(s)} ds dx \quad (2.1)$$

It is informative to also study the behavior of the inner integral, the "damage density" $D(x)$:

$$\bar{D} = \int_{x=0}^{\infty} D(x) dx; \quad D(x) = f_X(x) \int_{s=0}^{\infty} \frac{f_{S|X}(s|x)}{N_f(s)} ds \quad (2.2)$$

Physically, $D(x)dx$ is the contribution to mean damage \bar{D} due to values of the environmental variable, X , between x and $x + dx$. Thus, $D(x)$ shows the relative fatigue contribution of different x levels. As might be expected, it depends both on the long-term environmental variation, reflected by $f_X(x)$, and on the stress and fatigue properties for various x values.

Once obtained, \bar{D} can be used to directly estimate the fatigue life T_f . Considering the many cycles that contribute to high-cycle fatigue, the actual damage is assumed to vary negligibly from its average value \bar{D} per cycle, or equivalently $f_0\bar{D}$ per unit time

(f_0 =average response cycle rate). Assuming that failure occurs when this damage reaches a critical threshold Δ , and the structure is loaded some fraction of time, A , the failure time is then

$$T_f = \frac{\Delta}{A f_0 \overline{D}} \quad (2.3)$$

Note the generalization to cases where the measured cycle rate varies with the environmental variable X , i.e., $f_0 = f_0(x)$. In this case $f_0 \overline{D}$ in Eq. 2.3 is replaced by:

$$\overline{f_0 D} = \int_{x=0}^{\infty} \int_{s=0}^{\infty} f_0(x) \frac{f_{S|X}(s|x) f_X(x)}{N_f(s)} ds dx \quad (2.4)$$

If Miner's rule is correct one would assign $\Delta=1$. More generally, variability in Δ would reflect uncertainty in Miner's rule; i.e., the effect of predicting variable-amplitude fatigue behavior from constant-amplitude tests.

In general, Eqs. 2.1–2.3 can be evaluated numerically, permitting arbitrary functional choices of $f_X(x)$, $f_{S|X}(s|x)$, and $N_f(s)$. In the CYCLES formulation specific functional forms of each of these three quantities are chosen. These permit analytical expressions to be derived for Eqs. 2.1–2.3. As discussed earlier in Section 2 the assumed functional forms restrict the generality of the formulation however the resulting analytical form facilitates study of important parametric variations, e.g., of distribution parameters, S - N curve constants, etc. The following section describes the specific simplifying assumptions that permit this analytical formulation.

2.4 Analytical Fatigue Formulation

Described here are the basic assumptions which permit a closed-form, analytical expression for fatigue life. As noted earlier, these are based on a model suggested originally for fatigue of wind turbines (Veers, 1990). Some minor generalizations are included here as well. The resulting formulation is intended to be useful for a variety of applications beyond wind turbines, such as offshore structures, bridges, etc.

The assumptions are as follows:

- The long-term load variable, X , is assumed to have Weibull distribution. This

distribution involves two free parameters, which may be expressed in various ways. For example, in terms of its mean value \bar{X} and shape parameter α_x , the probability distribution of X satisfies

$$P[X > x] = \exp\left\{-\left[\frac{x}{\beta_x}\right]^{\alpha_x}\right\}; \quad f_X(x) = \frac{\alpha_x x^{\alpha_x-1}}{\beta_x^{\alpha_x}} \exp\left[-\left(\frac{x}{\beta_x}\right)^{\alpha_x}\right] \quad (2.5)$$

The parameter β_x in this result is related to the mean \bar{X} as follows:

$$\beta_x = \frac{\bar{X}}{(1/\alpha_x)!} \quad (2.6)$$

Resulting parameters: $\bar{X}, \alpha_x =$ mean, Weibull shape parameter of environmental parameter X (wave height, wind speed, etc.).

- The RMS of the (global) stress process is assumed to be of the form

$$\sigma_g(x) = \sigma_{ref} \left(\frac{x}{x_{ref}}\right)^p, \quad (2.7)$$

i.e., increasing in power-law fashion with the load variable x . The local stress at the fatigue-sensitive detail is further scaled by a stress concentration factor K . The resulting RMS $\sigma(x)$ is then finally

$$\sigma(x) = K \cdot \sigma_g(x). \quad (2.8)$$

Resulting parameters: $x_{ref}, \sigma_{ref}, p, K =$ reference level of load variable, reference level of RMS stress, power-law exponent, and stress concentration factor.

- Given load environment X , the stress amplitude S is also assumed to have Weibull distribution. From random vibration theory, the mean-square value

$$E[S^2] = 2\sigma(x)^2, \quad (2.9)$$

is assumed with $\sigma(x)$ from Eq. 2.8. The resulting density $f_{S|X}(s|x)$ is of the form given in Eq. 2.5, with shape parameter α_s , and scale parameter

$$\beta_s = \sigma(x)[2/(2/\alpha_s)!]^{1/2}. \quad (2.10)$$

Resulting parameter: α_s = Weibull shape parameter of stress S given X . Typical range: between $\alpha_s=1$ (exponential stress distribution) and $\alpha_s=2$ (Rayleigh stress distribution).

- The S - N curve is taken here as a straight line on log-log scale, with an effective intercept C_0 that includes the Goodman correction for mean stress effects:

$$N_f(s) = C \left(\frac{S}{1 - K|S_m|/S_u} \right)^{-b} = C_0 S^{-b}; \quad C_0 = C(1 - K|S_m|/S_u)^b \quad (2.11)$$

in which S_m and S_u are the mean and ultimate stress levels.

Resulting parameters: C, b = S - N curve parameters; S_m, S_u = mean, ultimate stress levels.

Substituting Eqs. 2.5–2.11 into Eqs. 2.1 and 2.3, the following expression for fatigue life T_f is found:

$$T_f = \frac{C\Delta}{Af_0} \left\{ \left(\frac{\sqrt{2}\sigma_{ref}K}{\sqrt{(2/\alpha_s)!(1 - K|S_m|/S_u)}} \right)^b \left(\frac{\bar{X}}{x_{ref}(1/\alpha_x)!} \right)^{bp} \left(\frac{b}{\alpha_s} \right)! \left(\frac{bp}{\alpha_x} \right)! \right\}^{-1} \quad (2.12)$$

Note that parameters directly scaling stress, such as σ_{ref} and the stress concentration factor K , are raised to the power b arising from the S - N curve. In contrast, parameters scaling the environmental variable X , such as its mean \bar{X} , are raised to the composite power bp , reflecting the combined nonlinear effect of Eqs. 2.7 and 2.11. If $p > 1$, this suggests that the uncertainty in these environmental parameters may have significant effect on fatigue life.

Finally, under the foregoing assumptions the damage density $D(x)$ from Eq. 2.2 may also be found:

$$D(x) \propto x^{bp+\alpha_x-1} \exp\left[-\left(\frac{x}{\beta_x}\right)^{\alpha_x}\right] \quad (2.13)$$

By finding the maximum of this function, the environmental level x_{max} that produces the largest damage is found to be

$$x_{max} = \beta_x \left(\frac{bp + \alpha_x - 1}{\alpha_x}\right)^{1/\alpha_x} = \frac{\bar{X}}{(1/\alpha_x)!} \left(\frac{bp + \alpha_x - 1}{\alpha_x}\right)^{1/\alpha_x} \quad (2.14)$$

For example, if X has exponential distribution $\alpha_x=1$, so that

$$x_{max} = bp\bar{X} \quad (2.15)$$

Thus, the most damaging X level depends not only its average value, \bar{X} , but also on the exponents b and p of the $S-N$ curve and RMS stress relation. Note that x_{max} may far exceed the mean \bar{X} ; e.g., $x_{max}=20\bar{X}$ if $b=10$ and $p=2$. This may be a rather extreme case, however. For example in a wind turbine application, common values of $\alpha_x=2$ (Rayleigh distribution) and $p=1$ (linear increase in stress with X) would result in x_{max} between 2 and 3 times \bar{X} for b values within a realistic range ($4 \leq b \leq 13$).

2.5 Solution Algorithm for Failure Probability

For the reliability analysis the failure criterion is taken to be the difference between the computed fatigue life (eqn. 2.12) and a specified target lifetime, T_t .

$$G(\mathbf{X}) = T_f - T_t \quad (2.16)$$

The vector \mathbf{X} contains the *resulting parameters* from the analytical fatigue formulation of Section 2.4; $\mathbf{X} = [\bar{X}, \alpha_x, x_{ref}, \sigma_{ref}, p, K, \alpha_S, C, b, S_m, S_u, \Delta, f_0, A]$. Equation 2.16, known as the failure state function, $G(\mathbf{X})$, is positive when the component is safe and negative when it has failed.

The solution for the failure probability is a four step procedure that has been described in Veers, (1990) and is reviewed here briefly for completeness. A more thorough description of reliability methods can be found in several references (Madsen et al, 1986, Ang and Tang, 1990, Thoft-Christensen and Baker, 1982, and, Melchers, 1987).

The first step of the solution procedure is the "formulation" of the limit state equation given above as Eq. 2.16. In the second step, the "transformation" requires that each random variable be associated with a uncorrelated, unit variance, normally distributed random variable. For independent variables this is achieved by equating the cumulative distribution functions of the input variable and its associated standard normal variate. Correlation can be included by working with conditional distributions (Madsen et al, 1986). Alternatively if only the marginal distributions and correlation coefficients among the x_i are known, transformation may proceed in two steps:

- With conventional methods, each x_i can be transformed marginally to a standard normal variable V_i . The resulting V_i variables will also be correlated, to a typically somewhat greater extent than the original physical (non-normal) variables x_i . Analytical methods have been developed to efficiently predict this correlation "distortion" due to non-normal physical variables (Winterstein et al, 1989).
- Correlation among the V_i 's may be removed by standard methods (e.g., Cholesky

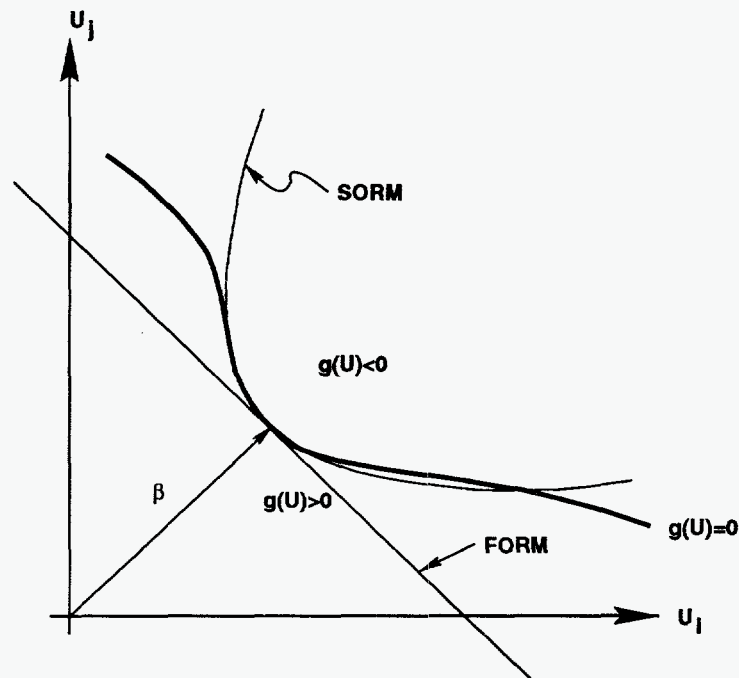


Figure 2.1: FORM and SORM approximations to $g(U) \leq 0$

decomposition of the covariance matrix) to obtain standard normal variables U_i .

This is the approach used in CYCLES. All random variables are transformed in this fashion and the calculations proceed in standard normal space, also called “normal” or U -space.

The failure state function (eqn. 2.16) is evaluated in normal U -space and gradient search methods are employed to find the point where it is closest to the origin, also known as the design point, U_i^* . (The design point in the original coordinates, X_i^* is determined through the inverse of the transformation step.) In the third step of the reliability calculation an “approximation” of the failure probability is obtained by fitting a tangent line (first order reliability method, FORM) or a parabola (second order reliability method, SORM) to the failure state function at the design point (see Figure 2.1). The direction cosines, α_i , of the vector β , that defines the design point are measures of the relative importance of each of the random variables.

The symmetry of standard normal space simplifies the "computation" of the failure probabilities and the importance factors as the final step of the solution algorithm. FORM probabilities are computed directly from the length of the vector identifying the design point. SORM estimates of failure probability are based upon the vector length and the curvatures of the surface at the design point.

2.6 Program CYCLES Capabilities

The current features of the CYCLES program are:

- Calculation of mean excess life
- First order (FORM) and second order (SORM) failure probabilities
- Importance factors for each random variable
- Sensitivity analysis for each parameter used to define the probability distributions of the random variables
- Option to run simulation
- Calculation of failure probabilities as a function of time
- Library of random variable distribution functions

The primary result of the CYCLES program is an estimate of the "failure" probability, p_f , i.e. the reliability is the probability that the fatigue life will be less than the target lifetime of the component. It is determined as described in section 2.5. The importance factors, which reflect the relative contribution of each variable to fatigue life uncertainty, are also reported.

The program estimates p_f over a range of target lifetimes (provided by the user) and sensitivities of the parameters for each random variable. The sensitivities are evaluated by varying each input parameter and dividing the change in reliability by the change in the respective parameter; dB/dp where dB and dp are change in reliability and change in parameter respectively. Note that this is effectively a partial

derivative; i.e., **CYCLES** reports sensitivities to each parameter individually while fixing the others at their input values.

Flowcharts depicting program execution and initial processing of random variables are shown in Figures 2.2 and 2.3 respectively.

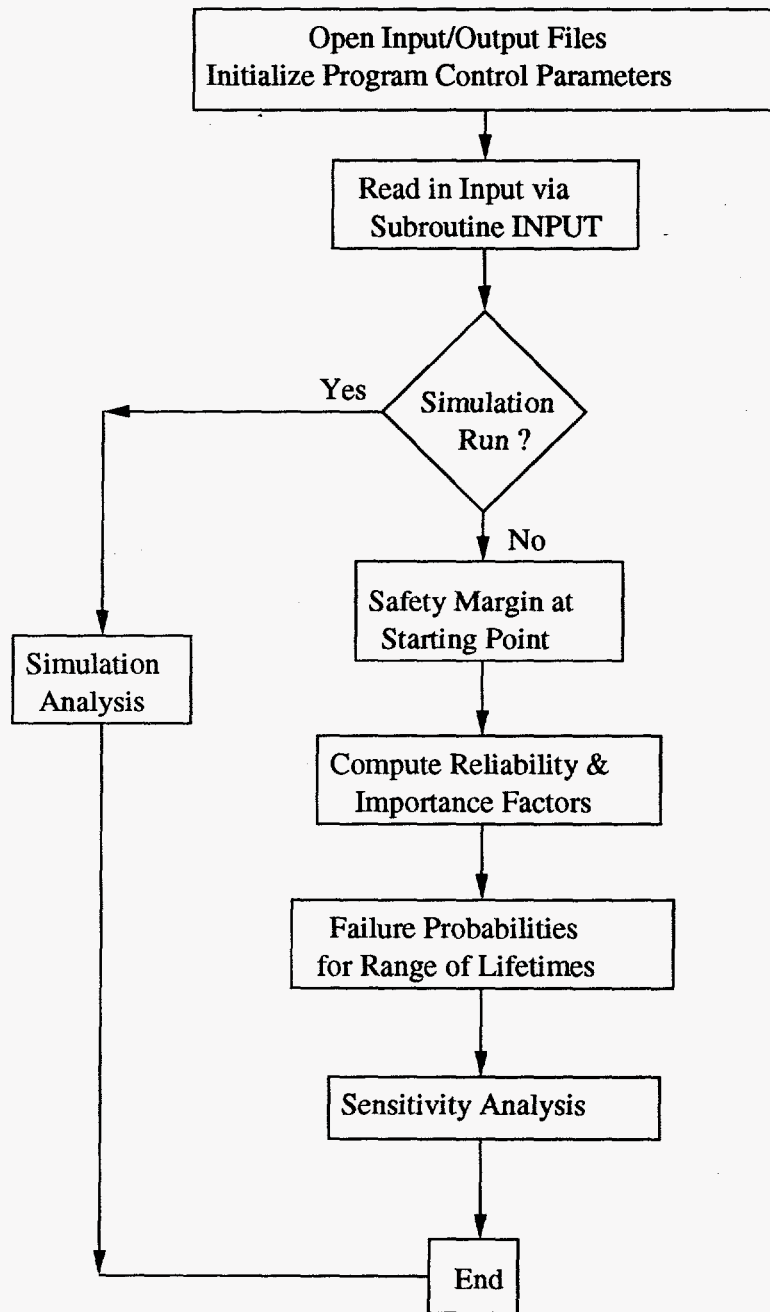


Figure 2.2: Flow chart, general CYCLES code execution.

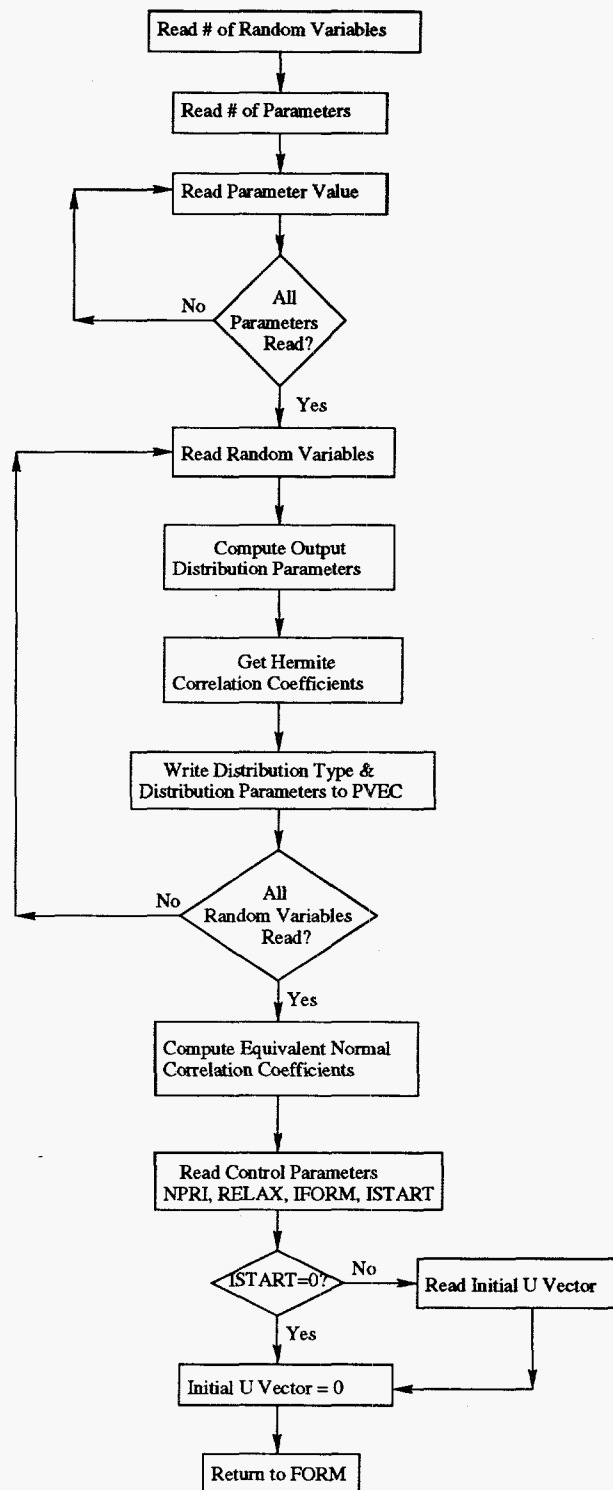


Figure 2.3: Flow chart, initial processing of CYCLES random variables.

2.7 Example Application: The Sandia 34-m Test Bed VAWT

The capabilities of the *CYCLES* reliability program is demonstrated by way of example. This example is intended to demonstrate a typical analysis one might encounter in the final design of a machine where there has already been extensive testing and data analysis, so that the uncertainty in many of the inputs is small. In particular, a research oriented 34-meter diameter Darrieus, vertical axis wind turbine (VAWT) erected by Sandia National Laboratories near Bushland Texas, has provided an abundance of test data useful to this reliability analysis.

This turbine has operated since 1988 with extensive instrumentation to collect wind-speed and operational-stress data. The aluminum material of which the blades are extruded has also been well characterized by constant amplitude fatigue tests. A reliability analysis for fatigue of blade joints on this turbine therefore has many inputs that are relatively well known. However, there has been no component testing to establish fatigue properties of the joints or stress concentration factors so that some inputs do have high uncertainty.

Much of the data used here has been taken from a deterministic fatigue analysis performed by Ashwill et al, (1990) on the same VAWT blade joint. This example reproduces the original probabilistic fatigue analysis performed by Veers, (1990), for the same turbine.

2.7.1 Definition of Input

The underlying assumptions and numerical values used to model:

1. the load environment,
2. the stress response, and
3. the resulting fatigue damage accumulation,

are described for this example to further illustrate the three aspects of the fatigue formulation described in section 2.2.

- **Load Environment.**

Following the approach used by Ashwill et al, (1990), V , the “10 minute mean wind speed” is used as the dominant environmental variable; X . Extensive measurements of V have been made at the Bushland site, as well as the Amarillo Airport about 30 miles away across flat terrain. The distributions measured at these two sites are plotted in Figure 2.4 along with a Rayleigh distribution. The mean of the “10 minute mean wind speeds,” \bar{V} , for Bushland and Amarillo are 6.2 and 6.6 m/s respectively. Note that the high wind tails of the distributions are different. Since the data sets are of different lengths, the following statistics are employed to model the local wind speed distribution;

$$E[V] = \bar{X} = 6.3 \text{ m/s} \quad (2.17)$$

with

$$\alpha_V = \alpha_X = 2.0. \quad (2.18)$$

The values in Eqs. 2.17 and 2.18 are based on limited data, and hence may differ from the true values we would find from infinite data. Therefore, these values are used as the *mean* values of \bar{X} and α_x , while assigning COV values of .05 and .10 to \bar{X} and α_X respectively. The result is a wind speed distribution with uncertain parameters that is a perturbation about a Rayleigh distribution (implied by the mean α_X of 2.0) with mean 6.3 m/s. Both parameters are assumed to be normally distributed.

- **Gross Stress Response.**

The wind turbine and its components have been equipped with a large array of sensors that permit characterization of the turbine under field conditions. Structural response measurements such as stationary and rotating natural frequencies, mean stresses, and operational stresses have been compared to analytical predictions with good agreement (Ashwill et al, 1990). The highest stressed region in the blade was found to be in the flatwise direction at the upper blade-to-tower joint, where the 48 inch chord blade section attaches to

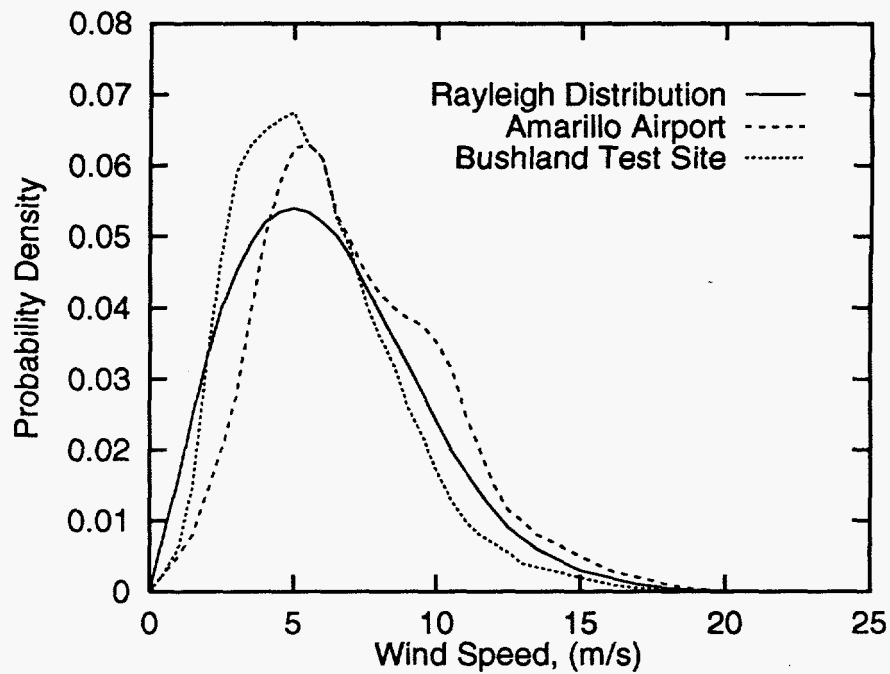


Figure 2.4: Wind speed distributions from Amarillo, Bushland, and the theoretical Rayleigh distribution with $\bar{V} = 6.3$ m/s

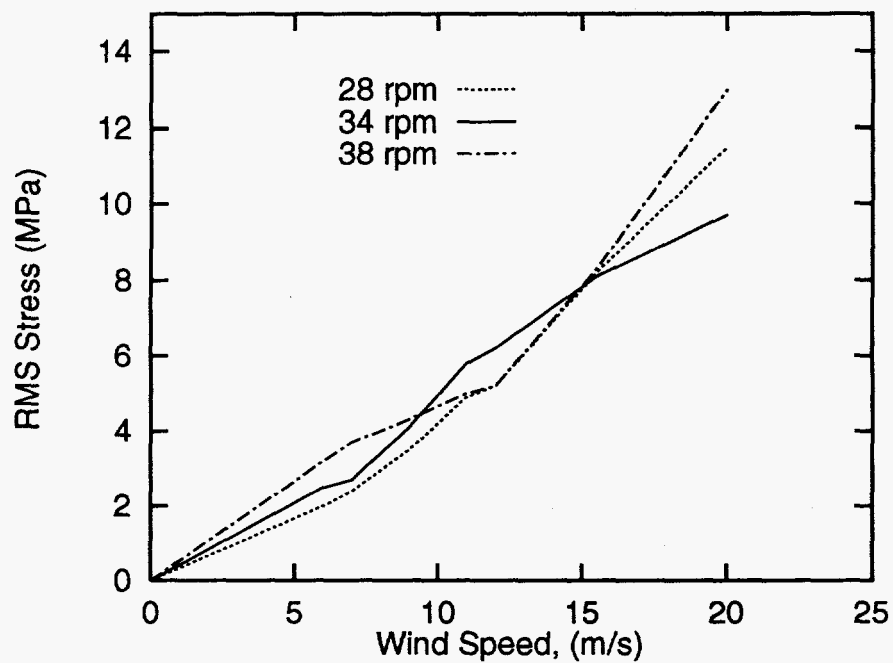


Figure 2.5: Measured RMS Stresses at the Blade Upper Root

the tower.

The stress states for the upper root were predicted using FFEVD (Lobitz and Sullivan, 1984), a Sandia written frequency response finite element code that assumes steady winds. Strain gages were employed to measure stress states at the upper root location. Figure 2.5 shows the measured RMS stresses for fixed speeds of operation at 28, 34, and 38 rpm. The trend is seen to be nearly linear for all three modes of operation.

For the power-law relationship used by CYCLES (Eq. 2.7), the following parameters are used to characterize the response: $x_{ref} = 10$ m/s, $\sigma_{ref} = 4.5$ MPa, and $p = 1$. Only the reference RMS level σ_{ref} is treated as a random variable while the exponent, p , and the characteristic wind speed, x_{ref} , are defined as constants. Because there is a great deal of data available a relatively small variation, $COV = 0.05$, was chosen for σ_{ref} which is assumed normally distributed. In Chapter 4 procedures useful for determining uncertainty measures from data will be shown. The COV used here for σ_{ref} is an assumed value believed to be representative of the existing uncertainty.

The remaining variables associated with the gross stress response of the machine are the stress concentration factor, K , and the shape factor, α_S , of the Weibull stress amplitude distribution. The stress concentration factor has not been predicted or measured with accuracy. As an approximation for the heavily bolted joint a mean K of 3.5 with 10% COV is used. Histograms of rainflow counted stress time histories show very good agreement with a Rayleigh distribution (Veers, 1982). In Chapter 3 we will see that typical data from horizontal axis wind turbines (HAWT) is more exponential in nature. Again, because there is an abundance of stress data and the observed fits are very good, the Weibull shape parameter is set to the constant value of 2.0 making the stress distribution Rayleigh.

- **S-N Curve**

The blades and joints are made of 6063-T6 aluminum extrusions for which extensive fatigue test data are available. The test data are shown in Figure 2.6,

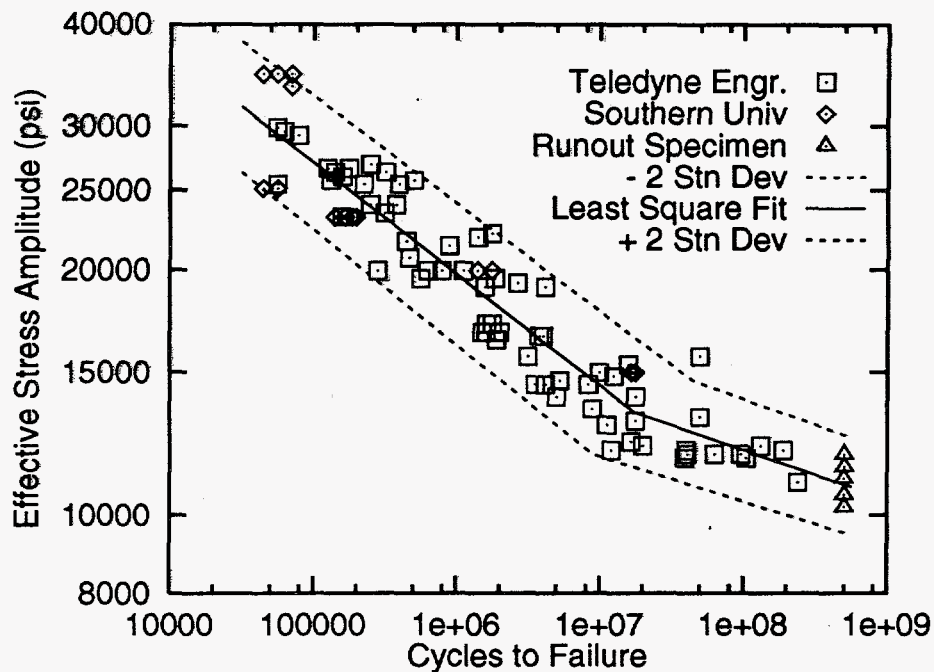


Figure 2.6: Effective stress amplitude versus cycles to failure for 6063 aluminum alloy

normalized to an effective stress amplitude as used by CYCLES (see Eq. 2.11). This data displays a commonly observed “fatigue limit” below which the fatigue lives are considerably extended. This effect is not included since cumulative damage assessments with occasionally applied larger stresses (as is the case here for wind turbines) may effectively eliminate the fatigue limit (Dowling, 1988). The higher stress peaks alter the way most materials respond and result in greater rates of fatigue damage than would be concluded based solely on constant amplitude results. The least squares fit to the data gives an $S-N$ exponent, $b = 7.3$, with intercept $C = 5.0E+21$ (based on stress units of MPa). The distribution of the data about the least squares line fits a Weibull distribution with $COV = 0.613$.

The mean stress and ultimate strength are needed to define the effective stress amplitudes using Goodman’s rule. The mean stress has been measured near the joint but may vary substantially along the blade span, resulting in high

Variable	Symbol	Definition	Distribution	Mean	COV
1	X	Mean Wind Speed	Normal	6.3 m/s	0.05
2	α_X	Wind Shape Factor	Normal	2.0	0.1
3	S_{ref}	Ref Stress	Normal	4.5 MPa	0.05
4	p	RMS exponent	Normal	1.0	-
5	K	Stress Conc	Normal	3.5	0.1
6	α_S	Stress Shape Fact	Normal	2.0	-
7	C	S-n Coeff	Weibull	5.0E+21	0.61
8	b	S-n Exponent	Normal	7.3	-
9	S_m	Mean Stress	Normal	7.0 MPa	0.2
10	S_u	Ultimate Strs	Normal	285 MPa	-
11	f_o	Cycle Rate	Normal	2.0 Hz	0.2
12	Δ	Miners Damage	Normal	1.0	-
13	A	Availability	Normal	1.0	-
14	T_t	Target Life	Normal	20.	-

Table 2.1: Sandia 34-m Test Bed VAWT, CYCLES Base Case Input Summary

uncertainty for the actual local mean. The mean stress is defined to be normally distributed with mean 7.0 MPa and 20% COV. The ultimate stress for the extruded aluminum material has been measured and is set to the constant value 285 MPa.

The three remaining parameters used to calculate the average fatigue damage rate are the average response cycle rate, f_0 , the actual value of Miner's damage at failure, Δ , and fraction of time the turbine is available, A . The cycle rate frequency has been measured and found to be relatively independent of wind speed but does vary from sample to sample. f_0 is assumed normally distributed with mean 2.0 (Hz) and 20% COV. For simplicity, both Δ and A are set to unity with no variation. Table 2.1 summarizes all the parameters used in this wind turbine fatigue reliability example.

2.7.2 Results: Base Case

The output from the CYCLES analysis for this example is given in Table 2.2 under the column heading identified as "Weibull". The results show a probability of failure of approximately 3% for a target lifetime of 20 years with a median excess lifetime of 294 years. The reliability analysis identifies the likelihood or probability that the turbine will achieve some desired lifetime. Of equal importance is the relative importance of each random variable on the fatigue life of the turbine. Results show that the leading coefficient in the S-N relationship is the most important source of variability supplying about half of the total variability in this example. The stress concentration factor, K , and wind speed shape factor, α_V , are next, having approximately 21% and 14% contribution respectively. The relative importance of each random variable provides valuable insight to the designer who is attempting to reduce the effects of fatigue damage.

2.7.3 Lognormal versus Weibull Distribution for $S-N$ Parameter: C

Finally, in order to investigate the effect of distribution type on the results of the reliability analysis, the example problem run here was repeated with the distribution type for the S-N coefficient changed to lognormal. Table 2.2 summarizes how the results vary between the two cases.

As might be expected the failure probability decreased to 1.5%. This result is due to the shift in probabilities of the resistance variable C towards larger values (e.g. the lognormal distribution has both a narrower lower tail and a fatter upper tail than the corresponding Weibull distribution). This model here predicts greater reliability, as it is applied to a resistance variable (fatigue life at given S) for which large values are favorable (non-failures). Note also the shifting of importance from the $S-N$ intercept to the stress concentration factor, K , and wind speed shape factor, α_V , as the analysis shifts from a blade with marginal resistance (e.g., a Weibull distribution for C) to one having potentially much higher resistance (e.g., the lognormal distribution for C).

The influence of distribution type on reliability is clearly case dependent as the

		Weibull	Lognormal
Excess life over 20 years:		294 yrs	277 yrs
FORM p_f (in %)		2.56	1.50
SORM p_f (in %)		3.01	1.55
Symbol	Definition	Importance Factors: (in%)	
X	Mean Wind Speed	4.9	7.9
α_X	Wind Shape Factor	14.4	27.6
S_{ref}	Ref Stress	4.9	7.9
p	RMS exponent	-	-
K	Stress Conc	21.2	32.6
α_S	Stress Shape Fact	-	-
C	S-n Coeff	52.2	20.3
b	S-n Exponent	-	-
S_m	Mean Stress	0.9	1.6
S_u	Ultimate Strs	-	-
f_o	Cycle Rate	1.4	2.2
Δ	Miners Damage	-	-
A	Availability	-	-
T_t	Target Life	-	-

Table 2.2: Sandia 34-m Test Bed VAWT, CYCLES Reliability Results

following example demonstrates. In this second example, it is assumed that sufficient testing was performed to reduce the uncertainty in the previous example for the stress concentration factor, K , and wind speed shape factor, α_V . Both COV's are now taken to be 5%. A new reliability analysis shows that the $S-N$ intercept, C , with a Weibull distribution, dominates the relative importance of all random variables, e.g. 79% importance. Results for this hypothetical case and one with a lognormal distribution for C are shown in Table 2.3.

Note that when the overall uncertainty in the problem has been reduced, the failure probability has also been reduced. Furthermore, with a lower p_f the shifting of importance away from the resistance variable to those constituting the load is much more dramatic. This is expected, due to the large role played by the random variable C in the reliability calculations.

The caution here is two-fold. First, the choice of distribution model for a critical

		Weibull	Lognormal
Excess life over 20 years:		294 yrs	277 yrs
FORM p_f (in %)		1.29	0.17
SORM p_f (in %)		1.37	0.16
Symbol	Definition	Importance Factors: (in%)	
X	Mean Wind Speed	5.0	14.2
α_X	Wind Shape Factor	2.8	9.4
S_{ref}	Ref Stress	5.0	14.2
p	RMS exponent	-	-
K	Stress Conc	6.0	17.3
α_S	Stress Shape Fact	-	-
C	S-n Coeff	79.0	38.4
b	S-n Exponent	-	-
S_m	Mean Stress	0.8	2.6
S_u	Ultimate Strs	-	-
f_o	Cycle Rate	1.4	3.8
Δ	Miners Damage	-	-
A	Availability	-	-
T_t	Target Life	-	-

Table 2.3: Effect of S-N Intercept Distribution Type with Reduced Uncertainty

random variable, when fit to the same mean and variance, can change failure probability estimates by one or more orders of magnitude. Second, although the lognormal model has been widely used in these fatigue strength and $S-N$ formulations, it may be considerably unconservative. At the least, if one knows nothing more than second-moment information (mean and variance), it is perhaps prudent to at least fit both a lognormal and Weibull models, and estimate the reliability under each assumption. Practical experience suggests that these two models provide useful bounds on the plausible range of reliability index, in view of distribution model uncertainty.

Chapter 3

Load Models for Fatigue Reliability

The fatigue reliability of wind turbines depends on the relative frequency, or probability distribution, of various cyclic load levels to be encountered during the turbine's operating life. These are typically required across a range of representative wind conditions.

For time scales of the order of minutes, these loads may be measured by relatively short-term experimental studies, or predicted by analytical methods. Practical questions then arise as to how these limited data should best be used (e.g., Jackson, 1992; Sutherland, 1993; Sutherland and Butterfield, 1994; Thresher et al, 1991). First, in seeking to estimate a representative fatigue life, is it sufficient to use the observed histogram of cyclic loads, or should a smooth theoretical probability distribution be fit to the limited data? If a smooth distribution is to be fit, what functional form is sufficiently flexible and how should it be fit? Finally, beyond forming a single best estimate of fatigue life, what is the uncertainty in this estimate due to limited data?

This chapter seeks to address these concerns. Subsequent sections address the following points in turn:

- 1. Fatigue Data and Damage Densities.** We first show several useful approaches to study fatigue load data and modeling needs. Damage density plots are constructed, to suggest which stress ranges are most important to model. In addition, Weibull scale plots are used to show systematic deviations from a range of standard Weibull models. While not completely new, these approaches have yet to

gain widespread use among wind turbine load modelers.

2. Model Uncertainty Effects. We fit a number of conventional load models to a particular data set, and determine the resulting scatter in fatigue damage they predict. Considerable scatter is found among common one-parameter load models, such as the Rayleigh and exponential models, when they are fit to the mean stress range or RMS level. This motivates the need for more general load models, with two or more parameters fit to the data.

3. New Statistical Loads Models. We introduce here a new generalized load model, which preserves the first four statistical moments of the data. By retaining these higher, more tail-sensitive moments, it is more faithful to the observed frequency of relatively large load levels. At the same time, it is a rather mild perturbation of a conventional 2-parameter load model, e.g., Weibull, Gumbel, or Gaussian. Of primary interest here is the generalized Weibull model which has found favor in various fatigue applications. Other applications include a generalized Gumbel model for extreme values, and a generalized Gaussian model useful for analyzing nonlinear vibration problems.

4. Uncertainty due to Limited Data. Finally, we discuss the implications of limited data. Techniques are shown to estimate the associated uncertainty in fatigue damage estimates. Acceptable levels of this uncertainty are also discussed, together with the data needs these imply. The result is strongly dependent on material properties; e.g., the slope of the $S-N$ curve that governs fatigue behavior.

Our application here concerns both flapwise and edgewise loads on a horizontal axis wind turbine (HAWT). A companion study (Sutherland and Veers, 1995) applies similar models to estimate loads on the Sandia 34-m vertical axis wind turbine (VAWT).

3.1 Fatigue Data and Damage Densities

In 1989 an extensive data set was obtained for a 100-kW wind turbine operated at Altamont Pass, California by Northern Power Systems. This turbine is a two-bladed, upwind HAWT with a teetering hub design utilizing full-span hydraulic passive pitch

control. The fiberglass rotor blades span 17.8 meters (rotor diameter). The root bending moment in both the flapwise (out-of-plane) and edgewise (in-plane) directions were measured in various wind conditions (Coleman and McNiff, 1989).

We consider first the flapwise moment. Figure 3.1 shows the histogram of rainflow counted ranges, taken from a 71-minute history during an average inflow wind speed of 10 m/s. Various studies have suggested a straight-line fit on this semi-log scale, implying an exponential probability model. We may question, however, whether a log-linear extrapolation adequately captures the frequency of rare, large stresses. Note, in particular, the single extreme stress range of around 32 [kN-m], which pairs the largest peak and smallest trough in the history. One may ask how much impact such extreme, rare loads have.

We address this issue here through the concept of the *damage density*. Fatigue tests are typically used to estimate $N(S)$, the number of cycles to failure under constant stress amplitude S . We adopt here a common power-law form of $N(S)$:

$$N(S) = \frac{1}{cS^b} \quad (3.1)$$

Here c and b are material properties where $c = 1/C$, C used in the earlier definition of the S - N Law, Eq. 2.11, from Chapter 2.

As shown in Figure 3.1, actual load histories produce a number of load cycles, $n(S_i)$, at various stress levels S_i . For each stress level, Miner's rule assigns fatigue damage

$$D(S_i) = \frac{n(S_i)}{N(S_i)} = cS_i^b n(S_i) \quad (3.2)$$

The latter form uses the S - N relation from Eq. 3.1. The total damage is then estimated as $D_{tot} = \sum_i D(S_i)$, the sum across all stress levels S_i .

In fitting loads models, it is useful to focus on the *relative* fraction of damage incurred at different levels. This is the damage density, herein denoted $d(S_i)$:

$$d(S_i) = \frac{D(S_i)}{\sum_i D(S_i)} = \frac{S_i^b n(S_i)}{\sum_i S_i^b n(S_i)} \quad (3.3)$$

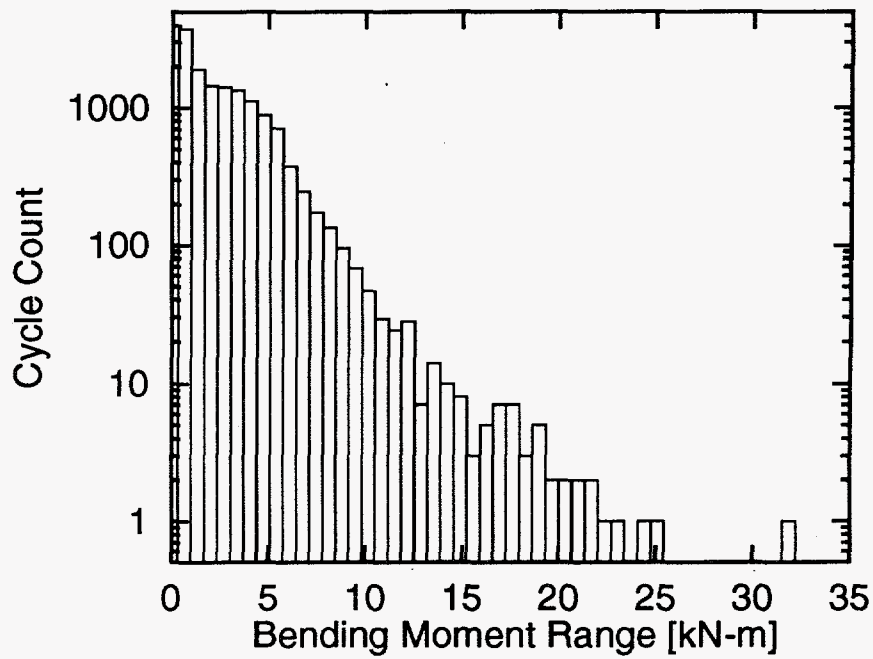


Figure 3.1: Histogram; Flapwise Data.

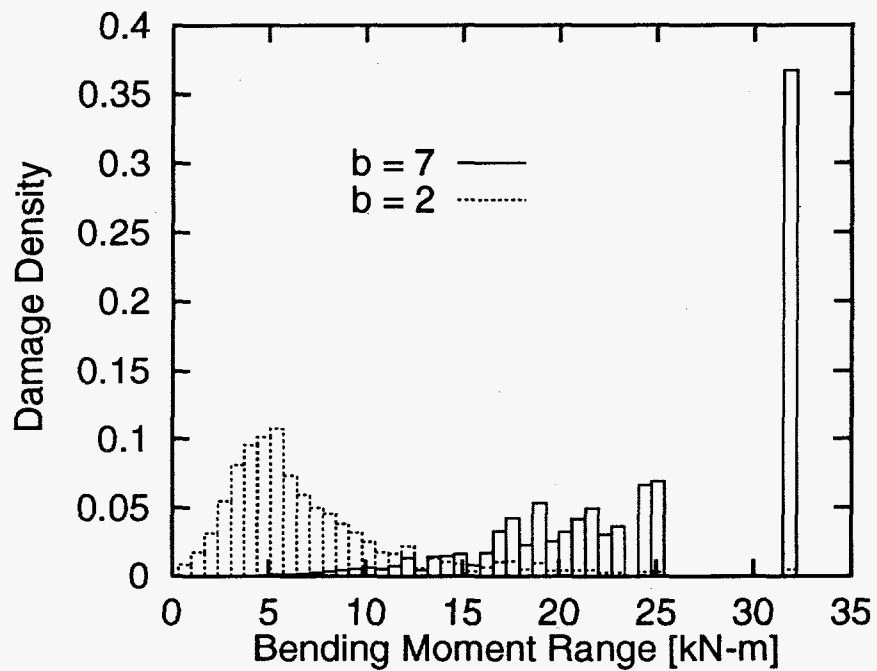


Figure 3.2: Damage Density; Flapwise Data.

Thus, the relative damage is independent of the intercept c of the S - N curve, but depends importantly on its slope b .

Figure 3.2 shows the damage densities of the flapwise loading for fatigue exponents $b=2$ and $b=7$. Fatigue exponents below 5 are typical of welded steel details, while exponents of 6 or above have been found from coupon tests of aluminums used in wind turbine blades (VanDenAvyle and Sutherland, 1987). Some fatigue studies of typical fiberglass blade materials have suggested even higher exponents; e.g., b values of 10 or above (Mandell et al, 1993).

Figure 3.2 shows that the most damaging stress level changes dramatically with the fatigue exponent, b . For welded steels, loads that lie within the body of the data (3–6 [kN-m]) are most damaging. In contrast, for aluminums with $b=7$, the single largest cycle contributes over 37% of the damage. For composites this single cycle may give still larger contribution. This leads to increasing uncertainty on fatigue life estimates given limited data. This effect is quantified in subsequent sections. In general, however, any loads model—whether observed or fitted—should be used with care if the largest observed load drives fatigue damage.

3.2 One and Two Parameter Load Models

As noted above, a common probability model suggested for HAWT blade loads is the exponential probability model. This model has a single parameter, essentially reflecting the slope of the expected histogram on semi-log scale (Figure 3.1). An alternative one-parameter model, based on random vibration theory of linear systems, is the Rayleigh distribution. Here we investigate the adequacy of these through the more general, two-parameter Weibull distribution.

For a general Weibull load model with parameters α and β , the cumulative distribution function $F(s)$ is given by

$$F(s) = P[\text{Load} < s] = 1 - e^{-(s/\beta)^\alpha} \quad (3.4)$$

This model includes the exponential and Rayleigh as special cases, corresponding

to $\alpha=1$ and $\alpha=2$ respectively. Note that $F(s)$ is the cumulative probability of all loads less than specified s . It is also useful to ask the inverse question: what fractile s_p has specified cumulative probability $F(s)=p$. Setting the left-side of Eq. 3.4 to p , solving for s yields

$$s_p = \beta[-\ln(1-p)]^{1/\alpha} \quad (3.5)$$

To determine the adequacy of a model such as Eq. 3.4, it is convenient to display the data on an appropriate "probability scale" plot. In general, probability scale is constructed for any distribution by transforming one or both axes to obtain a linear graph between cumulative probabilities and the corresponding values of the physical variable. For the specific case of Eq. 3.5, a linear result arises from taking logarithms:

$$\ln(s_p) = \ln(\beta) + \frac{1}{\alpha} \ln[-\ln(1-p)] \quad (3.6)$$

Thus, the observed load values are first sorted into ascending order ($s_1 \leq s_2 \leq \dots s_N$). We then plot $\ln(s_i)$ versus $\ln[-\ln(1-p_i)]$ on linear scale, with $p_i=i/(N+1)$. Equivalently, we may plot s_i versus $-\ln(1-p_i)$ on log-log scale; this is the alternative chosen here. The result is a linear plot in any Weibull case, including both the Rayleigh and exponential as important special cases. It also includes a still wider range of models, with the slope of the line directly showing whether the model should be Rayleigh, exponential, or something between (or outside).

Figure 3.3 shows the flapwise data from Figure 3.1 on this "Weibull scale." This plot also shows corresponding exponential and Rayleigh distributions, which preserve the mean of the data. Observe that with this graphical "goodness-of-fit" method it is fairly easy to discriminate between the two distributions, and confirm that the exponential model follows the data far better than the Rayleigh model.

Figure 3.4 repeats the flapwise data on Weibull scale, now plotted with the "best" Weibull distribution. The two parameters of this Weibull model have been chosen to match both the mean and standard deviation of the data. While providing an apparently better fit, we will consider below whether the difference between exponential model (Figure 3.3) and Weibull model (Figure 3.4) is statistically significant. In the

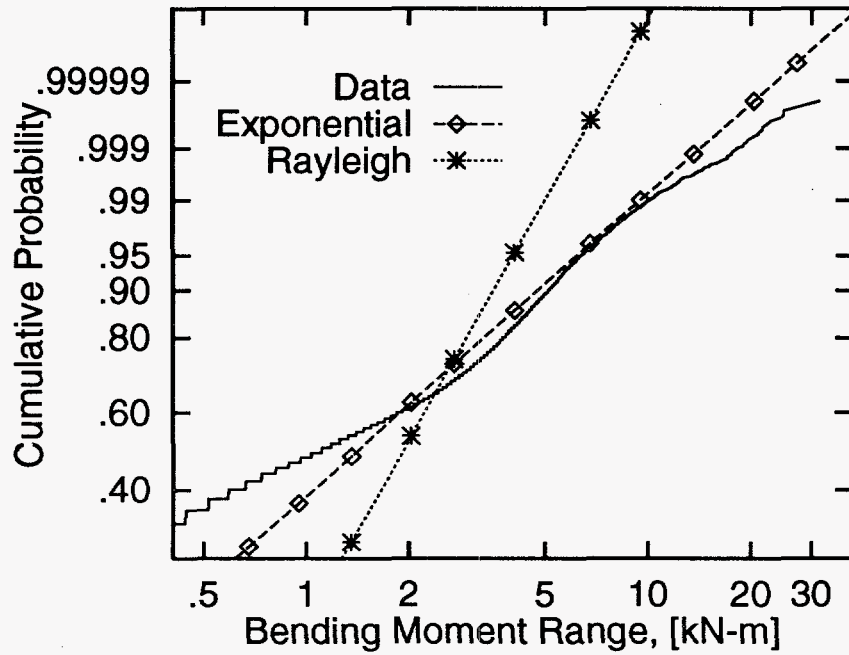


Figure 3.3: Exponential and Rayleigh Models; Flapwise Data.

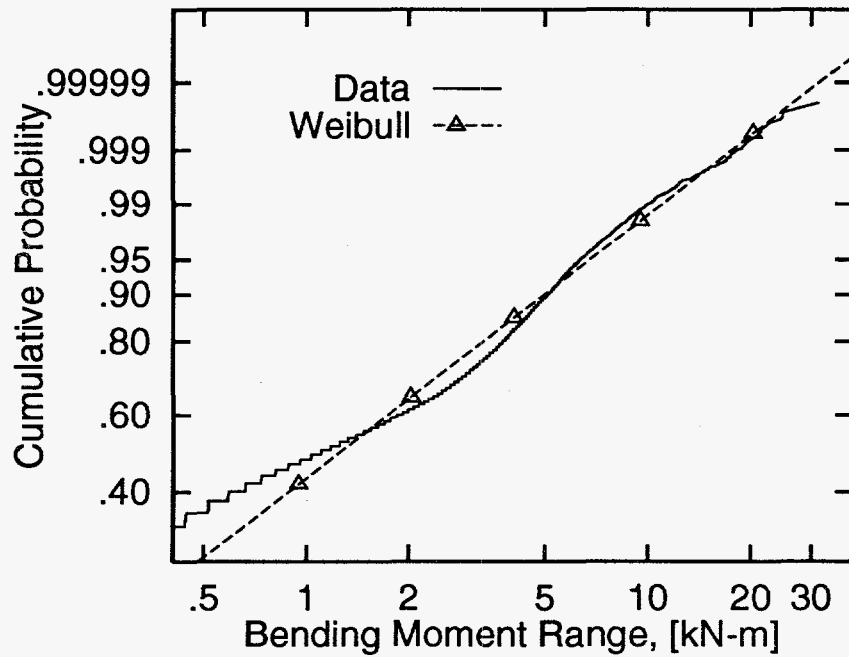


Figure 3.4: Weibull Model of Flapwise Data.

next section, we will also consider still more general models. In general, these figures show the advantage of using probability scale instead of the traditional histogram to discriminate between different models.

3.3 Generalized Four-Parameter Load Models

By using data to fit two parameters—both α as well as β in Eq. 3.4—it is not surprising that the Weibull fit seems visually superior to the 1-parameter exponential and Rayleigh models. In the same way, one may seek to introduce still more parameters, ultimately leading to seemingly perfect agreement as the number of parameters approaches the number of data. The tradeoff, of course, is that as one seeks to estimate more parameters from a fixed amount of data, our uncertainty in estimating each parameter grows. The practical effect of this should be measured by the resulting uncertainty (e.g., coefficient of variation or confidence interval) on our mean damage rate estimate. In general, adding more parameters to a probabilistic model is no longer beneficial if the resulting damage estimate does not vary significantly, in view of its uncertainty, from that given by a simpler model.

Comparing Figures 3.3 and 3.4, we may ask whether the difference between exponential and Weibull models is statistically significant. We will show below (e.g., Figure 3.13) that at least for high exponents b damage differences between Weibull and exponential models are statistically significant. This supports the effort of seeking a two-parameter Weibull model. To test in turn whether the Weibull model is sufficient, we require a still more detailed model with which to compare it. This is provided by the four-moment, “generalized Weibull” model defined below.

These generalized 4-parameter load models are perturbations of 2-parameter “parent” models that are based on fitting not only to the mean μ and standard deviation σ , but also the skewness α_3 and kurtosis α_4 of the data. (For a general random variable X , α_n is defined as the average value of $((X - \mu)/\sigma)^n$.) This section contains applications for not only a generalized Weibull model but also a generalized Gumbel and generalized Gaussian model as well. Each model is shown useful for a specific application. The emphasis however is on fatigue applications using the generalized Weibull model.

3.3.1 Model versus Statistical Uncertainty

Generalized four-parameter distributions have been developed to modify standard, commonly used two-parameter distributions to better match observed tail behavior. In particular, cubic distortions of these standard "parent" distributions are sought to match the first four moments of the data. We may then ask why precisely *four* moments are used to fit the probability distribution of X —and not two, three, five, ten, etc. Conventional models are of lower order, requiring only one or two moments. The problem is that a number of plausible models, with very different tail behavior and hence fatigue reliability, can be fit to the same first two moments. This scatter in reliability estimates is said to be produced by *model uncertainty*. This is prevalent in low-order, one- or two-moment models.

To avoid this model uncertainty, which is difficult to quantify, one is led to try to preserve higher moments as well. This will help to discriminate between various models, and hence reduce model uncertainty. The benefit does not come without cost, however: higher moments are more sensitive to rare extreme outcomes, and hence are more difficult to estimate from a limited data set. This is known as *statistical uncertainty*, which reflects the limitations of our data set.

Thus, our search for an "optimal" model reflects an attempt at balance between model and statistical uncertainties. Practical experience (e.g., Winterstein, 1988) suggests that four moments are often sufficient to define upper distribution tails over the range of interest. This experience motivates the generalized models developed here. It is again supported by the results of Section 3.3.4, in which extreme wave heights are insensitive to the choice of parent distribution, once four moments have been specified.

This issue of statistical uncertainty with moment estimates is discussed further in Appendix A. Methodology useful for estimating the first four statistical moments of a data set, especially when the number of data points is limited, is outlined. Of particular interest are cases with data limitations that introduce considerable bias into estimated values of normalized moments. The generalized Gumbel example (Section 3.3.4) is one such case and the effects of bias as well as corrective measures to compensate for it are presented.

3.3.2 Underlying Methodology

Development of a four-parameter distribution model begins with a theoretical, two-parameter “parent” distribution. Implementation has been achieved for Weibull, Gumbel, and Gaussian parent distributions. Denoting the parent variable as U , the physical random variable X is related to U through a cubic transformation:

$$X = c_0 + c_1U + c_2U^2 + c_3U^3 \quad (3.7)$$

An automated optimization routine then adjusts the coefficients c_n to minimize the difference between the measured skewness and kurtosis and those of the generalized variable X . Such a routine, **FITTING** (Winterstein et al, 1994) has been recently developed at Stanford University. Note also that for Eq. 3.7 to remain monotone we require $c_3 \geq 0$. The positive cubic term implies that X eventually has broader tails than U . When X has narrower tails than the parent distribution, the program automatically fits the alternate relation:

$$U = c'_0 + c'_1X + c'_2X^2 + c'_3X^3 \quad (3.8)$$

Here the positive cubic coefficient c'_3 plays the opposite role, expanding the distribution of the *physical* variable X to recover the parent model.

This switching between two dual models, based on the size of α_4 , occurs automatically within the **FITTING** program. Adding such a dual model has been found to greatly increase modeling flexibility for small kurtosis cases. These have been found to arise both in extreme and fatigue loading applications.

Finally, in whichever form the model is defined, the coefficients c_n are chosen to minimize the error ϵ , defined as

$$\epsilon = \sqrt{(\alpha_3 - \alpha_{3X})^2 + (\alpha_4 - \alpha_{4X})^2} \quad (3.9)$$

The speed of executing **FITTING** is governed largely by the speed of this optimization; i.e., by the amount of effort (trial c_n values) needed to achieve an acceptably small tolerance, ϵ_{tol} .

The **FITTING** report (Winterstein et al, 1994) supplies additional details and sub-routine documentation. The basic goal of these generalized load models is to reflect probabilistic engineering judgment—through the choice of basic two-parameter model (Weibull, Gumbel, etc.)—and then introduce a cubic distortion to better reflect rare extreme values through their higher statistical moments.

Numerical vs Analytical Four-Moment Models.

Another distinction among four-moment models concerns whether their coefficients (e.g., c_n in Eq. 3.7 or c'_n in Eq. 3.8) are found analytically or from some numerical algorithm. Implementation of Eqs. 3.7–3.8 as described above for the **FITTING** program is numerical where the coefficients c_n or c'_n are found by minimizing ϵ^2 , the sum of squared errors in skewness and kurtosis. This is done with constrained optimization, requiring Eq. 3.7 or 3.8 to remain monotone and often achieves perfect moment fits; i.e., $\epsilon^2=0$.

Although the numerical approach is not computationally burdensome, analytical four-moment models have been pursued (Winterstein and Lange, 1995), particularly in the case where U is standard Gaussian and $\alpha_{4X} > \alpha_{4U} = 3$. Here it is useful to rewrite Eq. 3.7 in terms of Hermite polynomials:

$$X = m_X + \kappa\sigma_X[U + c_3(U^2 - 1) + c_4(U^3 - 3U)]; \quad \kappa = (1 + 2c_3^2 + 6c_4^2)^{-1/2} \quad (3.10)$$

Results for c_3 and c_4 have been found to make ϵ^2 vanish to first-order (Winterstein, 1985) and second-order (Winterstein, 1988) in c_n . The most recent (and accurate) expressions have been fit to “exact” results from constrained optimization:

$$c_3 = \frac{\alpha_{3X}}{6} \left[\frac{1 - .015|\alpha_{3X}| + .3\alpha_{3X}^2}{1 + 0.2(\alpha_{4X} - 3)} \right] \quad (3.11)$$

$$c_4 = c_{40} \left[1 - \frac{1.43\alpha_{3X}^2}{(\alpha_{4X} - 3)} \right]^{1-0.1\alpha_{4X}^{0.8}}; \quad c_{40} = \frac{[1 + 1.25(\alpha_{4X} - 3)]^{1/3} - 1}{10} \quad (3.12)$$

The above expressions were produced using **FITTING** to generate a matrix of exact solutions for a range of requested skewness and kurtosis. The results were then

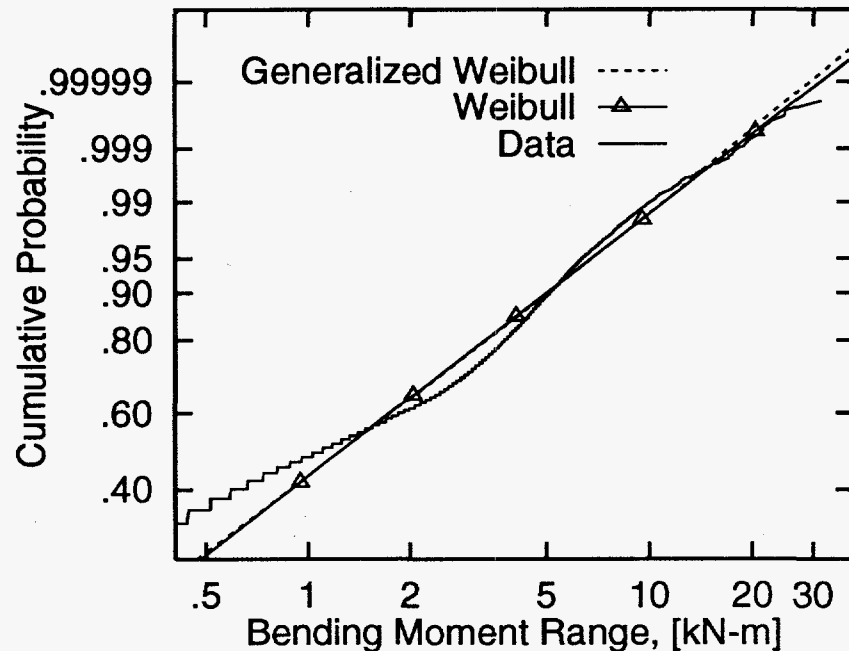


Figure 3.5: Weibull and Generalized Weibull models; Flapwise data

curvefit to produce expressions for c_3 and c_4 to be used in Eq. 3.10.

3.3.3 Generalized Weibull Model for Fatigue Loads

Figure 3.5 shows a generalized Weibull model of the NPS flapwise data, fit to its first four moments. Perhaps most notable is its similarity to the 2-parameter Weibull model. Unlike a least-squares or visual fit of a cubic model on this scale, this 4-moment fit does not bend to better match the cumulative probability at the highest level. Thus this single largest stress level, while visually striking, does not have sufficient impact to affect even a four-moment fit to the data. The net result is to support the general adequacy of the Weibull model for this flapwise case.

Somewhat different findings arise for the edgewise bending component, however.

Figure 3.6 shows the histogram of the edgewise bending history over the same 71-minute duration. This bimodal histogram shows the presence of fairly regular, large-amplitude stress cycles due to gravity, with small-amplitude oscillations superposed. Clearly, no single-mode distribution model, Weibull or other, can describe this entire load frequency pattern.

Fortunately, the small-amplitude load cycles need not be modeled for fatigue applications. This is seen in Figure 3.7, which shows that negligible fatigue damage is caused by cyclic loads below about $S_{min}=12$ [kN-m]. Therefore, we consider models of load ranges above S_{min} only. Above this value, Figure 3.8 shows that the generalized Weibull model gives quite a reasonable extrapolation of the observed trends in the data. It captures the curvature seen in the body of the data and the flattening characteristic of its upper tail. The generalized Weibull model appears to offer a significant improvement over the ordinary Weibull result in this case.

3.3.4 Generalized Gumbel and Generalized Gaussian Load Models

The primary motivation for a four-parameter load model here is the generalized Weibull model for fatigue applications. Generalized load models with other parent distributions are useful in other applications. They are presented here to both demonstrate these alternative uses and reiterate the important issue of statistical uncertainty in normalized moment estimates and its significance to the four-moment models.

Extreme Values: A Generalized Gumbel Example

Based on probabilistic engineering judgement the two-parameter Gumbel distribution is the natural choice for modeling extreme value problems. Although this example considers annual maximum significant wave heights, this generalized Gumbel model may also prove useful for extreme wind loads.

This application concerns the significant wave height H_s in a Southern North Sea location, for which 19 years of hindcast data are available (Danish Hydraulic

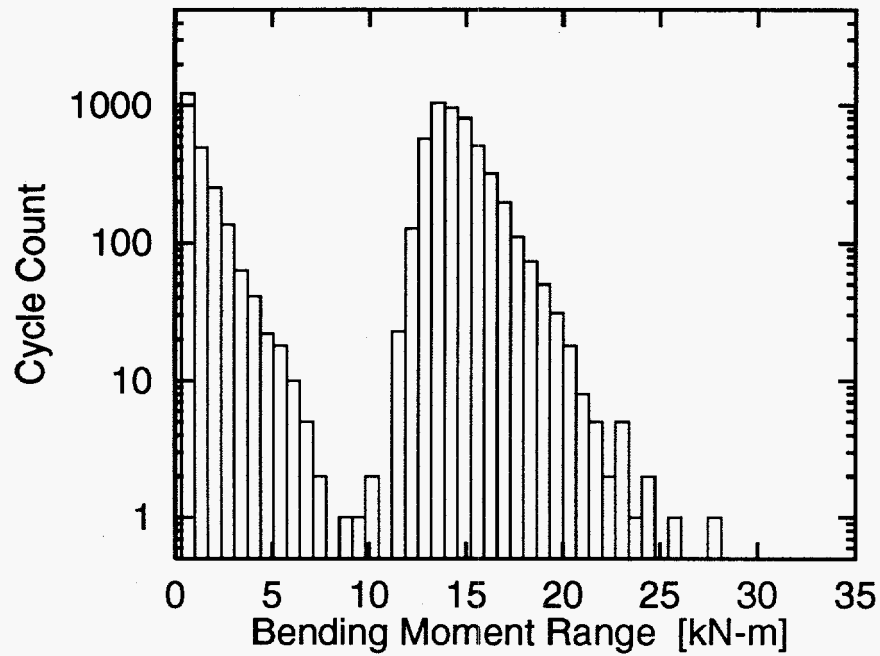


Figure 3.6: Histogram; edgewise data

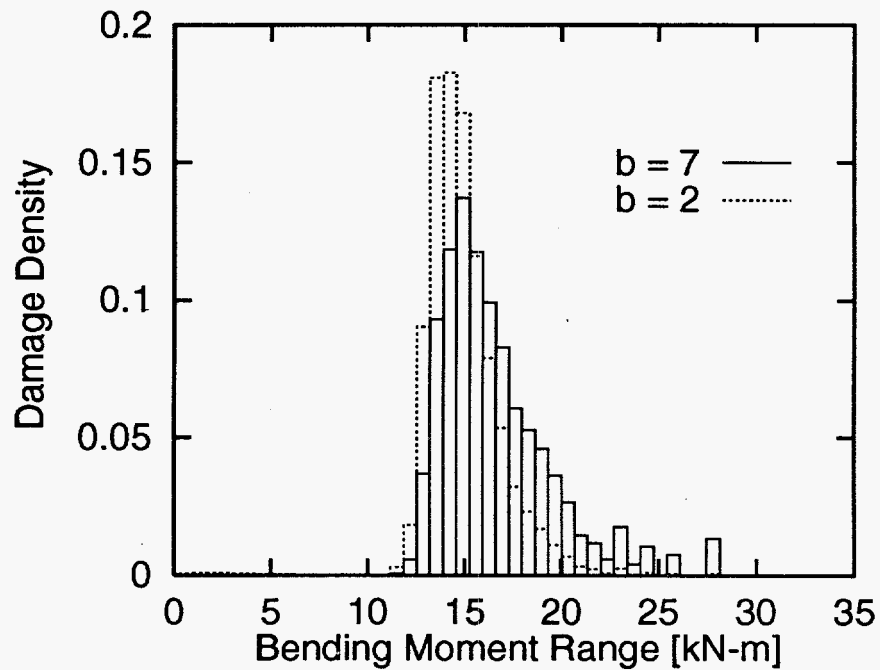


Figure 3.7: Damage Density; Edgewise Data.

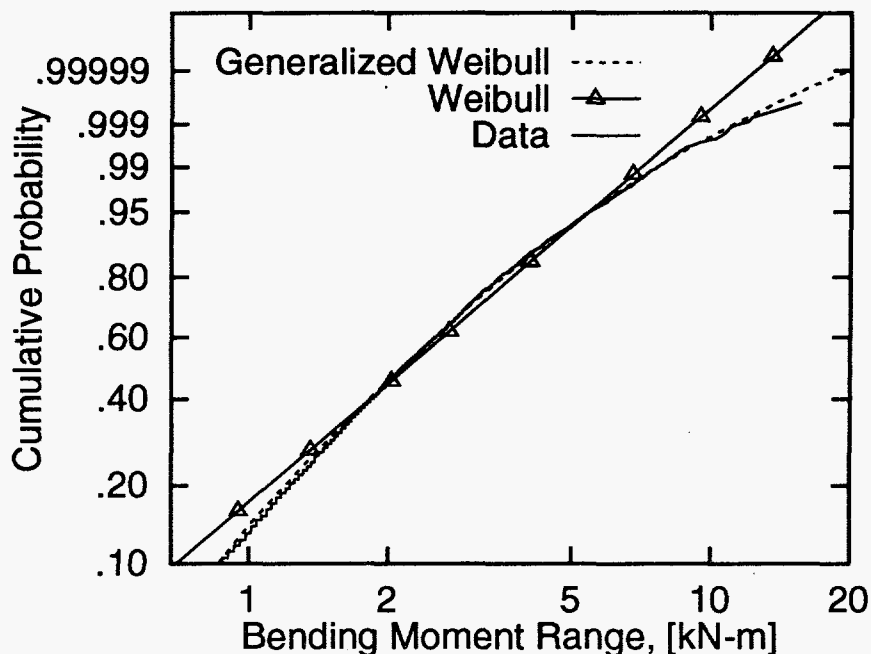


Figure 3.8: Weibull and Generalized Weibull Models; Edgewise Data (Ranges Plotted on Shifted Axis, $S-S_{min}$).

Institute, 1989). For each of these 19 years, a single storm event has been identified with maximum significant wave height H_s (i.e. the annual maximum values). This value ranges from $H_s = 6.92\text{m}$ (1972/1973) to 9.66m (1981/1982).

The generalized Gumbel distribution, plotted in Figure 3.9 along with the observed data values, is of the inverse cubic form given by Eq. 3.8. It appears to capture fairly well the systematic curvature of the data on the Gumbel probability scale used. As there are only 19 data points, the *statistical uncertainty* or bias in the estimated moments is of concern. Appendix A examines the magnitude of this bias and quantifies its significance.

It should be noted that an analytically based generalized Gumbel model has previously been fit to this data set (Winterstein and Haver, 1991). The results shown here are an improvement in two senses: (1) FITTING includes an inverse cubic transformation, which is particularly important in reflecting the narrower-than-Gumbel

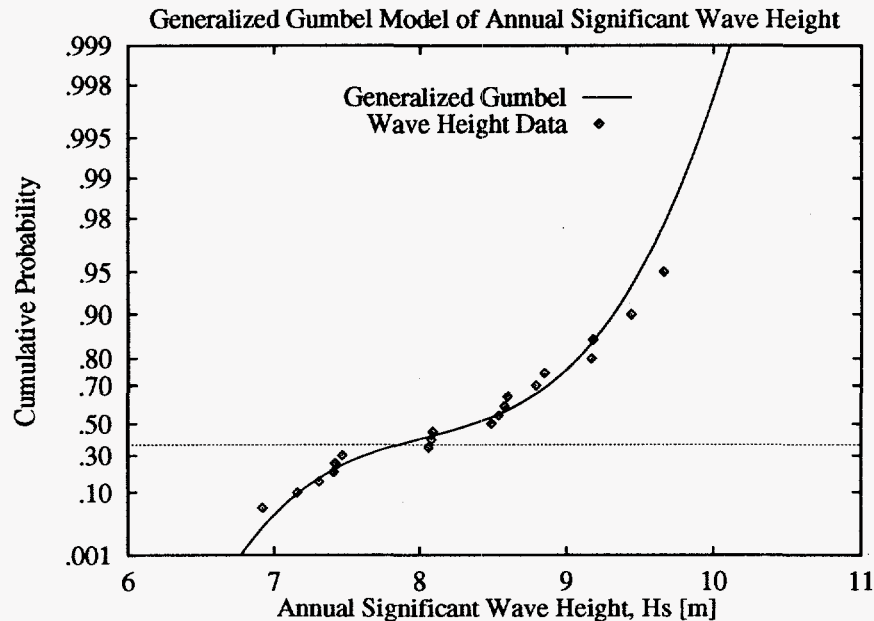


Figure 3.9: Generalized Gumbel Distribution for Annual Extreme Wave Height-19 Data.

tails; and (2) FITTING permits greater accuracy to be achieved in matching moments.

Because we deal here with annual extreme values, the Gumbel distribution is the natural choice of parent distribution. We may ask, however, what effect is achieved if a different choice of parent distribution is selected.

The three distributions are shown in Figure 3.10, The figure shows wave height results up to the 1000-year fractile, i.e. for which $p=.999$. The pattern of variation follows that of the underlying parent distributions: the Weibull has the narrowest upper tail and hence predicts the lowest extreme values, while the Gumbel predicts the largest. Most notably, however, all three parent distributions predict quite similar wave heights over this domain of interest.

This suggests that knowledge of four moments is sufficient to control the tail behavior of interest. This apparent robustness of the four-moment description is encouraging, particularly in cases where the optimal parent distribution is not obvious.

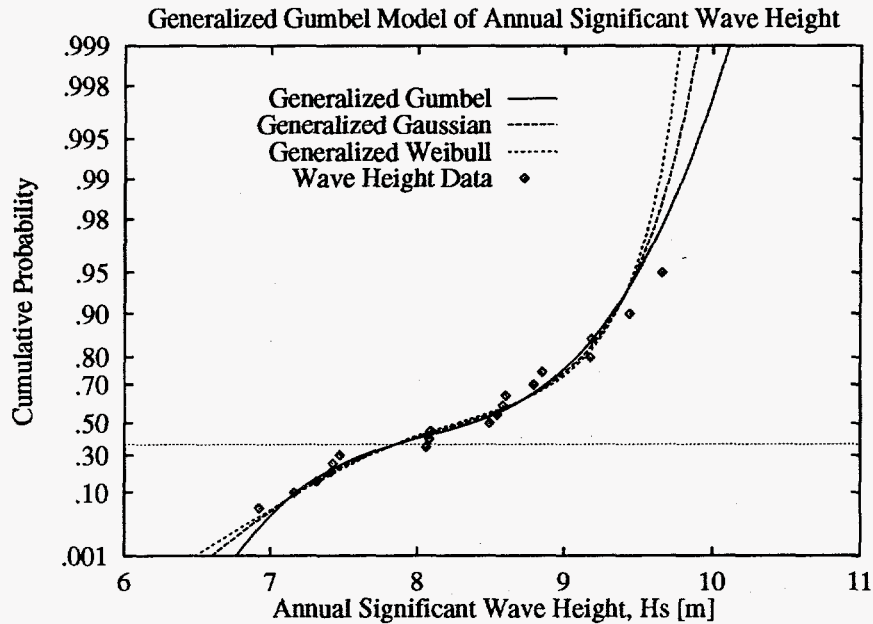


Figure 3.10: Comparison of Generalized Gaussian, Gumbel, and Weibull Distributions for Annual Extreme Wave Height.

Of course this conclusion may be problem-dependent; the user is encouraged to vary the choice of parent distribution for the problem at hand.

Nonlinear Vibration: A Generalized Gaussian Example

As a final example, we consider the vibration response of a linear structure under non-Gaussian loads. Such non-Gaussian loading may arise, in wind and wave applications, due to nonlinear relations between wind/wave velocities and applied forces. Adopting a simple 1DOF model of the response X ,

$$\ddot{X}(t) + 2\zeta\omega_n\dot{X}(t) + \omega_n^2X(t) = Y(t)^2 \quad (3.13)$$

in terms of the zero-mean Gaussian process $Y(t)$, and the system natural frequency

ω_n and damping ratio ζ . We consider a case studied previously (Grigoriu and Ariaratnam, 1987), for which $\omega_n=1.26$ [rad/sec], $\zeta=.30$, and the covariance between $Y(t)$ and $Y(t+\tau)$ is $\exp(-0.12|\tau|)$. As noted in that reference, this covariance ensures that $[X, \dot{X}, Y]$ is a Markov vector process, whose moments can be found from standard state-space moment relations. This yields $\alpha_{3X}=2.7$ and $\alpha_{4X} = 14.3$, quite far from their respective values (0 and 3) in the Gaussian case. (We also consider a more mild non-Gaussian case below, due to lower damping ratio $\zeta=.10$.)

Figure 3.11 shows the distribution of X , estimated by simulation, on normal probability scale. As expected, a two-moment Gaussian fit dramatically underestimates response fractiles x_p at levels of practical interest (e.g., p above .99). The generalized Gaussian model is a marked improvement, showing good agreement far into the response tails.

A maximum entropy model is shown here as a comparative model. The maximum entropy approach maximizes a quantity associated with the probability density $f_X(x)$ defined as "entropy" (Jaynes, 1957). The result, assuming four moments are known, is of the form

$$f_X(x) = \exp(-u(x)); \quad u(x) = \sum_{n=0}^4 \lambda_n x^n \quad (3.14)$$

A numerical algorithm is used to find constants $\lambda_1 \dots \lambda_4$ that preserve (or minimize error in) the four moments. Unit area is achieved through λ_0 . Note the similarity between Eq. 3.14 and Eq. 3.8 when U is Gaussian. Both ensure a hardening effect in the limit: $\lambda_4 > 0$ in Eq. 3.14 to achieve a proper pdf, and hence its distribution tails are ultimately narrower than the normal pdf $f_U(u)$.

The maximum entropy model underestimates response fractiles x_p systematically for p above .999; compensating errors occur at lower fractiles in its effort to preserve moments through an inconsistent functional form. As might be expected, similar though less dramatic effects are found when the damping is reduced to $\zeta=.10$ (Figure 3.12), as the response becomes more nearly Gaussian.

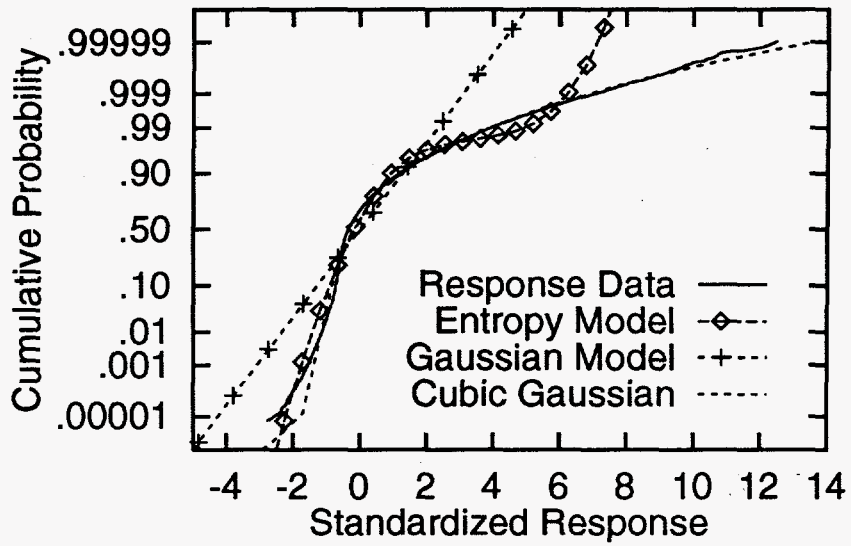


Figure 3.11: Oscillator Response; 30% Damping.

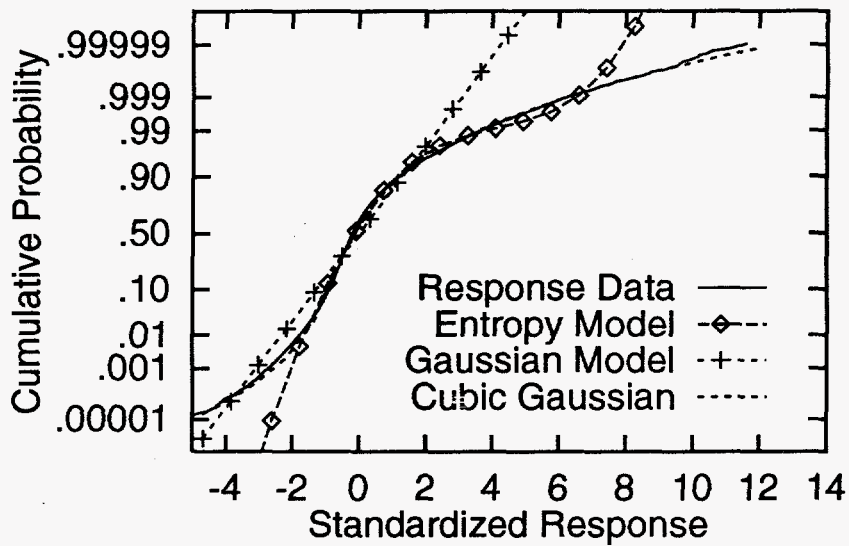


Figure 3.12: Oscillator Response; 10% Damping.

3.4 Fatigue Damage Estimates

Ultimately, the impact and adequacy of any probabilistic model must be viewed in the context of the application at hand. In our case, probabilistic models of stress ranges S_i are to be used to estimate the total fatigue damage:

$$D_{tot} = c \sum_i S_i^b n(S_i) = c N_{tot} \overline{S^b} \quad (3.15)$$

Thus, our interest focuses on estimating the normalized damage per cycle $\overline{S^b}$, the long-run average value of S^b over all stress cycles.

Figure 3.13 shows estimates of $\overline{S^b}$ found from the data, and from the various fitted probabilistic models. The generalized Weibull model follows the data quite well over the entire range of b values shown. The basic Weibull model also shows good agreement, with mild departure for exponents above around $b=10$. As might be expected from Figure 3.3, the Rayleigh model is extremely inaccurate. Somewhat more surprisingly, the visually plausible exponential model (Figures 3.1 and 3.3) appears to potentially underestimate damage, by about an order of magnitude for $b \geq 7$ and still more for higher b values.

Note that we need not expect more damage when the observed distribution tail is “filled in” with a continuous probability model. Indeed the observed normalized damage, $D_{obs} = \overline{S^b}$, is essentially a sample moment (of order b), and as such is always an unbiased estimate of the true long-run value, $D_{true} = \int s^b f(s) ds$. (Here $f(s)$ is the long-run probability density of stress S .) A caveat is in order here: in practice D_{obs} may vary rather asymmetrically around D_{true} . Consider, for example, an extreme case in which damage is governed by a single stress level bin, whose mean recurrence rate is one per 10 histories. (Multiple occurrences per history are thus negligible.) If we collect many such histories, on average 90% will show no occurrences in this critical bin—and hence will give mildly non-conservative damage estimates—while the remaining 10% show one occurrence, and hence strongly overestimate damage. Thus, while the correct average is achieved, the chance of (mild) non-conservatism is typically higher than that of (stronger) conservatism.

By fitting a smooth, continuous probabilistic model to all stress data, we hope

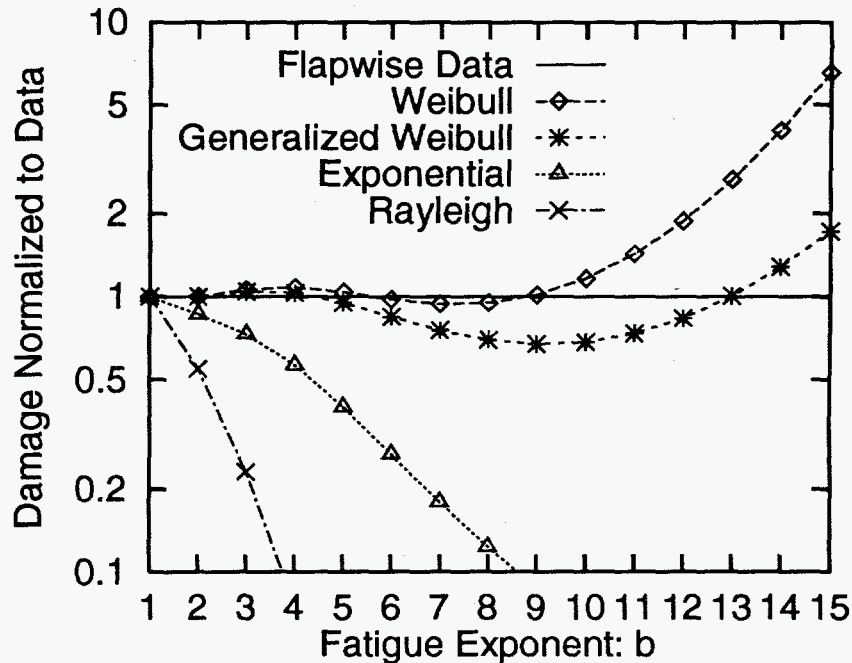


Figure 3.13: Normalized Damage per cycle; flapwise data

to avoid this extreme sensitivity of observed damage, D_{obs} , to the widely (and asymmetrically) varying tails of the observed stress distribution. In fitting this continuous model, however, it remains critical to well-represent the most damaging stress levels. High b values require better modeling of relatively large stress ranges; this is effectively done by matching at least two moments (Weibull) and still better by four moments (generalized Weibull).

3.5 Uncertainty Due to Limited Data

Finally, we consider the impact of uncertainty in damage due to our limited data history of 71 minutes. To do this we divide this history into subsets—e.g., $n_{seg}=4$ segments each with $N/4$ data—and produce damage estimates for each. The resulting variance among segment damages, σ_{seg}^2 , is then rescaled to estimate $\sigma^2 = \sigma_{seg}^2 / n_{seg}$, the damage variance based on all n_{seg} segments. While we take $n_{seg}=4$ here, the final

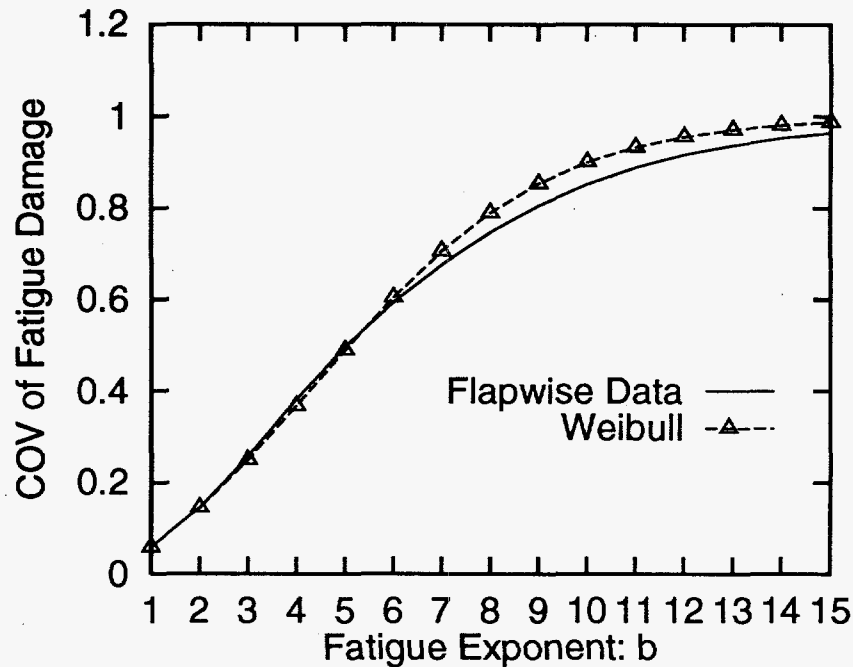


Figure 3.14: Damage coefficient of variation; flapwise data

variance σ^2 should be relatively insensitive to the number of segments used.

As the exponent b increases, we may expect damage estimates to grow in uncertainty due to their sensitivity to rare, high stresses. This is confirmed in Figure 3.14. This figure shows $V_{\bar{S}^b}$, the coefficient of variation (ratio of σ to mean damage) of the normalized damage, \bar{S}^b . $V_{\bar{S}^b}$ is shown to grow systematically with exponent b , reaching 50% for b of about 5 and nearing 100% for b values above 10. Note also that these results do not depend significantly on whether the damage estimates use the observed data or a Weibull model.

This worst-case value of $V_{\bar{S}^b}=1$ can be supported by a simple heuristic argument. Consider a stress history whose highest ranges fall into a bin at level S_{max} , in which there are $n(S_{max})$ data among the total of N_{tot} cycles. As b grows, the normalized damage \bar{S}^b becomes increasingly dominated by cycles at S_{max} only:

$$\bar{S}^b = \sum_i S_i^b \frac{n(S_i)}{N_{tot}} \approx S_{max}^b \frac{n(S_{max})}{N_{tot}} \quad (3.16)$$

The coefficient of variation can then be estimated as

$$V_{\bar{S}^b} \approx V_{n(S_{max})} \approx \frac{1}{\sqrt{n(S_{max})}} \quad (3.17)$$

If $n(S_{max})=1$ observation in this largest bin, as in Figure 3.1, this suggests 100% coefficient of variation in our damage estimate.

Finally, to determine data needs we need to consider what level of damage uncertainty is acceptable. This can only be addressed by comparing it with other uncertainty sources in fatigue life estimation. Here we define Δ as the actual damage level at failure. Setting $D_{tot}=\Delta$ in Eq. 3.15 and solving for the fatigue life $N_{tot}=N_{life}$ (in cycles):

$$N_{life} = \frac{\Delta}{cS^b} \quad (3.18)$$

The coefficient of variation of N_{life} is then roughly

$$V_{N_{life}} \approx \sqrt{V_{\Delta}^2 + V_c^2 + V_{\bar{S}^b}^2} \quad (3.19)$$

Here the three coefficient of variations, V_c , V_{Δ} , and $V_{\bar{S}^b}$, respectively reflect (1) scatter in the $S-N$ curve, (2) errors in Miner's rule, and (3) load modeling uncertainty due to limited data (e.g., as shown in Figure 3.14 for our 71-min. history). To ensure that load uncertainty has only moderate impact, we require

$$V_{\bar{S}^b} < \sqrt{V_{\Delta}^2 + V_c^2} \quad (3.20)$$

For most materials, typical values of $\sqrt{V_{\Delta}^2 + V_c^2}$ are 0.5 or higher. Thus, we need only seek a $V_{\bar{S}^b}$ value of 0.5, or perhaps a bit less. For cases in Figure 3.14 where $V_{\bar{S}^b}$ is about 1.0, this suggests that we obtain at least $n_{dat}=4$ times our current duration of 71 minutes. This should reduce $V_{\bar{S}^b}$ to about $1/\sqrt{n_{dat}}$, or 0.5. It should also yield multiple observations of the most damaging stress, unlike the current situation shown

in Figures 3.1–3.2. In other words, we seek at least $n(S_{max})=4$ observations at the most damaging stress level S_{max} ; this should give $V_{\overline{S}^b}$ of about 0.5 (Eq. 3.17).

3.6 Summary

Several techniques have been shown to better study fatigue loads data. Damage densities show which stress ranges are most important to model, reflecting fundamental differences between flapwise and edgewise data (Figures 3.2 and 3.7).

Common one-parameter models, such as the Rayleigh and exponential models, should be used with care. They may produce dramatically different estimates of load distributions (Figure 3.3) and damage (Figure 3.13). While the exponential model seems visually plausible for the flapwise data, it can potentially underestimate damage by an order of magnitude for S – N exponent $b \geq 7$ and still more for higher b values.

“Filling in” the distribution tail with a continuous model need not result in more damage (Figure 3.13). In fitting such a model, however, it is crucial to well-represent the most damaging stress levels. High b values require better modeling of relatively large stress ranges; this is effectively done by matching at least two moments (Weibull) and better by matching still higher moments. For this purpose, a new, four-moment “generalized Weibull” model has been introduced.

For edgewise data, the lower mode of the observed histogram gives negligible damage (Figure 3.7). Over the important range of larger stresses, the generalized Weibull model gives quite a reasonable extrapolation of the observed trends in the data (Figure 3.8). It appears to offer a notable improvement over the ordinary Weibull result in this case.

As the exponent b increases, damage estimates show growing uncertainty due to their sensitivity to rare, high stresses (Figure 3.14). This is quantified by Figure 3.14, and resulting data needs are discussed.

Chapter 4

LRFD for Fatigue

This chapter considers the design of wind turbine blades to resist fatigue failures. In particular, factors are developed for load and resistance factor design (LRFD) against fatigue. The use of separate load and resistance factors is consistent with a wide range of current, probability-based design codes (e.g., API, 1993).

This chapter combines several novel approaches to the blade fatigue problem. These include:

1. the use of FORM/SORM (first- and second-order reliability methods) to estimate failure probabilities and dominant uncertainty sources (Chapter 2);
2. new moment-based model of wind turbine loads, designed especially to reflect limited load data (Chapter 3); and
3. a parallel LRFD study of a specific Danish wind turbine, also based on FORM/SORM (Ronold et al, 1994).

4.1 Scope and Organization

The dominant fatigue blade loading is assumed here to be flapwise bending. We consider the following three different horizontal-axis wind turbines (HAWTs), for which measured load data are available.

Turbine 1:

Turbine 1 is the AWT-26 machine, a downwind, two-bladed, free-yaw, with 26-m diameter teetered rotor, and power rating of 275kW (McCoy, 1995). This turbine is used for our base case study, in view of the relatively large amount of load data available (197 10-minute segments).

Turbine 2:

Turbine 2 is an upwind, two-bladed HAWT with a rotor diameter of 17.8-m and a power rating of 100kW, operated by Northern Power Systems (Coleman and McNiff, 1989). It has a teetering hub design with full-span hydraulic passive pitch control. It affords a contrast to Turbine 1 both in mechanical design, and in the amount of available load data (only 20 10-minute segments).

Turbine 3:

Turbine 3 is a Danish machine, with hub height of 35-m and power rating of 500kW. This has been the subject of a similar LRFD study on wind turbine blade fatigue (Ronold et al, 1994). This study has been supported as one of four sub-projects within the 1994-1995 European Wind Turbine Standards (EWTS) project.

We seek here both to demonstrate basic methodology for fatigue reliability, and to identify the general impact of different load models on reliability calculations. We thus consider normalized bending loads from these various turbines, and fit different probability distributions to each. To focus on load modeling only, we adopt the same, hypothetical models of wind environment and blade properties in each case. Thus, our results are not intended to apply specifically to any of the machines in question. Rather, they should be seen as the result of applying various plausible load models to the same (hypothetical) wind turbine blade.

4.2 Background: Probabilistic Design

4.2.1 Probabilistic Design against Overloads.

Historically, codified probabilistic design has been most widely applied to “overload” failures, caused when the worst load, L , in the service life of a component exceeds its capacity R . This capacity may be associated with first yield, excessive deformation, buckling, or a similar criterion.

If both the load L and resistance R were known perfectly at the time of design, we would merely require that $R \geq L$. More generally, in load- and resistance-factor design (LRFD) separate factors, γ_L and ϕ_R , are used to scale the nominal load and resistance, L_{nom} and R_{nom} :

$$\phi_R R_{nom} \geq \gamma_L L_{nom} \quad (4.1)$$

Of course, in any single situation Eq. 4.1 can be replaced by a checking equation involving a single design factor SF_{des} on the net safety factor:

$$SF_{nom} = \frac{R_{nom}}{L_{nom}} \geq SF_{des}; \quad SF_{des} = \frac{\gamma_L}{\phi_R} \quad (4.2)$$

With the two factors γ_L and ϕ_R , however, Eq. 4.1 can more readily give uniform reliability across various cases—specifically, covering cases in which uncertainty in load may dominate over that of resistance, or vice versa. Similarly, different factors may be applied to separate load contributions which show different variability. Examples include separate factors for dead and live loads on offshore structures (API, 1993), or the separate factors recently suggested for static, wave-frequency, and slow-drift loads on floating structures (Banon et al, 1994).

4.2.2 Probabilistic Design against Fatigue

Because fatigue is the cumulative result of many loads, the choice of an “equivalent” load L and resistance R is somewhat ambiguous. Fatigue predictions are generally

based on tests with constant stress amplitude S (and mean stress $S_m=0$). The resulting number of cycles to fail, $N(S)$, is commonly modeled with a power-law relation:

$$N(S) = N_{ref} S_{norm}^{-b}; \quad S_{norm} = \frac{S}{S_{ref}}. \quad (4.3)$$

Here S_{ref} is a reference stress level, and N_{ref} the number of cycles to fail at that level. In Chapter 2 the S - N Law was written as $N = CS^{-b}$ where $C = N_{ref} S_{ref}^b$. Both N_{ref} and the power-law exponent, b , are material properties, both of which may generally be considered uncertain.

Miner's rule then assigns damage $D=1/N(S)$ per cycle, and hence average damage

$$\bar{D} = \frac{1}{N_{ref}} \overline{S_{norm}^b} \quad (4.4)$$

over the service life of the specimen. (Overbars are used here to denote average values.) More generally, this damage rate \bar{D} can be adjusted to reflect;

1. a stress concentration factor K relating local to far-field stresses;
2. an availability factor A , the fraction of time the wind turbine component operates; and
3. the effect of a non-zero mean stress S_m , which with the Goodman rule scales the fatigue life by $(1 - K|S_m|/S_u)$ (here S_u =ultimate stress);

as was done in the CYCLES limit state formulation (Chapter 2). The result is an effective damage rate

$$\bar{D}_{eff} = \frac{\overline{S_{norm}^b}}{N_{eff}}; \quad N_{eff} = N_{ref} \frac{(1 - K|S_m|/S_u)^b}{AK^b} \quad (4.5)$$

Finally, we can identify load and resistance variables, L and R , such that $L \geq R$ implies fatigue failure. If we seek the specimen to withstand N_{ser} cycles in its service life, Miner's rule predicts failure if $\bar{D}_{eff} N_{ser} \geq 1$. Here we generalize this failure criterion to read

$$\overline{D}_{eff} N_{ser} \geq \Delta, \quad (4.6)$$

where randomness in Δ reflects possible errors (both bias and uncertainty) in Miner's rule. This implies a failure criterion of the form $L \geq R$, in terms of the following "fatigue" load and resistance:

$$L = \overline{S_{norm}^b} \cdot N_{ser}; \quad R = N_{eff} \cdot \Delta \quad (4.7)$$

Note that in this formulation, fatigue load and resistance have units of cycles. Alternative formulations can instead assign load and resistance factors γ'_L and γ'_R in terms of stresses by taking the b^{th} root of the above expressions (Eq. 4.7); e.g., Ronold et al, 1994. Numerical values of these factors may differ notably; we may expect $\gamma'_L \approx \gamma_L^{1/b}$ because damage is related here to the b^{th} power of stress.

Our current formulation seeks to reflect common usage; e.g., a nominal value of N_{eff} that may be based on a lower-fractile $S-N$ curve. The resulting load factor γ_L then serves to inflate a number of load cycles to be withstood. For example, critical offshore facilities are often designed against $\gamma_L=10$ times the service life (e.g., demonstration of 200-year nominal life if the actual service life is 20 years).

In the following section we seek to;

1. model load variability given limited wind and load data;
2. study sensitivity to various modeling assumptions, different machines, etc.; and
3. suggest convenient choices of nominal fatigue load and resistance, and associated load and resistance factors γ_L and ϕ_R , to achieve desired reliability against fatigue failure.

4.3 Fatigue Load Modeling

Previously (Chapter 3) the use of smooth, analytical probability distributions conveniently fit to a limited number of statistical moments was evaluated with respect to fatigue load modeling. When fitting such models it was shown that, for high b values, proper modeling of relatively large stress ranges is required. This is achieved by matching at least two moments (Weibull) and sometimes improved further with the four-moment "generalized Weibull".

For this reason it is desirable to utilize the four-moment model in the partial safety factor calculations performed here. Unfortunately, the generalized Weibull as calculated by the FITTING routine is not easily integrated into a FORM analysis. Simultaneous solution of nonlinear equations to preserve the third and fourth moments becomes computationally burdensome as the iterative FORM calculations require repeated fits of the distribution.

However, our subsequent experience suggests that three-moment models may suffice for fatigue load ranges. Such a model, herein referred to as a "quadratic Weibull", is presented below in the following subsection. Its implementation for various wind conditions is also described.

4.3.1 Fatigue Loads for Given Wind Climate

We work here with the first three moments, defined as follows:

$$\mu_1 = \bar{S} \quad (4.8)$$

$$\mu_2 = \frac{\sigma_S}{\mu_1}; \quad \sigma_S^2 = \overline{(S - \bar{S})^2} \quad (4.9)$$

$$\mu_3 = \frac{\overline{(S - \bar{S})^3}}{\sigma_S^3} \quad (4.10)$$

Note that both μ_2 , the coefficient of variation, and μ_3 , the skewness coefficient, are normalized to be unitless. Successively higher moments provide increasingly detailed information about rare large loads, at the expense of being increasingly difficult to estimate from limited data. Alternatively, one may estimate the b -th moment (and

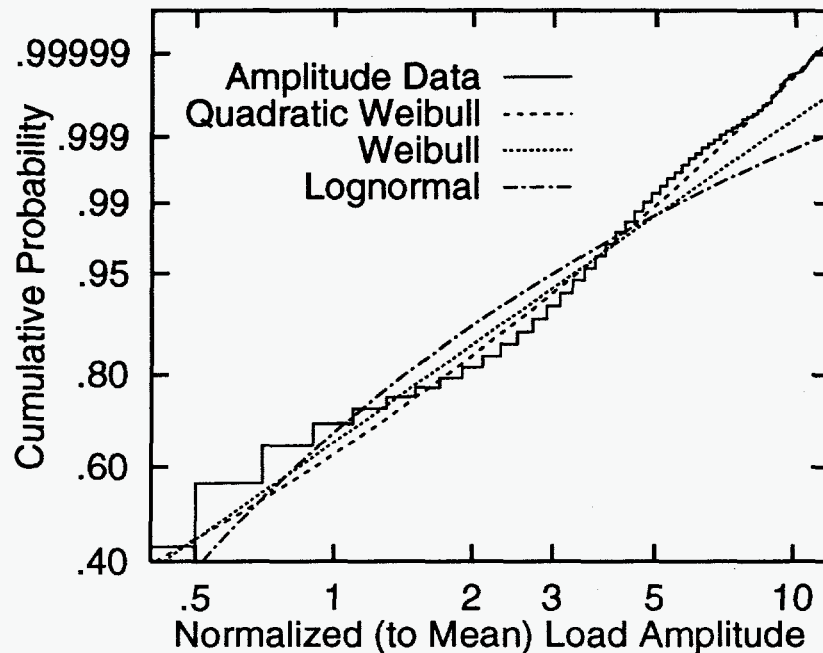


Figure 4.1: Distribution of normalized loads (Turbine 1: $V = 11.5$ m/sec, $I = .16$).

hence $\overline{S_{norm}^b}$) directly from data, thus avoiding the need to fit any theoretical probability model. Our use of lower-moment models, however, seeks to reduce the variability associated with estimating $\overline{S_{norm}^b}$, particularly for the relatively high b values (e.g., 10 or above) found for some composite materials (e.g., Mandell et al, 1993).

Following common wind turbine practice, we divide load histories into 10-minute segments. Rainflow-counted stress ranges, S , are identified for each segment, and the results binned by mean wind speed V and turbulence intensity I . This study employed an eight by eight bin scheme where the minimum and maximum values of the bins (for V and I) correspond to the minimum and maximum values of the data. Figure 4.1 shows a resulting distribution of flapwise bending loads, found for Turbine 1 at a wind climate bin centered at $V=11.5$ m/s and $I=.16$. This is a fairly frequently occurring bin, and Figure 4.1 reflects a total of approximately 5 hours of data. The results are shown on “Weibull scale,” along which any Weibull model of the form

$$\text{Prob [load } > s] = \exp[-(s/\beta)^\alpha] \quad (4.11)$$

will appear as a straight line. Recall that special cases of the Weibull include the exponential ($\alpha=1$) and Rayleigh ($\alpha=2$) models. Both of these have been previously applied to model HAWT and VAWT loads (Jackson, 1992; Kelley, 1995; Malcolm, 1990; Veers, 1982).

The Weibull model in Figure 4.1, fit to the first two moments μ_1 and μ_2 , appears to match the data fairly well. It fails, however, to reflect the systematic curvature the data display on this scale. An alternate two-moment model, the lognormal, shows curvature in the other direction, suggesting it notably overestimates loads at high-fractile levels. (A 4-moment variation on this lognormal model has been used in the Danish wind turbine study of Ronold et al, 1994.)

We also show results from a “quadratic Weibull” model, based on the first three moments of the data. It begins with the Weibull model S_{weib} of Figure 4.1, fit to μ_1 and μ_2 . If the skewness μ_3 of the data exceeds that of S_{weib} , a quadratic term is added to S_{weib} to broaden its probability distribution:

$$S = s_{min} + \kappa[S_{weib} + \epsilon S_{weib}^2] \quad (4.12)$$

When the skewness μ_3 of the data is less than that of S_{weib} , the roles of S and S_{weib} in Eq. 4.12 are interchanged:

$$S_{weib} = s_{min} + \kappa[S + \epsilon S^2] \quad (4.13)$$

(This quadratic equation is readily inverted to yield an explicit result for S in terms of S_{weib} .) In either case, the fitting proceeds in 3 steps:

1. ϵ is chosen to preserve the skewness, μ_3 ;
2. κ is chosen to recover the correct variance, σ_S^2 ; and
3. the shift parameter s_{min} is finally introduced to recover the correct mean, μ_1 .

Figure 4.1 shows that the quadratic Weibull model indeed provides an improved fit to the data. Note here that the best Weibull model, S_{weib} , overestimates the frequency of large loads, and hence the load skewness. Thus we select Eq. 4.13, with $\epsilon > 0$ to ensure that S has narrower distribution tails than S_{weib} . Similar trends are found for this turbine in other wind conditions, as shown in the next section. We focus in Section 4.5 on how such differences, among the three load distributions shown, impact resulting estimates of fatigue reliability. Note also that the data show $\mu_2=1.1$, so that the best Weibull model S_{weib} has broader distribution tails than the commonly used exponential model.

4.3.2 Fatigue Loads Across Wind Climates

To implement the preceding 3-moment load model for various wind conditions, best estimates $E[\mu_i]$ ("expected values") of the three moments μ_i ($i=1,2,3$) have been found for each $V-I$ bin. The following power-law relation has then been fit:

$$E[\mu_i] = a_{oi} \left(\frac{V}{V_{ref}} \right)^{a_{1i}} \left(\frac{I}{I_{ref}} \right)^{a_{2i}} \quad (4.14)$$

Figures 4.2–4.4 show resulting estimates of $E[\mu_i]$ for the three wind turbines. (All loads have been normalized by their respective mean values at $V=V_{ref}=7.5\text{m/s}$, so that all results in Figure 4.2 predict unit values of the normalized mean load at $V=V_{ref}$.) This approach of modeling the load moments, μ_i , across different wind conditions closely parallels that of the Danish fatigue reliability study (Ronold et al, 1994). This permits us to include results for that machine (Turbine 3), by substituting appropriate expressions for $E[\mu_i]$. Also, all results are shown versus mean wind speed V at a reference turbulence intensity $I=I_{ref}=0.15$. Because all quantities showed relatively moderate variation with I , (e.g., $.1 \leq a_{2i} \leq .3$) this dependence is not shown in the figures (although it is kept in the subsequent analyses).

Most notable in these figures is the similarity of the various turbines: Turbines 1 and 2 show similar estimates of all 3 moments, and Turbine 3 gives consistent μ_1 and μ_2 (albeit apparently lower μ_3 estimates). A notable distinction however between the two studies is that Ronold et al, (1994) employed a polynomial expression of the form

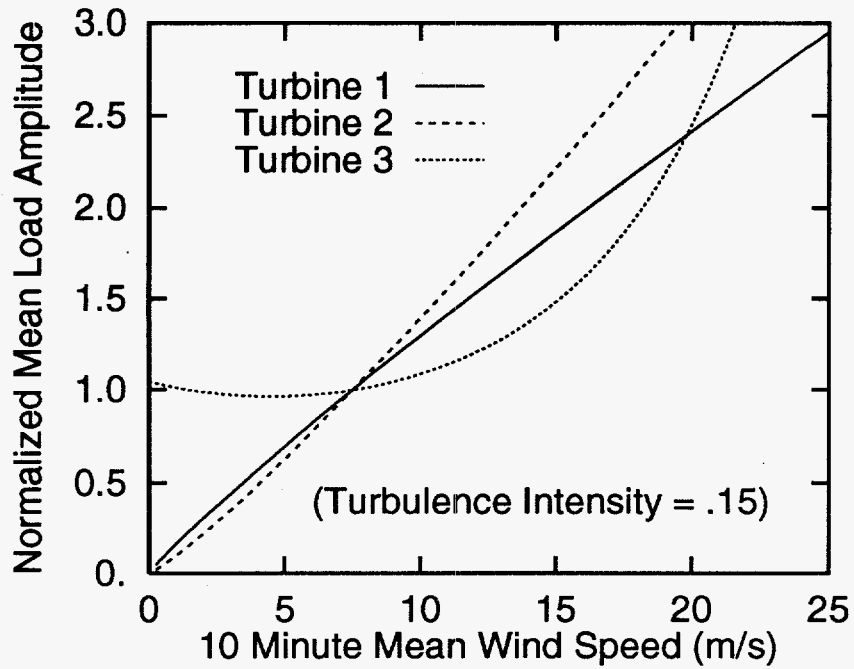


Figure 4.2: Estimated mean of normalized loads.

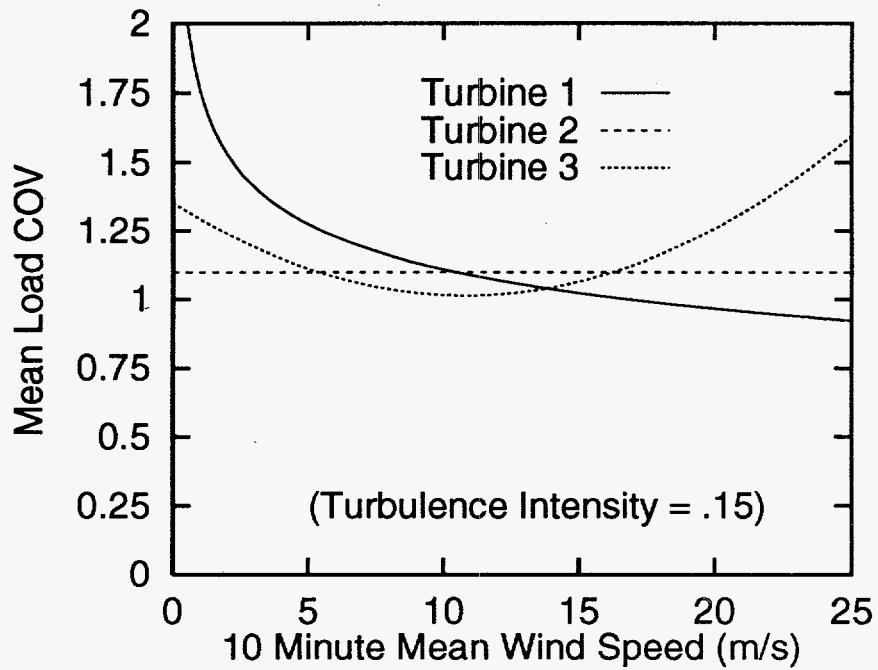


Figure 4.3: Estimated load coefficient of variation (COV).

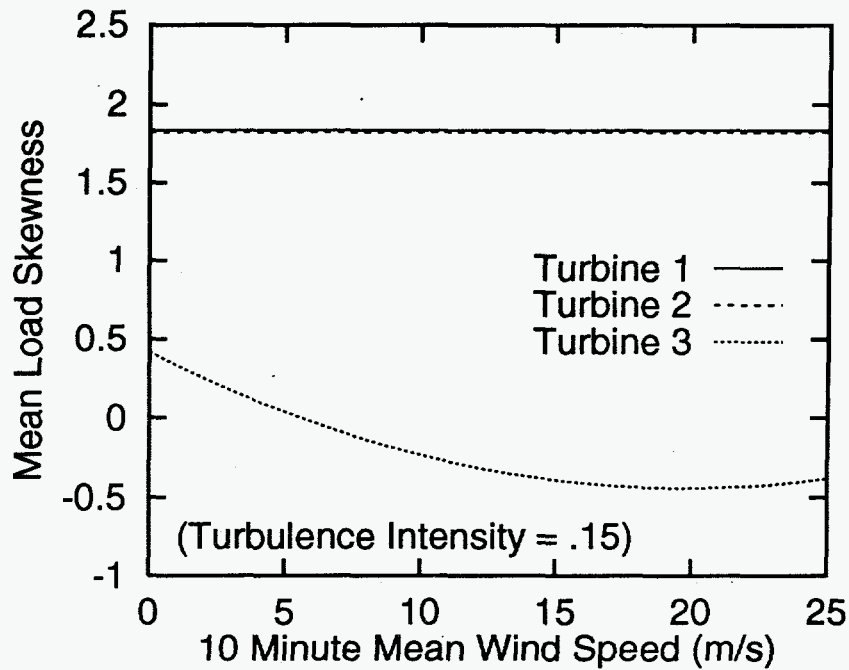


Figure 4.4: Estimated load skewness.

$$E[\mu_i] = a'_{0i} + a'_{1i}V + a'_{2i}V^2 + a'_{3i}I + a'_{4i}I^2 \quad (4.15)$$

which explains the nonzero mean load (at $V=0$) for Turbine 3 in Figure 4.2. It is also important to note that Turbine 3 results are inferred from cited results (Ronold et al, 1994) for the mean μ'_1 , standard deviation μ'_2 , and skewness μ'_3 of $S'=\ln S$. Figures 4.2–4.7 have been constructed from Taylor series approximations, which suggest the mean load $\mu_1 \approx \exp(\mu'_1)$, while the higher unitless moments $\mu_i \approx \mu'_i$ for $i=2$ and 3. These approximations may add to the discrepancy, however, for example in Figure 4.4.

In general, Figure 4.3 suggests that for all 3 turbines, the coefficient of variation μ_2 generally exceeds 1.0, its value for an exponential model. Thus the “best” two-moment Weibull model is broader in its tail, or more damaging, than the commonly

used exponential. However, the skewness μ_3 is generally less than 2.0, the corresponding value for an exponential variable. This implies that the basic Weibull fit, while more damaging than a body-fit exponential, in turn overestimates damage due to large load levels. In other words, the result shown in Figure 4.1 for Turbine 1 is symptomatic of various turbines in diverse wind climates: the data show curvature on Weibull scale, toward lower load levels at high fractiles than the Weibull model predicts. This effect will grow in importance as the fatigue exponent b increases; e.g., as we move from common metals to composites.

Analogous to Eq. 4.14, power-law fits have also been made of the corresponding standard deviations, $D[\mu_i]$, of the 3 moments $\mu_1 \dots \mu_3$. These have been estimated for each $V-I$ bin by a bootstrapping technique, in which "equally likely" rainflow range data (the same number as observed) are found by resampling from the observed ranges (Efron and Tibshirani, 1986). These quantities $D[\mu_i]$ directly reflect the impact of limited data, and approach zero as the amount of data grows. We should thus expect cases with little data (e.g., Turbine 2) to show relatively higher uncertainty levels, $D[\mu_i]$, than those with more data (Turbines 1 and 3). Again Turbines 1 and 2 are found to yield consistent results in Figures 4.5–4.7. Turbine 3 appears relatively more variable, especially in Figures 4.5–4.6 and at extreme wind speeds. It is not clear whether this reflects the observed data for this turbine, our approximation of moments of S from those reported of $\ln S$, or the extrapolation of functional forms beyond the range of observed data.

This difference, however, appears to propagate to the load- and resistance-factor calculation. In particular, the next section will show LRFD factors for both Turbine 1 (dense load data) and Turbine 2 (sparse load data). Because the uncertainty in Turbine 3 appears closer in Figures 4.5–4.7 to that of Turbine 2, LRFD factors reported in the Danish study more closely parallel our sparse-data case.

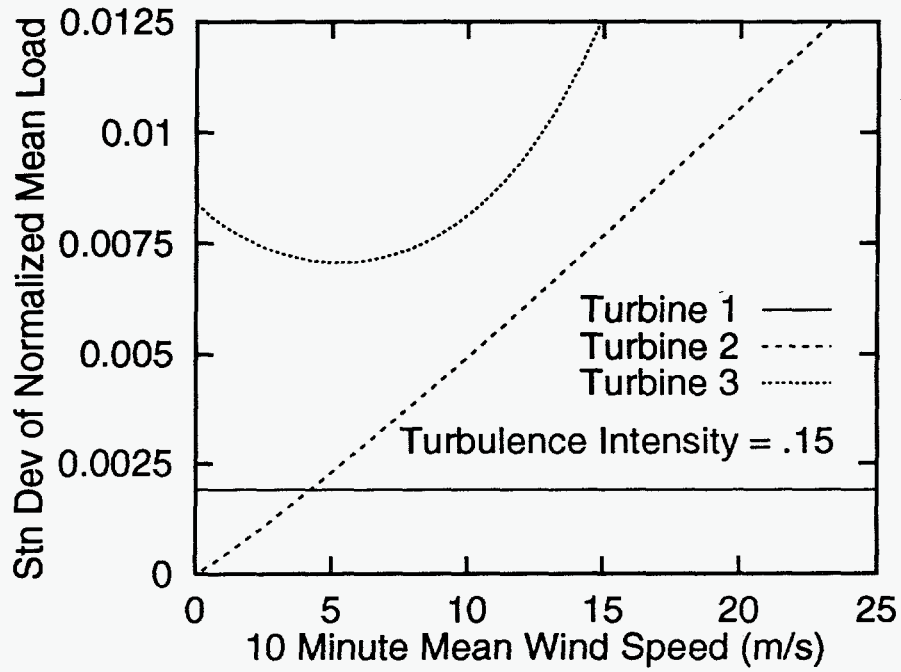


Figure 4.5: Standard deviation, estimated mean load.

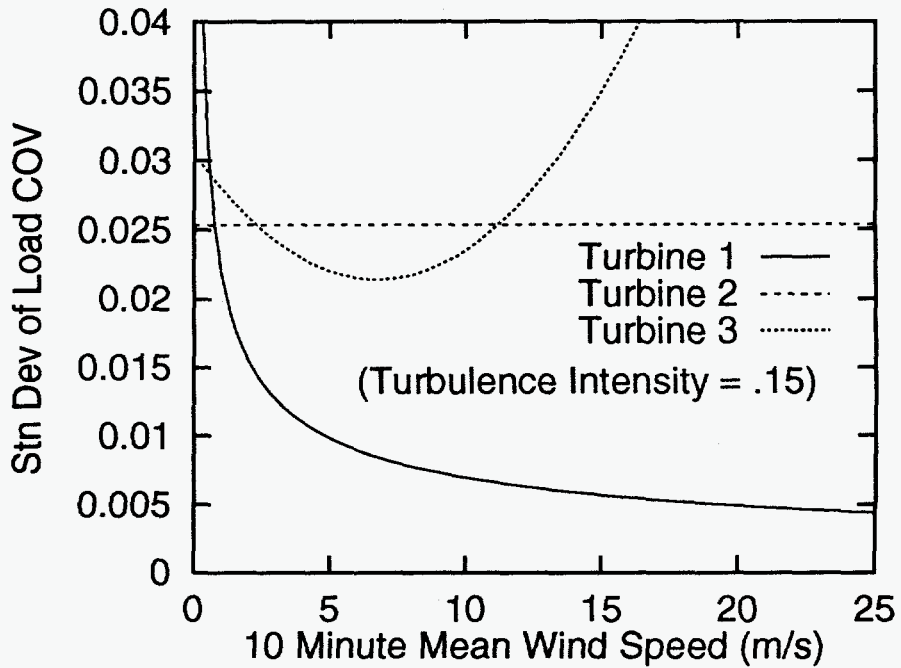


Figure 4.6: Standard deviation, estimated load COV.

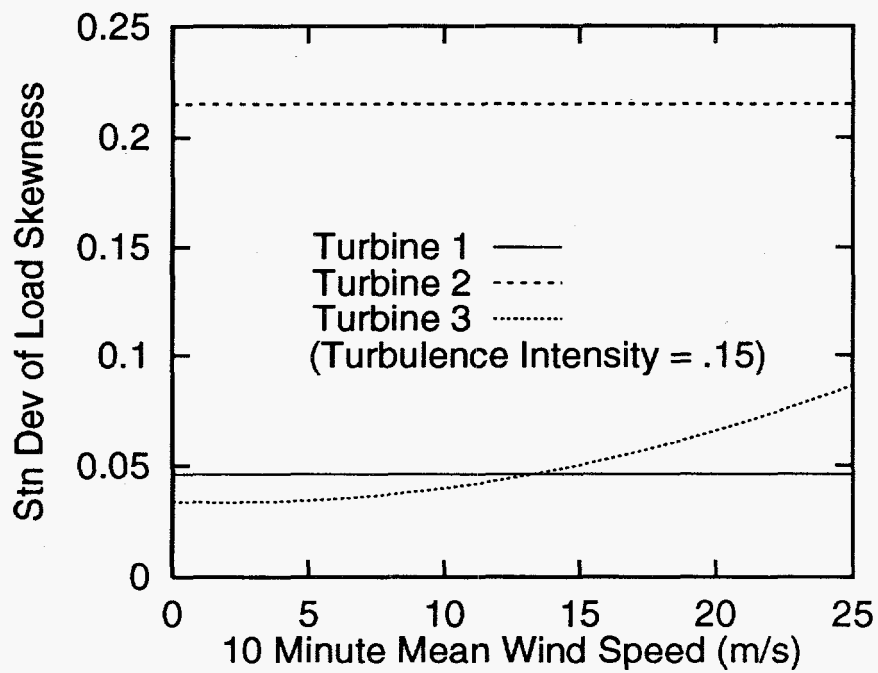


Figure 4.7: Standard deviation, estimated load skewness.

4.4 LRFD Assumptions and Computational Procedure

From Eq. 4.7, the fatigue loading involves the b^{th} moment $\overline{S_{norm}^b} = \overline{S^b}/S_{ref}^b$. This weights the conditional moment $\overline{S^b|V,I}$, given various values of V and I , by their joint probability density $f_{V,I}(v,i)$:

$$\overline{S^b} = \int \int_{\text{all } V, I} \overline{S^b|V,I} \cdot f_{V,I}(v,i) \, dv \, di \quad (4.16)$$

We assume here that the mean wind speed V has Weibull distribution, with average \overline{V} and shape parameter α_V . The turbulence intensity I is assumed independent of V , and assigned lognormal distribution with average \overline{I} and coefficient of variation COV_I . Finally, we estimate $\overline{S^b|V,I}$ from three moment-based fits: the Weibull, lognormal, and quadratic Weibull models as in Figure 4.1.

From the previous section, the necessary moments μ_i are modeled as

$$\mu_i = E[\mu_i] + D[\mu_i] \cdot U_i; \quad i = 1, 2, 3 \quad (4.17)$$

in terms of standard normal variables U_i . Correlations among the U_i are included, estimated from all the moment data irrespective of their V and I values. This approach directly parallels that suggested in the Danish fatigue reliability study (Ronold et al, 1994).

Thus, the fatigue load $L = \overline{S^b} \cdot N_{ser}/S_{ref}^b$ is modeled here as a function of seven uncertain quantities:

$$L = L(\mathbf{X}) = \frac{\overline{S^b}(\mathbf{X}) \cdot N_{ser}}{S_{ref}^b} \quad (4.18)$$

in which $\mathbf{X} = [\alpha_V, \overline{V}, COV_I, \overline{I}, U_1, U_2, U_3]$. Note that $\overline{S^b}/S_{ref}^b$ is unitless, so that this load definition has units of *cycles*. An alternative definition of load and resistance, in terms of stress, will be described later (cf. Eq. 4.23). The first four of these characterize the Weibull distribution of V and the lognormal distribution of I , respectively, which are assumed to be statistically independent. The latter three are used, with

Variable	Distribution	Mean	Stn Dev
α_V	Weibull	1.8	0.135
\bar{V}	Normal	7.5	0.563
COV_I	Weibull	0.25	0.019
\bar{I}	Normal	0.15	0.011
U_1	Normal	0.0	1.0
U_2	Normal	0.0	1.0
U_3	Normal	0.0	1.0
R	Weibull	2.42E+18	1.69E+18
N_{ser}	Constant	4.10E+09	-
b	Constant	8.0	-

Table 4.1: Random variables in reliability analyses.

Eq. 4.17, to reflect load uncertainty due to limited data.

Table 4.1 shows the distribution types and parameters for each of these variables, as well as of the net resistance variable $R = N_{eff} \cdot \Delta$ in Eq. 4.7. Generally, this would in turn require joint modeling of its various components; e.g., N_{ref} , K , S_m , S_u , and A in Eq. 4.5; cf Veers et al, 1993. Here, however, for simplicity we choose the value $b=8$ and the resistance variable R to have net coefficient of variation of 0.70.

Note that the computational procedure outlined will result in a limit state equation somewhat different from the CYCLES formulation described in Chapter 2. Thus an alternative version of CYCLES has been used here where the restrictive assumptions enforced in CYCLES (see Section 2.4) have been relaxed to permit more generality. (Incorporating such enhancements in future CYCLES versions may be a useful topic of future work; see the recommendations that follow in Chapter 5.) As our intent here is to study the impact of various load models on reliability calculations it was necessary to include those model types into the program input and modify the limit state formulation to accommodate different distribution types. With the additional complexity generated by the use of both wind speed, V , and turbulence intensity, I ,

as environmental parameters, closed form expressions for fatigue life become impracticable. Therefore the ensuing FORM analyses employ a limit state equation that is evaluated numerically using quadrature.

This implementation of numerical integration significantly enhances the flexibility of the FORM analyses. For example not only can the distribution types of the load be selected as an input option but also the environmental variables distribution types can be changed as well. The distributions are selected from the internal library of distribution types that exists within the original CYCLES program. A separate subroutine has been added to compute the conditional moment $\overline{S^b|V, I}$ required to determine the b^{th} moment of the load in Eq. 4.16. This subroutine includes the quadratic Weibull distribution as well as the Weibull and lognormal distributions, the three distributions considered in this study.

Of course this added capability does not come without cost. Numerical integration requires longer solution times; however, typical runs are on the order of minutes so this is not a big factor. Run-time costs are tied directly to the number of quadrature points selected; this number was varied and several runs were made to ensure stable results. Also, required input to the program is increased. In addition to the random variable definitions, the a_{0i} 's, a_{1i} 's, and a_{2i} 's of Eq. 4.14 must also be input for the three moments $E[\mu_i]$ and their standard deviations, $D[\mu_i]$.

This alternative FORM program with its added generality should not be considered as making the original CYCLES program obsolete. On the contrary, results show that CYCLES would likely have produced similar results for Turbine 2 with an assumed Weibull load distribution. This is because the turbulence intensity is relatively unimportant in this case, and the loads data here show relatively constant COV (see Figures 4.2 and 4.3) in accordance with the assumptions of CYCLES. While this enhanced version of CYCLES was necessary for the academic study performed here, the CYCLES program represents a useful compromise between level of detail and the existing knowledge of many structures and mechanical components.

	Stress Distribution Type	
	Log	Weibull
p_f :	4.4×10^{-1}	2.5×10^{-7}
Variable	Uncertainty Percentage	
α_V	0.5	0.1
\bar{V}	0.0	0.0
COV_I	19.9	0.1
\bar{I}	1.1	0.0
U_1	0.9	0.0
U_2	4.3	0.0
U_3	-	-
R	73.3	99.8

Table 4.2: Turbine 1 reliability results; effect of load distribution type

4.5 Variations with Load Distribution

We first consider results for Turbine 1, comparing the effect of switching between the three load models as in Figure 4.1: lognormal, Weibull, and quadratic Weibull. As in Figure 4.1, we pursue moment-based fits, matching μ_1 and μ_2 for the two-parameter models, and μ_1 through μ_3 for the quadratic Weibull. Thus all three models yield identical fatigue damage results for fatigue exponents $b=1$ and 2; the quadratic Weibull would also agree with the observed damage when $b=3$.

With the exponent $b=8$ chosen here, however, these models yield dramatically different estimates of fatigue damage, and hence of the probability p_f of fatigue failure within 20 years ($N_{ser}=4.1 \times 10^9$ cycles at an average rate of 6.5 Hz). Typical p_f values differ by more than 5 orders of magnitude: from less than 10^{-6} to above 10^{-1} . Table 4.2 shows the failure probabilities and relative importance of the different random variables for the lognormal and Weibull load distributions. Note that the relative importance of the load variables shifts from 27% for the lognormal distribution to less than 1% for the Weibull distribution of loads.

This highlights the importance of choosing an appropriate load model. It reflects

the well-known effect of tail-sensitivity in reliability, while the first two moments of S have been preserved here, the higher moment $\overline{S^b}$ can vary greatly among various models fit to the same data. This effect grows with b ; note that we choose here $b=8$, which is a relatively high value for metals but relatively low for many composites.

4.6 LRFD Calculations

The foregoing shows that if we consider an identically designed turbine blade, the calculated fatigue reliability is altered notably by the choice of load distribution. Conversely, vastly different load factors would be needed to achieve the same reliability for different load distributions—i.e., much higher load factors if the lognormal model were correct, much lower for the Weibull model, and so forth. This is demonstrated later with the results for Turbine 1.

To reduce this sensitivity of load factors to distribution choice, we can seek to reflect the load distribution type in our nominal load. Assume we consider a design parameter W , which relates the observed bending moment M to resulting stress S ; i.e., $S=M/W$. We may then seek to adjust W to preserve the mean damage, given our best estimates of the distributions of V , I and $S|V, I$ —in other words, choose W to preserve

$$L_{nom} = \overline{S_{norm}^b} \cdot N_{ser} = L(\mathbf{X} \text{ given } \mathbf{X}_i = \overline{\mathbf{X}}_i) \quad (4.19)$$

Thus, if applied moments M truly follow a lognormal model we would require a sturdier blade—i.e., higher W to preserve $\overline{S^b} = \overline{M^b}/W^b$ —than if a Weibull model of M were correct. Moreover, these differences between blade designs would increase with b , to reflect increasing sensitivity to distribution choice as b grows. Other design rules are also possible; e.g., choose W to preserve a specific upper fractile of the long-run stress distribution. An advantage of preserving L_{nom} in Eq. 4.19, however, is that it reflects not only the choice of load distribution but also the fatigue material behavior (i.e., choice of b).

Table 4.3 shows the resulting advantage of the nominal load definition in Eq. 4.19.

	Stress Distribution Type		
	Log	Weibull	Quad Weib
p_f :	4×10^{-4}	4×10^{-4}	5×10^{-4}
Variable	Uncertainty Percentage		
α_V	0.0	0.6	2.7
\bar{V}	0.1	1.6	3.3
COV_I	0.2	0.0	0.0
\bar{I}	2.6	1.2	1.0
U_1	0.1	0.0	0.2
U_2	0.6	0.1	0.0
U_3	-	-	0.3
R	96.4	96.6	92.5

Table 4.3: Turbine 1 reliability results; all results with same normalized fatigue load L_{nom} .

By preserving the nominal load L_{nom} in Eq. 4.19 for each distribution type, the results in Table 4.3 correspond to three different blade designs. Resizing the blade in each case scales the relative stress levels so that the $E[S^b]$ for each stress distribution type (and therefore L_{nom}) is the same for each blade. The results are seen to be only mildly sensitive to the choice of load distribution. In fact both two-moment models (lognormal and Weibull) give $p_f=4 \times 10^{-4}$, with almost all uncertainty due to R (96–97%). The three-moment model (quadratic Weibull) gives slightly higher p_f , due to the additional uncertainty in the higher-moment statistic μ_3 . (The uncertainty contribution of R is thus reduced to 92.5% in this case.)

We therefore suggest that load factors γ_L should be based on the nominal load defined in Eq. 4.19. This should promote relatively stable results across different materials, load modeling assumptions, and blade designs.

4.6.1 Turbine 1 Results

Finally, we consider the inverse problem of probabilistic design: what factors γ_L and ϕ_R should be used in Eq. 4.1, with nominal fatigue load L_{nom} and resistance R_{nom} , to achieve a target failure probability p_f over the service life? FORM/SORM methods are particularly useful for these purposes. In addition to providing estimates of p_f and uncertainty contributions, they provide load and resistance values, L^* and R^* , most likely to cause failure at the design lifetime (see Section 2.5). By setting our design load and resistance to these most likely values, we can estimate the necessary factors:

$$\gamma_L = L^*/L_{nom}; \quad \phi_R = R^*/R_{nom} \quad (4.20)$$

Regarding nominal loads and resistances, we again use Eq. 4.19 to define a “mean” nominal load L_{nom} . Recall that L_{nom} has units of “cycles” so that corresponding load factors are applied to an expected number of service lifetime cycles. In contrast, following common practice the nominal fatigue resistance, R_{nom} , is set at its lower 2.3% fractile, i.e., the underlying normal variable lies two standard deviations below the mean. An example utilizing units of “stress” is given in the next section using results for turbine 2.

Figures 4.8–4.9 show resulting load and resistance factors, respectively, for Turbine 1. As may be expected, the resistance factor ϕ_R decreases steadily as the target p_f is lowered. This reflects that while the nominal resistance R_{nom} was somewhat conservatively set (2.3% fractile), still lower resistances must be designed against if we require still rarer failure events.

In Figures 4.8–4.9 both the load and resistance factors are nearly identical for the assumed 2 parameter stress distribution cases while those for the 3 parameter quadratic Weibull are somewhat different. This can be explained by observing the relative levels of uncertainty reported for these results in Table 4.3. The lognormal and Weibull distribution cases have nearly the same levels of relative importance distributed between the resistance ($\sim 96.5\%$) and load ($\sim 3.5\%$) variables resulting in nearly identical load and resistance factors. Also from Figure 4.8, note that

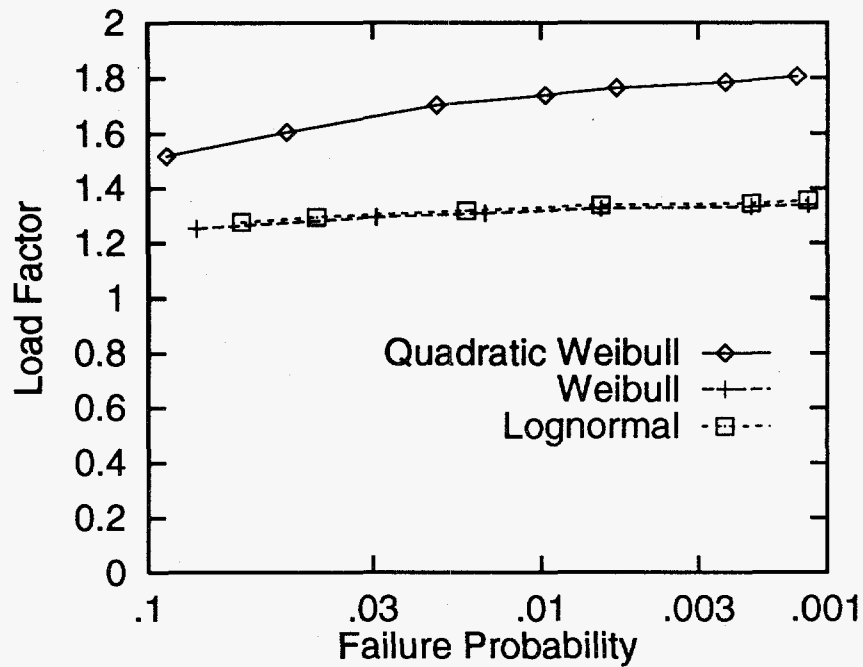


Figure 4.8: Load factors, Turbine 1. Note that these factors apply to a load defined in units of cycles (Eqs. 4.18–4.19).

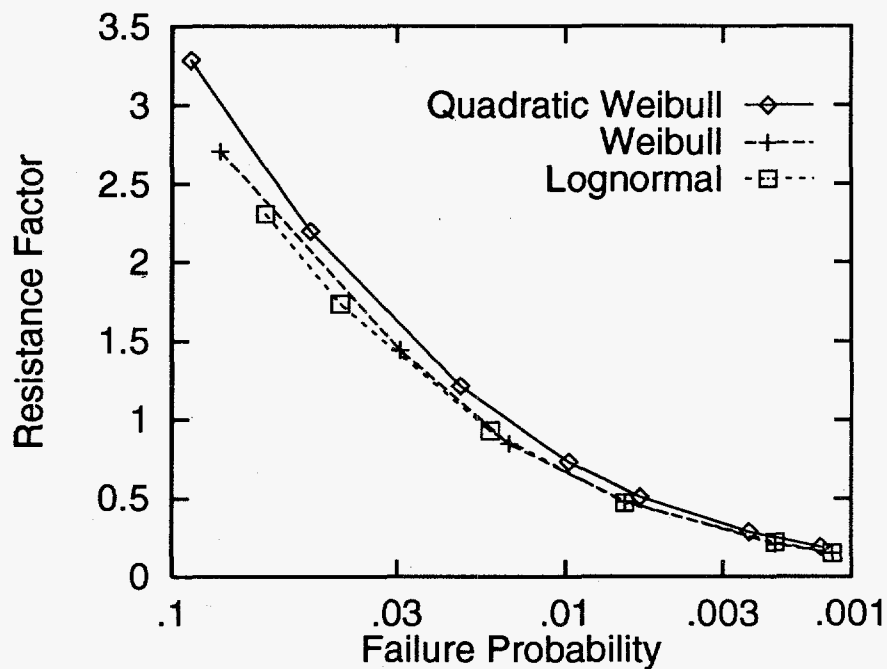


Figure 4.9: Resistance factors, Turbine 1. Note that these factors apply to a resistance defined in units of cycles (Eq. 4.7).

the required load factors γ_L are effectively constant over the several decades of p_f values shown. This is because load uncertainty is relatively unimportant (i.e., the uncertainty contributions from all 7 wind and load variables remains less than 7.5% throughout). The actual load factor γ_L is not 1.0, however; somewhat larger values ($\gamma_L=1.2-1.8$) are needed to cover not the uncertainty in load, but rather the *bias* between the nominal "mean" load L_{nom} and the actual load L^* most likely to cause failure.

In Section 4.5 the choice of load model on fatigue reliability was shown to be critical as p_f estimates differed by more than 5 orders of magnitudes for identically designed blades. Nominal load definitions that do not include load distribution type in their definition will produce load factors that also differ by orders of magnitude. To demonstrate, an alternative nominal load is defined where the design parameter, W , is chosen to preserve the conditional mean stress given a mean wind speed $V=50$ m/sec. Using Eq. 4.14 to evaluate $\bar{S} = E[\mu_1]$ with $V = 50$ m/s and $I = \bar{I}$, we define the nominal load by;

$$L'_{nom} = \frac{[\bar{S}|V = 50 \text{ m/sec}]^b \cdot N_{ser}}{S_{ref}^b} \quad (4.21)$$

The resulting load factors in Figure 4.10 differ by orders of magnitude as our alternative nominal load (L'_{nom}) does not reflect the distribution type. Note the critical distinction between \bar{S}^b here and \bar{S}^b in earlier nominal load definitions; Eq. 4.21 reflects only the mean stress \bar{S} at $V=50$ m/sec, which is a poor predictor of \bar{S}^b for high stress exponents b . These results clearly demonstrate the advantage of including distribution type in nominal load definitions as Eq. 4.19 does.

4.6.2 Turbine 2 Results

Figures 4.11 and 4.12 show load and resistance factors for Turbine 2 based on Eq. 4.19. Results vary markedly from those for Turbine 1. Due to the relatively sparse load data in this case, FORM results show roughly equal contribution from load and resistance uncertainty (see Table 4.4). As a result, the implied load and resistance factors in Figures 4.11–4.12 vary similarly over the range of p_f values

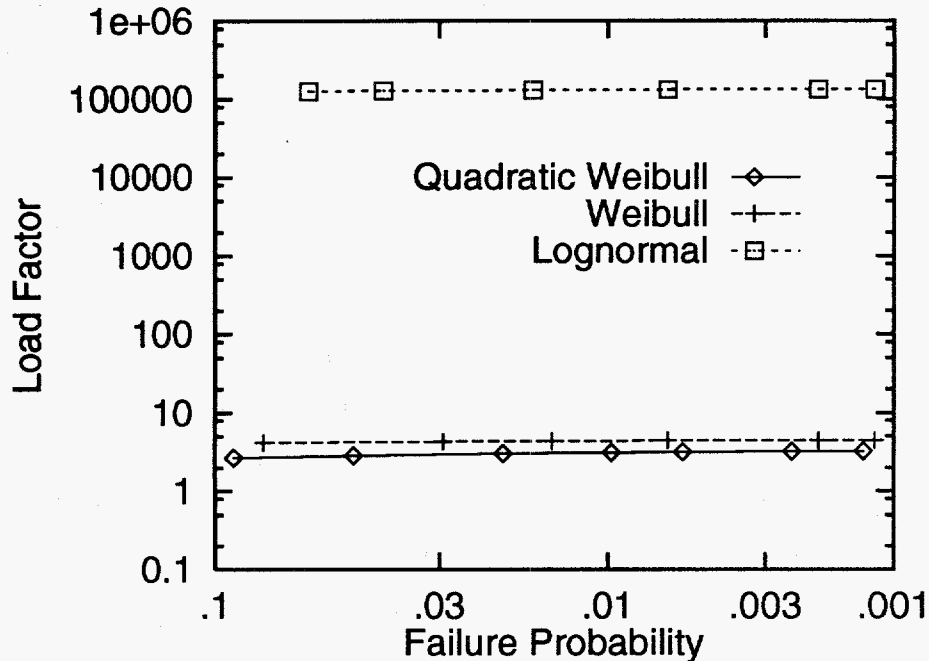


Figure 4.10: Load factors needed, for Turbine 1, if nominal load is based only on the mean stress for wind speed $V=50$ m/s.

reported: γ_L varies by about a factor of 3, and ϕ_R by about a factor of 7. Note also that for relatively high p_f values, the 2.3% fractile nominal resistance R_{nom} is too conservative; ϕ_R factors above 1.0 show that we may design with a less conservative $S-N$ curve. However, to cover load uncertainty we may need γ_L on the order of 5; i.e., ensure that our design life is an order of magnitude greater than the service life.

Finally, note again that our formulation applies all safety factors to a number of cycles: ϕ_R is applied to the number of cycles N to resist failure in a nominal $S-N$ curve, and γ_L to the number of cycles to be withstood in the service life. Alternatively, we may define nominal loads and resistances in terms of stresses, and find an equivalent set of factors γ'_L and ϕ'_R . In order to define nominal loads and resistances in terms of stresses recall the failure criterion defined in Section 4.2.2, e.g., $\bar{D}_{eff} N_{ser} \geq \Delta$, given by Eq. 4.6. Substituting for \bar{D}_{eff} from Eq. 4.5 and transposing terms results in;

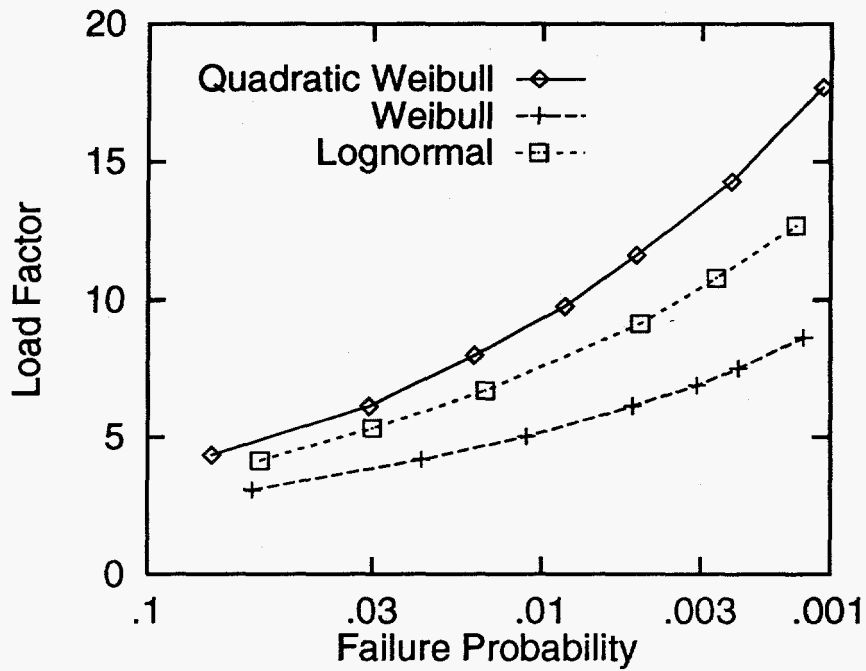


Figure 4.11: Load factors, Turbine 2. Note that these factors apply to a load defined in units of cycles (Eqs. 4.18–4.19).

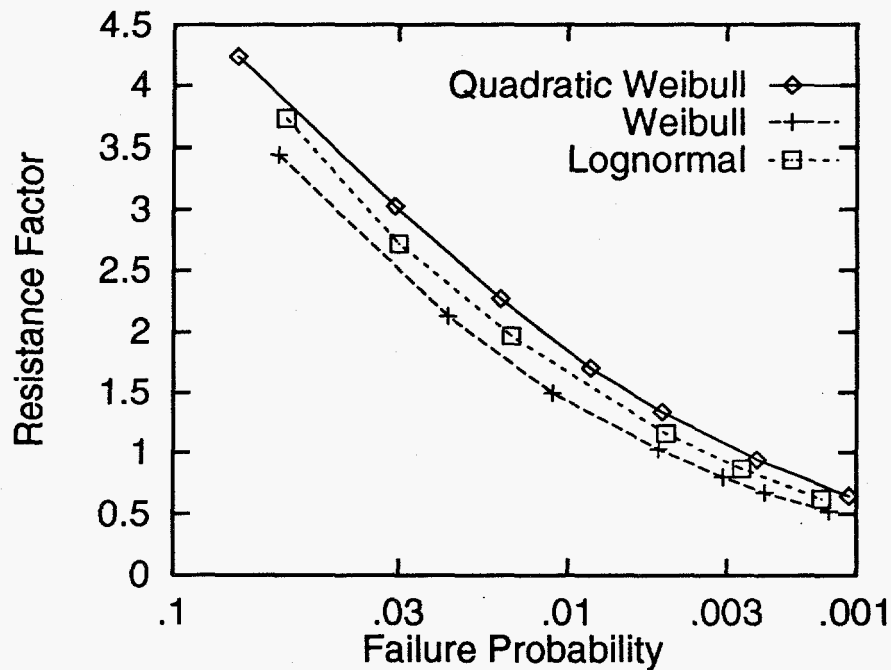


Figure 4.12: Resistance factors, Turbine 2. Note that these factors apply to a resistance defined in units of cycles (Eq. 4.7).

	Stress Distribution Type		
	Log	Weibull	Quad Weib
p_f :	4×10^{-4}	10×10^{-4}	17×10^{-4}
Variable	Uncertainty Percentage		
α_V	25.9	28.3	23.6
\bar{V}	7.3	7.1	7.3
COV_I	0.0	0.0	0.0
\bar{I}	0.4	0.4	1.4
U_1	0.3	0.3	3.5
U_2	8.9	2.1	5.2
U_3	-	-	7.0
R	57.2	61.7	52.5

Table 4.4: Turbine 2 reliability results; all results with same normalized fatigue load L_{nom} .

$$\bar{S}^b \geq S_{ref}^b N_{eff} \cdot \frac{\Delta}{N_{ser}} \quad (4.22)$$

Taking the b^{th} root produces expressions for load and resistance in units of stress;

$$L' = [\bar{S}^b]^{1/b}; \quad R' = \left[S_{ref}^b N_{eff} \cdot \frac{1}{N_{ser}} \right]^{1/b} \cdot \Delta^{1/b}. \quad (4.23)$$

The load term is simply the b^{th} root of the expected value of S^b integrated over the environmental variables V and I . For the resistance term recall our definition of the constant amplitude S - N relationship, Eqs. 4.3 and 4.5;

$$N(S) = N_{eff} \left(\frac{S}{S_{ref}} \right)^{-b} \quad \text{or} \quad S = \left[S_{ref}^b N_{eff} \cdot \frac{1}{N} \right]^{1/b} \quad (4.24)$$

The resulting resistance term then can be interpreted as the *stress* level associated with N_{ser} as given by the S - N relationship of Eq. 4.3 (and scaled by $\Delta^{1/b}$). Therefore R' reflects the material properties (e.g. the resistance) through the required service

cycles N_{ser} .

Figures 4.13 and 4.14 show load and resistance factors for Turbine 2 based on Eq. 4.23. Because damage is related to the b -th power of stresses, $\gamma'_L = \gamma_L^{1/b}$. To verify this equality consider the load definitions given by Eqs. 4.18 and 4.23 and observe that $L^{1/b} = L' \cdot [N_{ser}^{1/b}/S_{ref}]$. Since the load factors, γ_L are computed as the ratio of the design load L^* to the nominal load L_{nom} (see Eq. 4.20) the constant $N_{ser}^{1/b}/S_{ref}$ drops out of the calculation and the equality $\gamma'_L = \gamma_L^{1/b}$ holds. A similar argument can be made for the resistance term. In Figure 4.11 typical values of γ_L range from 5 to 20. For $b=8$, corresponding factors γ'_L on stresses range from 1.2 to 1.4. These factors lie in a similar range as those of the Danish study (Ronold et al, 1994).

4.7 Effects of Limited Data

The use of Eqs. 4.14 and 4.17 to model fatigue loads across wind climates is intended to include uncertainty in the loads due to limited data through the standard deviations ($D[\mu_i]$'s) of the moments $\mu_1 \dots \mu_3$. The difference in $D[\mu_i]$'s, observed in Figures 4.5 - 4.7, is expected to propagate through the load- and resistance-factor calculations. This approach apparently works quite well as Turbine 1, with approximately 10 times more data than Turbine 2, has much lower load factors (Figures 4.8 and 4.11).

Closer inspection of the results shows that the effects of data limitations in this case are more subtle. Table 4.4 shows reliability results and uncertainty contributions for Turbine 2. As for Turbine 1, the nominal load L_{nom} has again been preserved across the three load distribution types, by appropriate choice of blade section modulus, W . One would expect Turbine 2, with higher $D[\mu_i]$'s and load factors to show a shift of importance away from the resistance R to the moments U_i . Results show only a moderate shift to the U_i 's and a dramatic shift to the wind speed shape factor, α_V . These results would suggest that there are sufficient blade load data for Turbine 2 and the other sources of uncertainty are dictating the reliability. Table 4.4 shows that the dependence upon wind speeds and the uncertainty in those wind speeds is an important factor to consider for Turbine 2.

The dependence of Turbine 2 upon wind speeds, in contrast to Turbine 1, can be

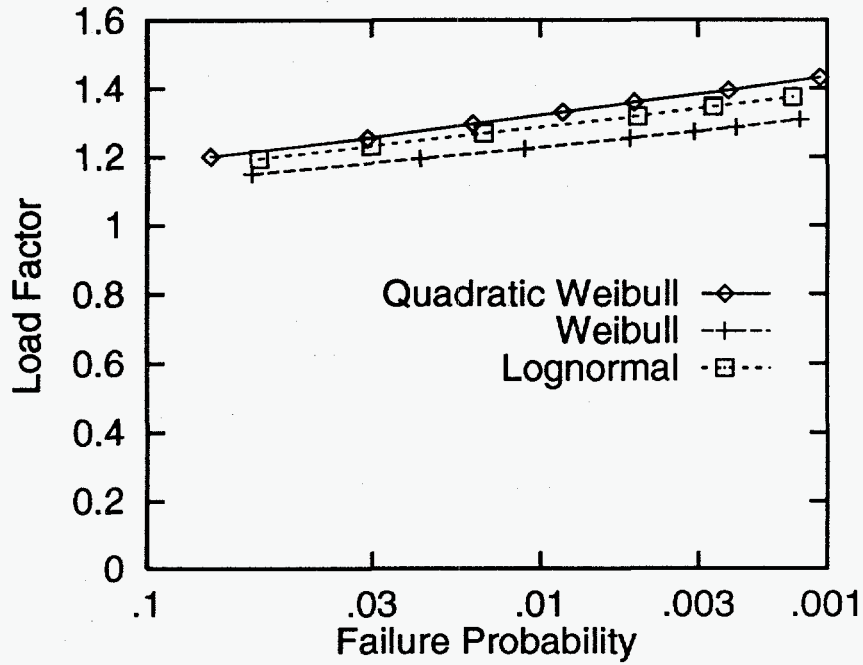


Figure 4.13: Load factors, Turbine 2. Note that these factors apply to a load defined in units of stress (Eq. 4.23).

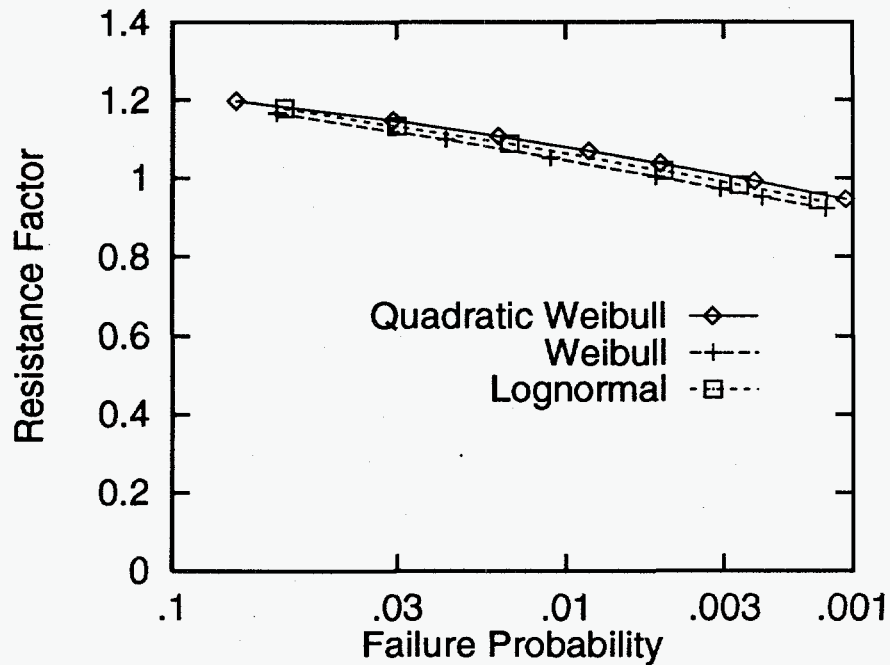


Figure 4.14: Resistance factors, Turbine 2. Note that these factors apply to a resistance defined in units of stress (Eq. 4.23).

explained by considering the trends in the mean blade loads rather than the standard deviations. That is, it is the $E[\mu_i]$'s in Figures 4.2–4.4 and not the $D[\mu_i]$'s (from Figures 4.5–4.7) that are responsible for the shift in uncertainty. This has been confirmed through an additional case study, in which the FORM analyses used to generate the results of Table 4.4 are repeated with the $D[\mu_i]$'s set to zero (to assume perfect data). In this case the results in Table 4.4 change very little since load uncertainty (e.g., U_1 , U_2 , and U_3) is small. Since identical distribution parameters were used for all random variables (except the loads) in the reliability analyses, we conclude that apparent differences in mean blade damage, \bar{S}^b , are attributed to different turbine designs.

It is also useful to examine most damaging wind speeds (Eq. 2.14) for the two turbines and compare them against the range of available data for each machine. Table 4.5 gives the most damaging wind speeds obtained from the associated FORM analyses at their converged, most-likely failure points. Figure 4.15 shows mean load ($E[\mu_1]$) relationships from Figure 4.2 plotted over the range of data used to produce the power-law fits. The most damaging wind speeds for Turbine 1 are within the range of measured data. This is desirable as the results of the regression analysis used to produce the curve-fits in Figure 4.15 are not valid outside the range of available data. Turbine 2 on the other hand is predicted to receive most damage from wind speeds that far exceed the associated data seriously compromising the results.

There are two important points to be made here. First, there are data limitations associated with the reliability analysis of Turbine 2 but it is the lack of blade load data at higher wind speeds rather than the paucity of the data at the more moderate wind speeds for which measurements are available. (Recall that the wind environment model has been chosen arbitrarily in this study, with no regard to the specific environment in which Turbine 2 is planned to operate.) In general these results reflect the clear need for prototype machines, on which load measurements are made, to be subjected to wind conditions that span the range of envisioned operating conditions.

A second point to be considered is the potential danger that may be encountered when using automated curve-fitting models to describe blade loads across a broad range of wind conditions. When the critical (most damaging) environment is far outside the range of observations as Turbine 2 is, results are likely to be governed

Distribution	Turbine 1	Turbine 2
Lognormal	9.2	24.0
Weibull	15.0	24.2
Quad Weib	22.1	36.0

Table 4.5: Most Damaging Wind Speeds (m/s) from Reliability Analyses

not by the data but by the curve-fit. In such cases it seems likely a range of answers are possible depending upon the assumed functional form of the relationship, fitting method, etc..

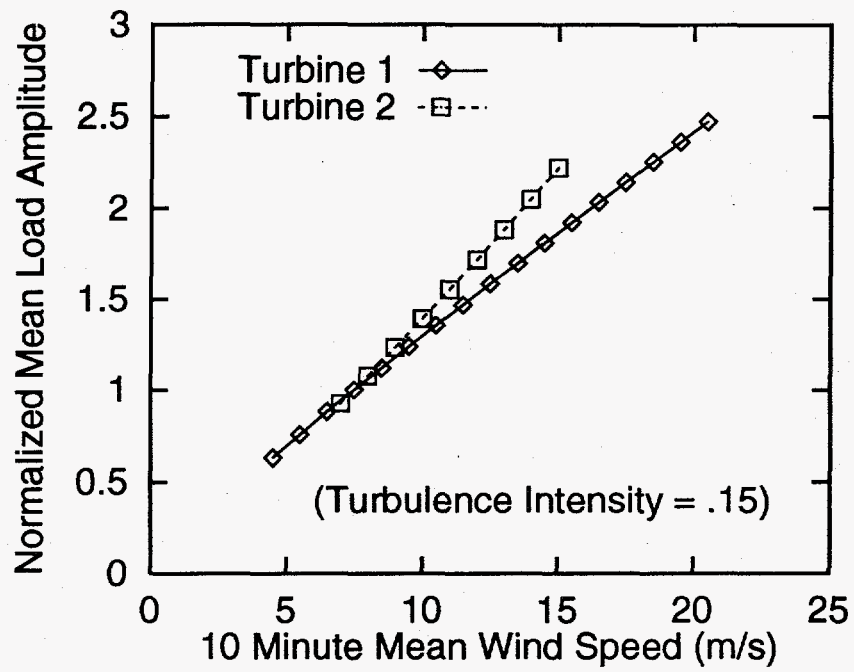


Figure 4.15: Estimated Mean of Normalized Loads showing range of measured data

4.8 Summary

We have directly studied the fatigue reliability of two horizontal-axis wind turbines, one with rather dense load data (Turbine 1) and another with relatively sparse data (Turbine 2). We have also tried to infer similar results for a Danish machine, reported in a parallel fatigue reliability study (Ronold et al, 1994). Our findings include the following.

To estimate fatigue damage, flapwise loads have been represented by their first three statistical moments across a range of wind conditions. The first two moments, μ_1 and μ_2 , show similar trends for all 3 machines (Figures 4.2–4.3). Despite their rather different designs, Turbines 1 and 2 also show similar third moment μ_3 in Figure 4.4. This tends to support the goal of establishing a fairly general set of load distributions, at least for specific load components, HAWT designs, etc.

Based on the moments $\mu_1 \dots \mu_3$, we have introduced new “quadratic Weibull” load distribution models. By preserving μ_3 , they more faithfully reflect the upper fractile of observed loads (e.g., Figure 4.1) than common two-moment models such as the Weibull or the lognormal. At the same time, they are rather simpler to implement than our earlier 4-moment models (e.g., Winterstein et al, 1994). This leads to particular savings when many fits are required; e.g., to estimate damage contributions over a range of wind speeds V and turbulence intensities I .

The fatigue reliability is found to be notably affected by the choice of load distribution model. When lognormal, Weibull, and quadratic Weibull models are fit to the same 3 moments of loads data, typical failure probabilities for a 20-year life were found to differ by more than 5 orders of magnitude: from less than 10^{-6} to above 10^{-1} . This effect will grow with b ; note that we choose here $b=8$, which is a relatively high value for metals but relatively low for many composites. Once an appropriate load distribution has been selected, this choice can be directly reflected in the fatigue design by seeking to preserve the nominal load L_{nom} in Eq. 4.19. Resulting load- and resistance factors are then only mildly sensitive to the choice of load distribution (e.g., Figures 4.8–4.12).

Because a broad range of load data is available for Turbine 1, its fatigue reliability

is governed by the uncertainty in fatigue resistance R (e.g., uncertainty in $S-N$ curve, Miner's rule, etc.). The required resistance factor ϕ_R —applied to the nominal $S-N$ curve—is shown in Figure 4.9 to decrease steadily as the target p_f is lowered. This reflects that while the nominal resistance R_{nom} was somewhat conservatively set (2.3% fractile), still lower resistances must be designed against if we require still rarer failure events. In contrast, the load factor γ_L in this case is relatively flat, reflecting only the bias between the nominal “mean” load L_{nom} and the actual load most likely to cause failure.

Because relatively sparse load data is available for Turbine 2, load and resistance uncertainties are found to be of comparable importance in this case. (This lack of data however is associated more with the range over which the data was acquired than with the quantity of data itself.) Thus the implied load and resistance factors in Figures 4.11–4.12 vary similarly over the range of p_f values reported: γ_L varies by about a factor of 3, and ϕ_R by about a factor of 7.

Chapter 5

Summary and Recommendations

5.1 Overview of Important Conclusions

CYCLES Fatigue Reliability Formulation

A computer program (CYCLES) that estimates fatigue reliability of structural and mechanical components has been developed. A FORM/SORM analysis is used to compute failure probabilities and importance factors of the random variables. The limit state equation includes uncertainty in environmental loading, gross structural response, and local fatigue properties.

The CYCLES fatigue reliability formulation assumes specific functional forms for the controlling quantities of fatigue life so that a closed form expression for fatigue damage can be derived. While these assumptions limit the program's generality, the CYCLES formulation represents a useful compromise between level of detail in probabilistic modeling and the state of knowledge of many components to which it may be applied.

Load Models for Fatigue Reliability

Several techniques have been shown to better study fatigue loads data. Damage densities show which stress ranges are most important to model, reflecting fundamental differences between flapwise and edgewise data.

Common one-parameter models, such as the Rayleigh and exponential models, should be used with care. They may produce dramatically different estimates of load distributions and fatigue damage. Improved fits may be achieved with the two-parameter Weibull model.

"Filling in" the distribution tail with a continuous model need not result in more damage. In fitting such a model, however, it is crucial to well-represent the most damaging stress levels. High b values require better modeling of relatively large stress ranges; this is most effectively done by matching at least two moments (Weibull) and better by matching still higher moments. For this purpose, a new, four-moment "generalized Weibull" model has been introduced.

As the exponent b increases, damage estimates show growing uncertainty due to their sensitivity to rare, high stresses. This effect has been quantified and resulting data needs have been discussed.

LRFD for Fatigue

We have directly studied the fatigue reliability of two horizontal-axis wind turbines (Turbines 1 and 2), and tried to infer similar results for a Danish machine, reported in a parallel fatigue reliability study (Ronold et al, 1994).

To estimate fatigue damage, flapwise loads have been represented by their first three statistical moments across a range of wind conditions. The first two moments, μ_1 and μ_2 , show similar trends for all 3 machines. Turbines 1 and 2 also show similar third moment μ_3 . This tends to support the goal of establishing a fairly general set of load distributions, at least for specific load components, HAWT designs, etc.

Based on the moments $\mu_1 \dots \mu_3$, we have introduced new "quadratic Weibull" load distribution models. By preserving μ_3 , they more faithfully reflect the upper fractile of observed loads than common two-moment models such as the Weibull or the lognormal.

The fatigue reliability is found to be notably affected by the choice of load distribution model. When lognormal, Weibull, and quadratic Weibull models are fit to the same 3 moments of loads data, typical failure probabilities for a 20-year life were found to differ by more than 5 orders of magnitude. This effect will grow with b ; note

that we choose here $b=8$.

Because a broad range of load data is available for Turbine 1, its fatigue reliability is governed by the uncertainty in fatigue resistance R (e.g., uncertainty in $S-N$ curve, Miner's rule, etc.). The required resistance factor ϕ_R —applied to the nominal $S-N$ curve—decreases steadily as the target p_f is lowered. In contrast, the load factor γ_L in this case is relatively flat, reflecting only the bias between the nominal “mean” load L_{nom} and the actual load most likely to cause failure. Because relatively sparse load data is available for Turbine 2, load and resistance uncertainties are found to be of comparable importance in this case.

5.2 General Recommendations of Future Work

There are a few recommendations of a general nature that will be mentioned before more specific recommendations, that are direct extensions of this study, are presented. First it would be instructive to repeat the reliability analyses for the LRFD study in Chapter 4 with data from additional turbines. The similarity of trends for the two turbines considered gives promise to establishing a general set of load distributions for specific components, blade designs, etc. Additional data from different turbines would help establish the feasibility of such distributions.

Note too that our predictions and load factors have been based here entirely on observed (empirical) loads data from prototype machines. It may also be useful to consider modeling errors, and resulting load factors, that arise when analytical load predictions are used. In this case one trades statistical uncertainty, due to a limited quantity of observed data, for modeling uncertainty due to simplifying assumptions made in the analysis. This modeling error could be assessed by comparing predicted and measured loads, statistically, for different wind regimes (and possibly different turbine types). Results would parallel common practice in the offshore industry, in which LRFD design reflects both natural variability in the ocean climate, and model uncertainty in load prediction inferred from measured loads on offshore structures. Such results could be used to improve design against both overload and fatigue failures.

A final recommendation of general interest is to further study, and characterize, the set of wind characteristics that best explain blade loads and hence fatigue damage. There is nothing in CYCLES that limits the analysis to considering wind speed and/or turbulence intensity; other wind parameters could in principle be propagated through the analysis in a similar way. The main challenge remains in identifying which wind parameters best “explain” blade loads and resulting damage; this is a question that classical statistics is often well-suited to address. New methods have also been developed to efficiently predict, and display, all sets of environmental variables that may likely contribute to overload failure independent of structural concept (e.g., Winterstein et al, 1993). While commonly applied to predict overload failures of offshore structures, such concepts may prove useful for the wind industry as well—again for both overload and fatigue failure applications.

5.3 Specific Recommendations to Extend Current Work

Through the course of this thesis, a number of basic developments have been made; e.g., in modeling loads from limited data, and in propagating this uncertainty efficiently into fatigue reliability calculations. Based on this experience, we focus here on suggesting specific avenues of further work, both in the form of documenting/implementing our improved algorithms and in further studying the areas we found challenging to model.

Directing attention first to the reliability algorithm (g -function) used here, further work could profitably be directed to include formal development and documentation of an “enhanced” version of CYCLES. The capabilities of such a version could parallel those used in the LRFD analysis of Chapter 4. Our research efforts suggest that it is conceptually straightforward, and of little numerical cost, to generalize our load models to include dependence on both wind speed and turbulence intensity (or another vector set of wind attributes). We believe this generalization, through numerical quadrature methods to calculate the mean damage required in our fatigue

g -function, should be made to significantly broaden the applicability of these methods. (This more general quadrature routine would also permit other generalizations; e.g., non-smooth S - N relations.)

An additional generality has been offered through the creation of generalized, moment-based load models. These distributions have been used in research versions of CYCLES, and deserve incorporation into its standard distribution library for dissemination. A cause of concern had been its numerical robustness, particularly when four moments are sought to be fit, with minimum error, from a numerical optimization routine. The simpler, 3-moment fits (e.g., quadratic Weibull model) avoid this numerical optimization, and are believed to be good candidates to include in an automated package such as CYCLES. Note also that these distributions may have two distinct uses: (1) to model long-term uncertainties (e.g., in parameters of wind or load distributions); and (2) to model short-term variations in loads given wind. In case (2), these generalized distributions need to be included not in the CYCLES distribution library but rather in its g -function. This has already been incorporated in our in-house CYCLES version; it is recommended that it be included in a newly distributed version of CYCLES as well.

5.4 Challenges for Future Study

Parametric Models. Finally, we seek to elaborate on some of the practical aspects of our turbine-specific studies, and how they may suggest challenging avenues for future study. Important issues regarding loads modeling were encountered during the development of the "enhanced" version of CYCLES for the LRFD analyses, required to best model the practical cases encountered with the two turbines in Chapter 4.

The technique reported in Chapter 4 is based on a *parametric* load model, in which a power-law relationship is used to define the variation of predicted load moments (and their standard deviations) across different wind climates. It is perhaps useful to note here that this was not the first model adopted. We first sought a still simpler parametric model, in which it was assumed that only the mean load $\mu_L(V, I)$ varied systematically as a function of mean wind speed V and turbulence intensity I . Data

of the normalized, unit-mean load $L_{norm}=L/\mu_L(V, I)$ were then created, and pooled over all wind conditions. (An analogous treatment could be made of fatigue life data: observed cycles N to fail at different stresses S could be normalized by their predicted mean, $\mu_N(S)$, and pooled to fit a single distribution of normalized resistance $N_{norm}=N/\mu_N(S)$.)

When this single (normalized) load model was implemented for the turbines considered here, uncertainty due to limited data was typically found to have little or no impact. This is to be expected: the assumption of a common (parametric) distribution model reduces data needs enormously, as all data can be pooled/lumped, after proper normalization, into a common "bin" for fitting purposes. The corresponding danger of this method is that it is only as good as its assumptions; namely, it obscures any true variations that the unit-mean normalized load, L_{norm} , may show with wind conditions.

Note that our final model was also of parametric form, fitting analytical, power-law form to observed statistics. It was, however, somewhat more general than the original 1-parameter normalized load model considered above: the first three load moments μ_n ($n=1,2,3$) were permitted to vary with wind conditions, and power-law relations were fit to both the mean and uncertainty of each $\mu_n(V, I)$. Our limited results showed some promise for simpler 1-moment models; e.g., the observed COV for two turbines remained nearly constant (near unity) for various wind conditions. This would tend to support the assumption of a common (exponential) distribution of blade loads, in which only the mean load needs to be fit as a function of wind conditions. Preliminary experience with other turbine blade loads data suggest that this conclusion may not be universal. We believe, however, that sufficient loads data exist to permit critical study of this question; i.e., which load statistics are permissible to be assumed constant, and which must be kept free to vary with wind parameters such as V and I . An associated question concerns which parametric form—e.g., power-law or polynomial—is most appropriate if one seeks to fit one such form.

As a final caution regarding parametric models, we note our experiences with the limited-data case of Turbine 2. We predict rather different results than for Turbine 1—e.g., greater importance of wind vs fatigue resistance uncertainty. However, for

Turbine 2 the greatest damage contribution comes from wind conditions for which we have little or no data. Thus our conclusions in this case are driven less by our data than by our assumed curve-fits. This is a common danger of parametric models: while easy to automate, they create a danger that users will apply them indiscriminately, outside the range for which the data can validate them. Based on this experience, at a minimum we propose that future CYCLES versions will also report the most damaging wind conditions (at the design point most likely to cause fatigue failure). The user can then be cautioned as to whether the results are based on wind conditions for which adequate data are available.

Non-Parametric Models. Finally, we note that as an alternative to the parametric load models described above, we have also considered and implemented non-parametric loads models. These assume no specific functional (“parametric”) form of any load statistic with V or I . Instead they simply sort data into discrete bins; here, in 2 discretized dimensions involving bins of V and I values. Loads distributions—and uncertainty in their parameters—are sought separately from the data in each bin. The results are then propagated through the fatigue reliability analysis, using a numerical quadrature routine to estimate fatigue damage by summing contributions from each bin. (Several numerical strategies are possible here: 1. optimal quadrature points may be chosen for the integration, and load statistics at these optimal points may be interpolated from those observed at prescribed bin locations; or 2. the bins may be kept as given, and the probabilities lumped optimally into these prescribed bins.)

Our preliminary experience with these models was that they provide a flexible load representation, more faithful to observed trends (and uncertainties) found in the loads data. However, due to their discrete nature, it was found difficult to use them to achieve converged, FORM-based analysis to predict fatigue reliability. This is typical with “noisy,” non-smooth g -functions: gradient-based searches for the most likely failure point are likely to have convergence difficulty, due to non-systematic variations in g and its derivatives with one or more uncertain variables.

Therefore, we believe that both nonparametric as well as parametric load modeling methods provide useful topics for future study. Regarding the non-parametric models,

new *Inverse-FORM* methods, which switch the objective function (failure probability) and the constraint (limit state function g), may be more stable for noisy g -functions (Winterstein et al, 1993). Simulation and other analysis methods are also appropriate for these cases.

A practical implementation question in these non-parametric models concerns the choice of optimal binning strategy. Indeed, any binning is effectively parametric; i.e., load statistics are at least assumed to be equal for all data that fall within the prescribed wind-condition bin. Thus, the extent of the bin width (in one or more dimensions) reflects the modeler's assumption as to how uniform the turbine loads are with varying wind conditions. This bin width will in turn govern how much data are accumulated per bin, and hence the requisite data needs.

References

- API, RP2A-LRFD (1993). *Recommended practice for planning, designing and constructing fixed offshore platforms—load and resistance factor design*, 1st edition, American Petroleum Institute.
- Ang, A. and W.H. Tang (1990). *Probability Concepts in Engineering Planning and Design: Volume II - Decision, Risk, and Reliability*, Published by Authors.
- Ashwill, T.D., H.J. Sutherland, and P.S. Veers (1990). Fatigue Analysis of the Sandia 34-Meter Vertical Axis Wind Turbine. *Ninth ASME Wind Energy Symposium*, New Orleans, Louisiana.
- Banon, H., R.G. Toro, E.R. Jefferys and R.S. De (1994). Development of reliability-based global design equations for TLPs. *Proc., 13th Intl. Offshore Mech. Arctic Eng. Symp.*, ASME, Vol. II, 335–343.
- Coleman, C. and B. McNiff (1989). *Final report: Dynamic response testing of the Northwind 100 kW wind turbine*, Subcontractor Report DE-FC02-86CH10311, Solar Energy Res. Inst..
- Committee on Fatigue and Fracture Reliability, ASCE (1982). Fatigue reliability: review papers 1–4. *J. Struc. Div.*, ASCE, Vol. 108, No. ST1, 3–88.
- Danish Hydraulic Institute, (1989). *Environmental Design Conditions and Design Procedures for Offshore Structures*, Copenhagen.
- Dowling, N.E. (1988). Estimation and Correlation of Fatigue Lives for Random Loading. *Intl. J. Fatigue*, Vol. 10, No. 3, 179–185.
- Efron, B. and R. Tibshirani (1986). Bootstrap Methods for Standard Errors, Confidence Intervals, and Other Measures of Statistical Accuracy. *Statistical Science*, Vol. 114, No. 1, pp. 54-77.

- Fisher, R.A. (1928). Moments and product moments of sampling distributions. *Proc. London Math. Soc.*, Vol. 30, 199–238.
- Golweitzer, S., T. Abdo, and R. Rackwitz (1988). *FORM (First Order Reliability Method) Manual*, and S. Golweitzer, F. Guers, and R. Rackwitz, *SORM (Second Order Reliability Method) Manual*, RCP GmbH, Munich.
- Grigoriu, M. and S.T. Ariaratnam (1987). Stationary response of linear systems to non-gaussian excitations. *Proc., ICASP-5*, ed. N.C. Lind, Vancouver, B.C., Vol. II, 718–724.
- Jackson, K. (1992). Deriving fatigue design loads from field test data. *Proc., Wind-Power 92*, AWEA.
- Jaynes, E.T. (1957). Information theory and statistical mechanics. *Phys. Rev.*, Vol. 106, 620–630.
- Kelley, N.D. (1995). A comparison of measured wind park load histories with the WISPER and WISPERX load spectra. *Proc., Wind Energy 1995*, ASME, SED Vol. 16, 107–114.
- Lobitz, D.W. and W.N. Sullivan (1984). *Comparisons of Finite Element Predictions and Experimental Data for the Forced Response of the DOE 100 kW Vertical Axis Wind Turbine*, Report SAND82-2534, Sandia National Laboratories.
- Madsen, H.O., S. Krenk, and N.C. Lind (1986). *Methods of structural safety*, Prentice-Hall, Inc., New Jersey.
- Malcolm, D.J. (1990). Predictions of peak fatigue stresses in a Darrieus rotor wind turbine under turbulent winds. *Proc., 9th Wind Energy Symp.*, ASME, SED Vol. 9, 125–135.
- Mandell, J.F., R.M. Reed, D.D. Samborsky, and Q. Pan (1993). Fatigue performance of wind turbine blade composite materials. *Proc., 13th Wind Energy Symp.*, ASME, SED Vol. 14.
- McCoy, T.J. (1995). Load measurements on the AWT-26 prototype wind turbine. *Proc., Wind Energy 1995*, ASME, SED Vol. 16, 281–290.
- Melchers, R. (1987). *Structural Reliability Analysis and Predictions*, Limited, Halsted Press: a division of John Wiley & Sons, Inc. New York.
- Ronold, K.O., J. Wedel-Heinen, C.J. Christensen, and E. Jorgensen (1994). Reliability

- based calibration of partial safety factors for design of wind-turbine rotor blades against fatigue. *Proc., 5th European Wind Energy Conf.*, Vol. II, Thessaloniki, Greece, 927-933.
- Rubinstein, Y. (1981). *Simulation and the Monte Carlo Method*, Wiley.
- Sutherland, H.J. (1989). *Analytical framework for the LIFE2 computer code*, Report SAND89-1397, Sandia National Laboratories.
- Sutherland, H.J. (1993). Effect of flap and edgewise bending moment phase relationships on the fatigue loads of a typical HAWT blade. *Proc., 13th Wind Energy Symp.*, ASME, SED Vol. 14181-188.
- Sutherland, H.J. and S. Butterfield (1994). A summary of the workshop on fatigue life methodologies for wind turbines. *Proc., WindPower 94*, AWEA.
- Sutherland, H.J., P.S. Veers, and T.D. Ashwill (1994). Fatigue Life Prediction for Wind Turbines: A Case Study on Loading Spectra and Parameter Sensitivity. *Case Studies for Fatigue Education, ASTM STP 1250*, American Society for Testing and Materialspp. 174-207.
- Sutherland, H.J. and P.S. Veers (1995). Fatigue analysis of WECS components using the generalized Weibull model. *Proc., Wind Energy 1995*, ASME, SED Vol. 16, 83-90.
- Thoft-Christensen, P. and M.J. Baker (1982). *Structural Reliability Theory and Its Applications*, Springer Verlag.
- Thresher, R.W., S.M. Hock, and R.M. Osgood (1991). Data record length effects on rainflow analysis. *Proc., 11th Wind Energy Symp.*, ASME, SED Vol. 12.
- VanDenAvyle, J.A. and H.J. Sutherland (1987). Fatigue characterization of a VAWT blade material. *Proc., 8th Wind Energy Symp.*, ASME, SED Vol. 9.
- Veers, P.S. (1982). Blade fatigue life assessment with application to VAWTs. *J. Solar Energy Eng.*, Vol. 104, No. 2, 106-111.
- Veers, P.S. (1990). Fatigue Reliability of Wind Turbine Components. *Proc., WindPower 90*, AWEA.
- Veers, P.S., S.R. Winterstein, and C.H. Lange (1993). FAROW: A tool for fatigue and reliability of wind turbines. *Proc., WindPower '93*, American Wind Energy Association.

- Winterstein, S.R. (1985). Nonnormal responses and fatigue damage. *J. Engrg. Mech.*, ASCE, Vol. 111, No. 10, 1291-1295.
- Winterstein, S.R. (1988). Nonlinear vibration models for extremes and fatigue. *J. Engrg. Mech.*, ASCE, Vol. 114, No. 10, 1772-1790.
- Winterstein, S.R., R.S. De, and P. Bjerager (1989). Correlated Non-Gaussian Models in Offshore Reliability FORM. *Proc.*, 5th International Conference on Structural Safety and Reliability (ICOSSAR), Vol. 1., San Francisco, California.
- Winterstein, S.R. and S. Haver (1991). Statistical uncertainties in wave heights and combined loads on offshore structures. *J. Offshore Mech. Arctic Eng.*, ASME, Vol. 114, No. 10, 1772-1790.
- Winterstein, S.R., T.C. Ude, C.A. Cornell, P. Bjerager and S. Haver (1993). Environmental parameters for extreme response: Inverse FORM with omission factors. *Proc.*, *ICOSSAR-93*, Innsbruck.
- Winterstein, S.R. and C.H. Lange (1994). *CYCLES: Fatigue Reliability Formulation and Analysis*, Rept. RMS-13, Rel. Marine Struc. Prog., Civil Eng. Dept., Stanford University.
- Winterstein, S.R., C.H. Lange, and S. Kumar (1994). *FITTING: A subroutine to fit four moment probability distributions to data*, Rept. RMS-14, Rel. Marine Struc. Prog., Civil Eng. Dept., Stanford University.
- Winterstein, S.R. and C.H. Lange (1995). Moment-based probability models for wind engineering applications. *Proc.*, *10th Eng. Mech. Spec. Conf.*, ASCE, 159-162.

Appendix A

Statistical Moment Estimation

A brief background in statistical moment estimation is provided here. If we seek to estimate the ordinary mean value $E[X]=\mu$ from data $X_1 \dots X_n$, a natural estimate is the simple average value $\bar{X}=\sum_{i=1}^n X_i/n$. Similarly, the k -th order "ordinary" moment, $E[X^k]$, is naturally estimated by the corresponding average $\sum_{i=1}^n X_i^k/n$.

The difficulties arise when we instead seek, as in many applications, to estimate not ordinary but *central* moments; i.e., of the form $\mu_k=E[(X - \mu)^k]$ for $k=2, 3, 4, \dots$. Note that only the first four moments are required, e.g., $k=4$: $\sigma_x=\mu_2^{1/2}$, $\alpha_3=\mu_3/\mu_2^{1.5}$, and $\alpha_4=\mu_4/\mu_2^2$ for the generalized models developed in Section 3.3.

The problem here lies in its circular aspect: we must first estimate the unknown first moment μ before seeking to estimate $\mu_k=E[(X - \mu)^k]$. And, if we use the same data set for both purposes, we typically find too-low estimates of μ_2, μ_3, μ_4 , etc. because our μ value is artificially tuned to best match the mean of the observations. Those exposed to a standard statistics course will best recognize this phenomenon when estimating the variance μ_2 : to inflate the sample variance to account for this bias, the sum of squared deviations is divided by $n - 1$ rather than n .

While unbiased estimates of the higher moments μ_3, μ_4, \dots are less familiar, they are available in the statistical literature (Fisher, 1928):

$$\mu = \bar{X} = \frac{1}{n} \sum_{i=1}^n X_i \quad (\text{A.1})$$

$$\mu_2 = \frac{n}{n-1} m_2 \quad (\text{A.2})$$

$$\mu_3 = \frac{n^2}{(n-1)(n-2)} m_3 \quad (\text{A.3})$$

$$\mu_4 - 3\mu_2^2 = \frac{n^2}{(n-1)(n-2)(n-3)} [(n+1)m_4 - 3(n-1)m_2^2] \quad (\text{A.4})$$

in terms of the sample central moment $m_k = \sum_{i=1}^n (X_i - \bar{X})^k / n$. Eq. A.1 is the conventional result for the sample variance.

Remaining Bias.

The routine **FITTING** which produces generalized load models using constrained optimization, employs a companion routine, **CALMOM**, to compute statistical moments of a given data set. The routine **CALMOM** uses Equations A.1 thru A.4 to estimate the quantities σ_x by $\mu_2^{0.5}$, α_3 by $\mu_3 / (\mu_2^{1.5})$, and α_4 by $\mu_4 / (\mu_2^2)$. Because these vary nonlinearly with μ_n , they may still contain some bias although the μ_n estimates do not.

For example, if we fit a Gumbel model to the 19 wave height data from Section 3.3.4, the true skewness and kurtosis values are 1.14 and 5.40. However, simulating 10000 data sets of size $n=19$ and running each through **CALMOM**, we find on average the skewness 0.79 and kurtosis 3.89 (Winterstein and Haver, 1991).

To address this problem, the **FITTING** routine has an automatic check for remaining bias through simulation. After **FITTING** constructs a distribution with moments from the input data, many similar data sets (of identical size) are simulated from this distribution. If the moments predicted from **CALMOM** differ appreciably on average from the input values, new theoretical estimates of the moments are constructed. This estimation-simulation loop is continued iteratively until satisfactory convergence is found.

Figure A.1 shows the effect of enabling this "unbiased" option and disabling it

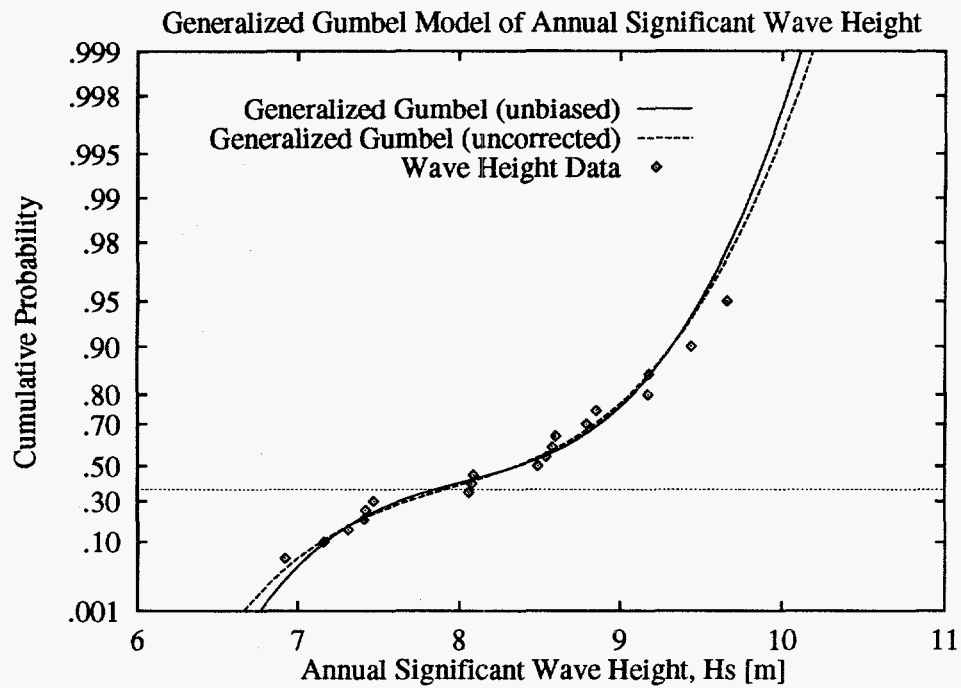


Figure A.1: Effect of Ignoring Bias: Wave Height Example.

(using “raw” moments from CALMOM directly) for the generalized Gumbel model produced for the example given in Section 3.3.4. There is relatively little difference found in these cases. Larger effects may be found for cases of (1) fewer data and/or (2) distributions with broader tails.

DISTRIBUTION:

R. E. Akins
Washington & Lee University
P.O. Box 735
Lexington, VA 24450

H. Ashley
Dept. of Aeronautics and
Astronautics Mechanical Engr.
Stanford University
Stanford, CA 94305

E. Ausman
Polarconsort Alaska
1503 W. 33rd Avenue
Suite 310
Anchorage, AK 99530

B. Bell
FloWind Corporation
990 A Street
Suite 300
San Rafael, CA 94901

K. Bergey
University of Oklahoma
Aero Engineering Department
Norman, OK 73069

J. R. Birk
Electric Power Research Institute
3412 Hillview Avenue
Palo Alto, CA 94304

C. P. Butterfield
NREL
1617 Cole Boulevard
Golden, CO 80401

G. Bywaters
New World Power Technology Center
Box 999
Waitsfield, VT 05673

J. Cadogan
U.S. Department of Energy
Office of Photovoltaic & Wind Tech.
Energy Efficiency & Renewable Energy
E-11
1000 Independence Avenue SW
Washington, DC 20585

R. N. Clark
USDA
Agricultural Research Service
P.O. Drawer 10
Bushland, TX 79012

C. Coleman
Northern Power Systems
Box 659
Moretown, VT 05660

Allin Cornell
Stanford University
Civil Engineering Department
Stanford, CA 94305-4020

K. J. Deering
The Wind Turbine Company
515 116th Avenue NE
No. 263
Bellevue, WA 98004

E. A. DeMeo
Electric Power Research Institute
3412 Hillview Avenue
Palo Alto, CA 94304

A. J. Eggers, Jr.
RANN, Inc.
260 Sheridan Ave., Suite 414
Palo Alto, CA 94306

D. M. Eggleston
DME Engineering
P.O. Box 5907
Midland, TX 79704-5907

P. R. Goldman, Acting Deputy Director
Office of Photovoltaic & Wind Technology
Energy Efficiency & Renewable Energy, EE-11
U.S. Department of Energy
1000 Independence Avenue
Washington, DC 20585

G. Gregorek
Aeronautical & Astronautical Dept.
Ohio State University
2300 West Case Road
Columbus, OH 43220

C. Hansen
University of Utah
Department of Mechanical Engineering
Salt Lake City, UT 84112

L. Helling
Librarian
National Atomic Museum
Albuquerque, NM 87185

E. N. Hinrichsen
Power Technologies, Inc.
P.O. Box 1058
Schenectady, NY 12301-1058

S. Hock
Wind Energy Program
NREL
1617 Cole Boulevard
Golden, CO 80401

W. E. Holley
3731 Oak Brook Court
Pleasanton, CA 94588

B. J. Im
McGillim Research
11299-C San Pablo Avenue
El Cerrito CA 94530

K. Jackson
Dynamic Design
123 C Street
Davis, CA 95616

G. James
Dept. of Mechanical Engineering
University of Houston
4800 Calhoun
Houston, TX 77204-4792

O. Krauss
Division of Engineering Research
Michigan State University
East Lansing, MI 48825

C. Lange
841 Byerley Avenue
San Jose, CA 95125 (20)

R. Lynette
AWT/RLA
425 Pontius Avenue North
Suite 150
Seattle, WA 98109

D. Malcolm
Advanced Wind Turbines, Inc.
425 Pontius Avenue North
Suite 150
Seattle, WA 98109

J. F. Mandell
Montana State University
302 Cableigh Hall
Bozeman, MT 59717

R. N. Meroney
Dept. of Civil Engineering
Colorado State University
Fort Collins, CO 80521

P. Migliore
NREL
1617 Cole Boulevard
Golden, CO 80401

A. Mikhail
Zond Systems, Inc.
13000 Jameson Road
P.O. Box 1910
Tehachapi, CA 93561

S. Miller
2321 Osprey Lane
Richland, WA 99352-9182

D. Morrison
New Mexico Engineering
Research Institute
Campus P.O. Box 25
Albuquerque, NM 87131

W. Musial
NREL
1617 Cole Boulevard
Golden, CO 80401

NWTC Library
NREL
1617 Cole Boulevard
Golden, CO 80401

V. Nelson
Department of Physics
West Texas State University
P.O. Box 248
Canyon, TX 79016

G. Nix
NREL
1617 Cole Boulevard
Golden, CO 80401

R. Osgood
NREL
1617 Cole Boulevard
Golden, CO 80401

M. Papadakis
Aero Engineering Department
Wichita State University
Wichita, KS 67260-0044

C. Paquette
The American Wind Energy Association
122 C Street NW
Fourth Floor
Washington, DC 20002

R. G. Rajagopalan
Aerospace Engineering Department
Iowa State University
404 Town Engineering Bldg.
Ames, IA 50011

R. L. Scheffler
Southern California Edison
Research and Development Dept.
Room 497
P.O. Box 800
Rosemead, CA 91770

L. Schienbein
CWT Technologies, Inc.
4006 S. Morain Loop
Kennewick, WA 99337

T. Schweizer
Princeton Economic Research, Inc.
1700 Rockville Pike
Suite 550
Rockville, MD 20852

J. Sladky, Jr.
Kinetics Group, Inc.
P.O. Box 1071
Mercer Island, WA 98040

M. Snyder
Aero Engineering Department
Wichita State University
Wichita, KS 67208

L. H. Soderholm
Agricultural Engineering
Room 213
Iowa State University
Ames, IA 50010

K. Starcher
AEI
West Texas State University
P.O. Box 248
Canyon, TX 79016

W. J. Steeley
Pacific Gas and Electric Co.
3400 Crow Canyon Road
San Ramon, CA 94583

F. S. Stoddard
Dynamic Design-Atlantic Office
P.O. Box 1373
Amherst, MA 01004

W. V. Thompson
410 Ericwood Court
Manteca, CA 95336

R. W. Thresher
NREL
1617 Cole Boulevard
Golden, CO 80401

K. J. Touryan
NREL
1617 Cole Boulevard
Golden, CO 80401

W. A. Vachon
W. A. Vachon & Associates
P.O. Box 149
Manchester, MA 01944

B. Vick
USDA, Agricultural Research Service
P.O. Drawer 10
Bushland, TX 79012

L. Wendell
Battelle-Pacific Northwest
Laboratory
P.O. Box 999
Richland, WA 99352

W. Wentz
Aero Engineering Department
Wichita State University
Wichita, KS 67208

R. E. Wilson
Mechanical Engineering Dept.
Oregon State University
Corvallis, OR 97331

S. R. Winterstein
Civil Engineering Department
Stanford University
Stanford, CA 94305

B. Wolff
Renewable Energy Program Manager
Conservation and Renewable Energy System
6918 NE Fourth Plain Boulevard
Suite B
Vancouver, WA 98661

M. Zuteck
MDZ Consulting
931 Grove Street
Kemah, TX 77565

S. Schuck
Renewable Technology
Pacific Power
P.O. Box 5257
GPO Sydney, New South Wales 2001
AUSTRALIA

V. Lacey
Indal Technologies, Inc.
3570 Hawkestone Road
Mississauga, Ontario L5C 2V8
CANADA

A. Laneville
Faculty of Applied Science
University of Sherbrooke
Sherbrooke, Quebec J1K 2R1
CANADA

B. Masse
Institut de Recherche d'Hydro-Quebec
1800, Montee Ste-Julie
Varenes, Quebec J3X 1S1
CANADA

I. Paraschivoiu
Dept. of Mechanical Engineering
Ecole Polytechnique
CP 6079
Succursale A
Montreal, Quebec H3C 3A7
CANADA

R. Rangi
Manager, Wind Technology
Dept. of Energy, Mines and Resources
580 Booth 7th Floor
Ottawa, Ontario K1A 0E4
CANADA

P. Vittecoq
Faculty of Applied Science
University of Sherbrooke
Sherbrooke, Quebec J1K 2R1
CANADA

P. H. Madsen
Riso National Laboratory
Postbox 49
DK-4000 Roskilde
DENMARK

T. F. Pedersen
Riso National Laboratory
Postbox 49
DK-4000 Roskilde
DENMARK

M. Pedersen
Technical University of Denmark
Fluid Mechanics Dept.
Building 404
Lundtoftevej 100
DK 2800 Lyngby
DENMARK

H. Petersen
Riso National Laboratory
Postbox 49
DK-4000 Roskilde
DENMARK

A. F. Abdel Azim El-Sayed
Dept. of Mechanical Design &
Power Engineering
Zagazig University
3 El-lais Street
Zeitun
Cairo 11321
EGYPT

M. Anderson
Renewable Energy Systems, Ltd.
Eaton Court, Maylands Avenue
Hemel Hempstead
Herts HP2 7DR
ENGLAND

M. P. Ansell
School of Material Science
University of Bath
Claverton Down
Bath BA2 7AY
Avon
ENGLAND

A. D. Garrad
Garrad Hassan
9-11 Saint Stephen Street
Bristol BS1 1EE
ENGLAND

D. I. Page
Energy Technology Support Unit
B 156.7 Harwell Laboratory
Oxfordshire, OX11 0RA
ENGLAND

D. Sharpe
Dept. of Aeronautical Engineering
Queen Mary College
Mile End Road
London, E1 4NS
ENGLAND

D. Taylor
Alternative Energy Group
Walton Hall
Open University
Milton Keynes MK7 6AA
ENGLAND

P. W. Bach
Netherlands Energy Research Foundation, ECN
P.O. Box 1
NL-1755 ZG Petten
THE NETHERLANDS

J. Beurskens
Programme Manager for
Renewable Energies
Netherlands Energy Research
Foundation ECN
Westerduinweg 3
P.O. Box 1
1755 ZG Petten (NH)
THE NETHERLANDS

O. de Vries
National Aerospace Laboratory
Anthony Fokkerweg 2
Amsterdam 1017
THE NETHERLANDS

J. B. Dragt
Institute for Wind Energy
Faculty of Civil Engineering
Delft University of Technology
Stevinweg 1
2628 CN Delft
THE NETHERLANDS

R. A. Galbraith
Dept. of Aerospace Engineering
James Watt Building
University of Glasgow
Glasgow G12 8QG
SCOTLAND

M. G. Real, President
Alpha Real Ag
Feldeggstrasse 89
CH 8008 Zurich
SWITZERLAND

M.S. 0167 J. C. Clausen, 12630
M.S. 0437 E. D. Reedy, 9118
M.S. 0439 D. W. Lobitz, 9234
M.S. 0439 D. R. Martinez, 9234
M.S. 0557 T. J. Baca, 9741
M.S. 0557 T. G. Carne, 9741
M.S. 0557 B. Hansche, 9741
M.S. 0557 T. Paez, 9741
M.S. 0615 A. Beattie, 9752
M.S. 0615 W. Shurtleff, 9752
M.S. 0708 H. M. Dodd, 6214 (50)
M.S. 0708 T. D. Ashwill, 6214
M.S. 0708 D. E. Berg, 6214
M.S. 0708 M. A. Rumsey, 6214
M.S. 0708 H. J. Sutherland, 6214
M.S. 0708 P. S. Veers, 6214
M.S. 0708 T. A. Wilson, 6214
M.S. 0833 J. H. Strickland, 9116
M.S. 0836 W. Wolfe, 9116
M.S. 9018 Central Technical Files, 8523-2
M.S. 0899 Technical Library, 13414 (5)
M.S. 0619 Print Media, 12615
M.S. 0100 Document Processing, 7613-2 (2)
For DOE/OSTI